Table of contents Page

1. Background

The Bushveld Igneous Complex of South Africa hosts the world's largest reserves of platinum-group elements (PGEs). The Merensky reef was the first PGE-bearing reef to be exploited due to its relative ease of processing given the fairly large quantities of sulphides hosting the well-associated platinum-group minerals (PGMs) (Jones, 1999). Recent developments in flotation technology have led to the exploitation of the more difficult to process chromite-bearing UG-2 reef. New expansions are focused on exploiting the UG-2 reef on the Eastern Limb of the Bushveld Igneous Complex. Deep-level mining and difficulties encountered with mechanised mining due to the inadequate thickness of the reef, have contributed to consideration of the Platreef and the Great Dyke of Zimbabwe as possible sources of PGEs. The Great Dyke of Zimbabwe is commonly believed to host the second largest reserves of PGEs after the Bushveld Igneous Complex of South Africa. However, the exploitation of this reef has been slow, which can be partly attributed to the lack of infrastructure, political instability and complexity of the ore. The Platreef in South Africa has recently been classified as an economically viable reef; it can be accessed by conventional open-pit mining (Merkle *et al.*, 2002). Both the Platreef and the reef from the Great Dyke of Zimbabwe host very complex ores and require innovative design to process these altered ores. In addition to this, these ores contain appreciable quantities of exotic platinum group minerals (such as [Pt,Pd]-bismuthotellurides, PGE sulpharsenides), which are believed to contribute to the low PGE recoveries, especially from ores of the Great Dyke.

Research on platinum flotation in the past was mainly focused on the flotation of base metal sulphides because of the association of the PGMs with these minerals. However, the assumption that all PGMs remain associated with the base metal sulphides was challenged by the findings of Penberthy *et al.* (2000) who conducted a comprehensive study on the recovery of platinum-group elements from UG-2 chromite from the Bushveld Igneous Complex. The platinum-group mineral assemblage of the UG-2 chromite consists mainly of PGE-sulphides (predominantly, cooperite, braggite, malanite and laurite) and a significant component of alloys (such as Pt-Fe alloy) and various tellurides. The PGMs identified in the ore sample were

indeed mainly associated with the base metal sulphides (>74 %), occurring either within or at the sulphide-gangue grain boundary. However, Penberthy *et al.* (2000) found that up to fifty percent of the PGMs were liberated during milling. This clearly emphasises the importance of studying the flotation behaviour of the liberated PGMs themselves with the main aim to optimise their flotation response. Most of the PGMs associated with the sulphides reported to the concentrate during flotation, while PGMs associated with the silicates were not recovered. The response of the liberated PGMs to the flotation stimulus was difficult to investigate due to their small size (< 10 μm). Most of the liberated grains did float, albeit with a slower response than the base metal sulphides. In general the rate of PGM flotation was, in decreasing order, braggite, cooperite, malanite, ferroplatinum and laurite. No indication was given on the rate at which sperrylite and (Pt,Pd)-bismuthotellurides float. Nevertheless, it is expected that the PGE-sulphides will float at a higher rate than sperrylite and (Pt,Pd)-bismuthotellurides, especially the latter which are possibly prone to chemical attack, as discussed below.

Elvy *et al.* (1996) reported the incongruent oxidation of minerals in the Pd-Te-Bi system leading to the formation of a layer of tellurium and/or bismuth oxide covering the palladium-rich substrate. Both Te and Bi oxidise from the bismuth-telluride minerals despite the fact that these elements do not oxidise readily, in their pure state, in air. The reactivity of the minerals increased in the order of: PdTe < PdTeBi < PdBi. This is in the same order as the reactivities of Pd, Te and Bi in the pure form. This implies that merenskyite (ideal formula: $PdTe_2$) should be more resistant to oxidation than michenerite (ideal formula: PdBiTe).

The next section on the platinum-group mineralization of the platinum reefs of Southern Africa will highlight the importance of studying the flotation characteristics of sperrylite and (Pt,Pd)-bismuthotellurides.

2. Literature review on platinum-group minerals

2.1. Platinum-group element mineralogy

2.1.1. Introduction

The distribution of PGEs (platinum-group elements) in an ore is directly related to the type of ore, which in turn, dictates the mineralogical constitution. PGE ores can be divided into the following main classes (Stribrny *et al.*, 2000):

- Alluvial ores: These ores contain almost no sulphide and are composed of individual particles of rock and liberated minerals: an example is the Colombian deposit.
- Layered intrusions (e.g. Bushveld, Stillwater, Great Dyke)
- Magmatic nickel sulphide deposits (e.g. Noril'sk-Talnakh, Sudbury)

The layered intrusion ores contain by the far the world's largest reserves of PGE. The mineralization and occurrence of the PGEs are of utmost importance considering the very low concentrations of these elements in the ores (1-15 g/t).

PGE deposits can be divided into two categories: discrete platinum-group minerals (PGMs), and those hosted as "impurities" within other minerals. The latter category also includes the so-called "invisible" portion of the precious-metal distribution (Oberthür *et al.*, 2002a). The reason for the "invisibility" is not always known but can be twofold in nature: PGEs are present in submicroscopic particles or they occur as a dilute solid-solution. The understanding of the PGE associations is of utmost importance in order to construct mineralogical balances.

2.1.2. Hosted platinum-group elements

The PGE distribution between and content of the base-metal sulphides, sulpharsenides, oxides, and silicates are largely speculative, without substantial experimental evidence. However, the invention of the electron microprobe has led to

an explosion in the number of discrete PGM species being identified. It has also contributed to the understanding of the PGE distributions within other minerals as indicated by the results of the studies given below.

2.1.2.1. PGEs hosted in sulphides

There is little doubt at this stage that sulphides are a major repository of PGEs and these minerals can contain PGEs in variable amounts up to a few percent (by mass).

2.1.2.1.1. Pentlandite $(Fe,Ni)_9S_8$.

The best known carrier of PGEs is pentlandite (which can contain up to 12.1 wt% Pd). Pentlandite from Stillwater contains between 8.6-12.1 % Pd (Cabri, 1992). Reported maximum levels of Pd in pentlandite in (ppmw) (ppmw refers to parts per million by weight) are: J-M reef (46000), Platreef (20000), Lac des Iles (6500), Medvezhy Creek (2540), Great Dyke (1990), Penikat (1800) and Merensky reef (1164) (Cabri, 1992). Strirny *et al.* (2000) reported Pd and Rh partioning up to 2236 and 259 ppmw, respectively, in pentlandite from the Hartley Mine in the Great Dyke. In addition to this Prendergast (1990) reported a maximum of around 0.2 wt% Pd in pentlandite and that these low Pd concentrations could not account for the "missing Pd". "Missing" PGMs were also reported by Oberthür *et al.* (1998) from the Hartley Mine in the Great Dyke.

Lidsay *et al.* (1988) reported that the Pt content of the pentlandite from the Merensky reef is usually less than 36 ppmw and has a mean content of around 10-13 ppmw. Pentlandite from the Hartley Mine in the Great Dyke has a mean content of around 8.5 ppmw Pt. In contrast to this Prendergast (1988a) reported no association of Pt with pentlandite from samples taken at Mimosa Mine in the Great Dyke. The maximum reported solubilities of Pd, Rh and Ru in pentlandite are 12.5%, 12.4% and 12.9%, respectively, but no Pt could be detected at the analytical sensitivity value of 0.05% (Makovicky, 1986). This clearly indicates that pentlandite is mainly a Pd carrier and that high pentlandite recoveries are essential to optimise the Pd recoveries.

2.1.2.1.2. Pyrrhotite ($Fe_{1-x}S$)

Pyrrhotite can accommodate considerable quantities of PGE in solid solution at elevated temperatures, up to 11% Pd, 1.3 % Ru, 10.5% Rh and 2.2 %Pt, but upon cooling most of these PGM are expelled. A higher Fe content in the pyrrhotite is also detrimental to the solubility limit of PGMs in the mineral. Cabri (1988) reported a maximum of 47 ppmw Pd in pyrrhotite from the J-M reef. The contents of the rest of the PGEs in pyrrhotite from the most important PGE deposits are usually lower than 20 ppmw. The detection limit of many of the PGMs is of the order of 10 ppmw. These results indicate that pyrrhotite contains PGEs very close to the detection limit; indeed Oberthür *et al.* (1997) reported that pyrrhotite usually contains PGEs at concentrations close to or lower than the detection limit. Another important aspect is the occurrence of pentlandite as flame-shaped exsolutions in pyrrhotite (typical in ore from Mimosa Mine, Great Dyke). Hence the flotation characteristics of pyrrhotite will impact on the recovery of the PGEs, largely due to the occurrence of pentlandite within pyrrhotite.

2.1.2.1.3. Pyrite (FeS_2)

Pyrite does not accommodate appreciable quantities of PGM as shown by the experimental work performed by Makovicky (1986). However, Strirny *et al.* (2000) reported that pyrite from the Hartley Mine in the Great Dyke can contain on average about 36 ppmw Pt (range from 0.4 to 244; mean of 35.5 ppmw).

2.1.2.1.4. Chalcopyrite ($CuFeS_2$)

Chalcopyrite usually contains PGE at concentrations lower than the detection limit [(Oberthür *et al.*, 1997) and (Cabri, 1992)]. In addition to this, experimental studies also indicate the low solubility of PGMs in Cu-Fe sulphides (Lindsay *et al.*, 1988).

2.1.2.2. PGEs hosted in oxides

The most important oxides currently under investigation are chromite ($FeCr_2O_4$) and magnetite (Fe_3O_4). Cabri (1981) reported the presence of Pt in magnetite, but this needs verification (Cabri, 1981), since magnetite can be associated with Pt-Fe alloys. Parry (1984) reported PGE values of typically less than 1 ppmw for mixtures of magnetite and ilmenite.

2.1.2.3. PGEs hosted in silicates

There is little information on the PGE content of silicates. Michell *et al.* (1987) reported values less than 5 ppb and typically of the order of 1ppb. It is postulated that the Sudbury ores contains a significant portion of minute PGMs, which occur interstitially in silicates (Sizgoric, 1984) and that the Merensky reef contains PGMs in solid solution within oxides and silicates (Kinloch, 1982; Peyerl, 1983). It remains difficult to assess whether large or small quantities of PGEs are associated with the silicates.

2.1.2.4. PGEs hosted in sulpharsenides, arsenides and tellurides

These groups of minerals can contain appreciable levels of PGE. For example cobaltite (CoAsS) contains up to 600 ppmw Pt, 2800 ppmw Pd, 25000 ppmw Rh and 2600 ppm Ir (Cabri, 1981).

2.1.3. Platinum-group minerals

2.1.3.1. Platinum-group element mineralogy of the Merensky Reef, UG-2 Reef and the Great Dyke of Zimbabwe

Microbeam techniques enable the investigator to analyse the PGMs quantitatively to understand better the platinum-group element (PGE) distribution between discrete PGMs. As stated earlier, the number of identified PGMs exploded after the development of the microprobe. Broadly, PGMs can be grouped into metals, intermetallic compounds and alloys especially with Sn, Fe, Pb, Hg, Cu and Ni. The

remaining PGMs are formed with Bi, Te, As, Sb and S. The latter group of PGMs and compounds is of great interest and this study focused on characterising the flotation behaviour of two members of this group. Usually it is believed that the most common PGMs are the sulphides, arsenides and tellurides. The proportions and textures of these minerals vary considerably locally and regionally. Very informative surveys on PGMs and PGEs, covering all aspects of identification, composition, properties and recoveries may be found in Cabri (1981).

Table 1 and 2 list the most common Pt and Pd minerals in alphabetical order. The lists represent estimates of PGMs bearing Pt and Pd on a world basis, taking into consideration amounts produced from different deposits (Cabri, 1994). Although these lists are not intended to be highly accurate (Cabri, 1994), they do give a good account of the most common PGMs of Pt and Pd found in the world, with their ideal compositions and common substitutions in these PGMs. According to Cabri (1994) sperrylite is the most common PGM worldwide, and it can be found in every type of geological environment.

Table 1: Most common Pt minerals (Cabri, 1994).

Mineral	Ideal formula	Common substitutions
Braggite	(Pt,Pd)S	Ni
Cooperite	PtS	Pd, Ni
Isoferroplatinum	Pt_3Fe	Ru, Rh, Ir, Pd, Os, Cu, Ni
Moncheite	$PtTe_2$	Pd, Ni, Sb
Sperrylite	$PtAs_2$	Rh, Ir, Sb, S
Unknown, UG2	Pt-Cu-S	Rh, Ir, Pb

Table 2: Most common Pd minerals (Cabri, 1994).

Mineral	Ideal formula	Common substitutions
Braggite	(Pt,Pd)S	Ni
Cabriite	Pd_2SnCu	Pt, Ag, Sb
Isomertieite	$Pd_{11}As_2Sb_2$	Te
Kotulskite	PdTe	Pt, Ni, Bi, Sb
Merenskyite	$PdTe_2$	Pt, Ni, Bi, Sb
Michenerite	PdBiTe	Pt, Ni, Sb
Plumbopalladinite	Pd_3Pb_2	Ag, Cu, Bi, Sn, Sb
Polarite	Pd(Bi,Pb)	Pt
Stannopalladinite	Pd_5Sn_2Cu	Pt
Sudburyite	PdSb	Ni, Te, Bi, As
Taimyrite	$Pd_9Sn_4Cu_3$	Pt
Vysotskite	PdS	Pt, Ni

In general the dominant platinum-group minerals (with their proportions by number) of the Merensky reef are the Pt-Pd sulphides (braggite, cooperite) at 60% (braggite and cooperite at 30% each), PGE tellurides (11%) and arsenides and sperrylite (6%) (the balance is mostly PGE alloys and Au/Ag phases) (Wilson, 1998). An average distribution of PGM for the Rustenburg facies (reef associated with potholes) is: PGE sulphides, 36%, Pt- and Pd-bearing bismuthotellurides, 32%, Ru phases, 15%, PGE alloys, 7%, and PGE arsenides 7% and Au/Ag phases 3% (Wilson, 1998). Potholes comprise about 15% of the total reef area. These areas are generally highly disturbed and represent areas of reef loss. UG-2 ores contain in general more PGE – sulphides such as braggite, cooperite, malanite and laurite. In sharp contrast to this the principal platinum-group mineral phases found in the Wedza-Mimosa platinum deposit in the Great Dyke of Zimbabwe are, in order of decreasing abundance, sperrylite ($PtAs_2$), Pt- and Pd-bearing bismuthotellurides (moncheite and merenskyite, respectively) and hollingworthite (RhAsS) (Prendergast, 1990). These results were obtained from 47 precious-metal mineral grains and groups (i.e. grains close together or clearly associated), or 111 individual grains in total. In contrast to this Weiser *et al.* (1998) suggested Pt- and Pd-bearing bismuthotellurides (michenerite, merenskyite,

moncheite and kotulskite) to be the most frequent PGM whereas sperrylite is subordinate. However no indication was given of the number of samples analysed.

The proportions given in Table 3 for Mimosa Mine (data from Oberthür *et al.*, 2002a) are mostly in agreement with mineralogical investigations performed by Mintek (Van Wouw, 2000). The Mintek investigations showed that the most common PGMs are the Pt-Pd-Bi-Te minerals - including Pd-Bi-Te, Pt-Pd-Bi-Te and Pt-Bi-Te (probably michenerite, merenskyite, moncheite and kotulskite) - and sperrylite ($PtAs_2$) (Van Wouw, 2000). PGE sulpharsenides, cooperite (PtS), braggite ((Pt,Pd,Ni)S) and Au-Ag compounds were also detected (Van Wouw, 2000). Platinum occurs predominantly as $PtAs_2$, Pt-Bi-Te, Pt-Pd-Bi-Te and PGM sulpharsenides. In addition to occurring as bismuthotellurides of Pt and Pd, Pd also occurs in variable amounts in solid solution in pentlandite.

For these deposits, the Pd-bearing bismuthotellurides and to a lesser extent the Pt-bearing bismuthotellurides are the only PGMs containing appreciable amounts of palladium.

As an example, a back-scattered electron image of a sample of the concentrate of Mimosa mine is shown in Figure 1. This mineral (see white arrow) has been identified qualitatively by energy dispersive X-ray analysis (EDS-analysis) to belong to the class of Pd-Bi-Te.

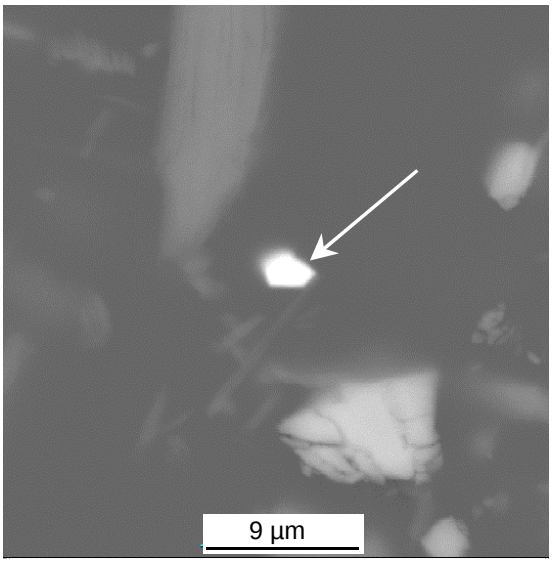

Figure 1: Back-scattered electron image (25kV) of a small liberated Pd-Bi-Te particle (arrowed) in the concentrator effluent stream of Mimosa platinum (Great Dyke, Zimbabwe).

The palladium recovery is on average about 5% lower than that of platinum (for the Mimosa Mine in Wedza-Mimosa platinum deposit) (Van Wouw, 2004). It seems, therefore, that the platinum and palladium recoveries are decoupled, which reflects differences in mineralisation. There is also a physical separation of the minerals in the ore deposit: Weiser *et al.* (1998) reported that the platinum peak lies 50-60 cm below the top of the reef profile whereas Pd peak lies 50-70 cm below the Pt peak. Similar profiles have been reported by Oberthür *et al.* (1998) for the Hartley mine (see Figure 2) and more generally on the Great Dyke (Oberthür, 2002b).

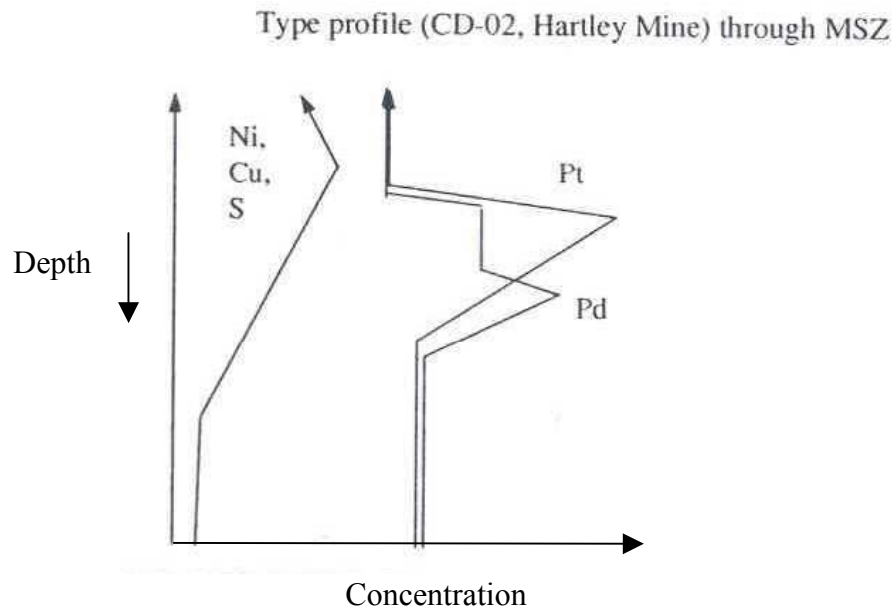

Figure 2: Schematic profile of the Main Sulphide Zone (MSZ) from the Hartley Mine (Oberthür *et al.*, 1998).

The proportions and textures of these minerals vary considerably locally and regionally. For instance the relative prevalence of Pt- and Pd-bearing bismutho-tellurides varies from 20 – 80% (See Table 3 and Appendix 1).

Table 3. The PGM proportions (proportions are by number) of a number of MSZ localities from the Great Dyke in Zimbabwe (Oberthür *et al.*, 2002a).

Locality →	Hartley	Mhondoro	Ngezi	Unki	Mimosa
PGM *(n)* → *Type* [%]	*181*	*43*	*199*	*250*	*134*
(Pt,Pd)(Bi,Te)	71	58	60	39	28
$PtAs_2$	11	9	11	28	26
(Pt,Pd)S	11	5	16	4	3
PGE-AsS	2	4	2	16	33
Pt-Fe alloys	1	11	6	-	-
Others	4	11	5	12	13
Gold *(n)*	*26*	*7*	-	*12*	-

It is evident that $PtAs_2$ and (Pt,Pd)(Bi,Te) are the principal PGM classes along the Great Dyke in Zimbabwe, except at Mimosa where the PGE-AsS phase can also be found in appreciable quantities.

According to Weiser *et al.* (1998), the grain sizes of the PGMs are very small (< 20 μm diameter) and only rarely exceed 100 μm. The PGE and Au mineral grains of the Mimosa ore sample are smaller than 10 μm diameter, compared with the 10 - 31μm of the Merensky reef (Wilson, 1998). Prendergast (1990) reported that the mean grain size of sperrylite and moncheite is ~ 1000 μm^3, and of merenskyite, ~ 400 μm^3 corresponding to 12μm and 9μm equivalent diameters of spheres. Daily plant size-assay data from Mimosa Mine in Zimbabwe indicate that the -45 μm fraction has by far the highest PGM recovery (86.5%) compared to the recovery of the +45 – 75 μm fraction of 59%. This confirms that one of the possible reasons for low recoveries is that of insufficient liberation (Van Wouw, 2004).

The platinum-group minerals of the Merensky Reef (10-30 and 50-350 μm in diameter; these two ranges are for different PGMs) are in general larger than that of

the UG-2 Reef (6-10 µm in diameter) and Great Dyke (less than 10 µm). The textural association of the PGM will greatly influence their recovery potential during flotation. Good associations of base metal sulphides with PGMs are evident for the Merensky and UG-2 reefs. In contrast to this, ores from the Great Dyke show poorer association with the base metal sulphides and a significant portion is associated with the silicate minerals (Van Wouw, 2000). Regrinding of the ore is the only option to avoid significant losses to the tailings.

According to Weiser *et al.* (1998) and Prendergast (1990) the PGMs occur as inclusions in the base-metal sulphides, as irregular grains on the sulphide-silicate (also hydrosilicate) boundary, and interstitially in silicate minerals. No statistical indication was given of the number of grains analysed (for the Mimosa Mine sample) and the occurrence distributions. All the gold grains were located within the hydrosilicates. A mineralogical investigation of the Mimosa flotation feed samples showed that the major modes of occurrence in order of decreasing abundance, are as liberated grains, at the grain contact of base-metal sulphides and silicates, and at the grain contact of silicates (Van Wouw, 2003). A very small fraction of the PGMs is locked in the base-metal sulphides. Unfortunately, only about 86 grains were analysed during this investigation. Literally hundreds of PGM grains would have to be investigated to reduce the statistical uncertainty to acceptable levels (Merkle, 2004).

In addition to this, investigations performed by Mintek on the Mimosa Mine tailings indicated that the vast majority (70%) of the (unrecovered) PGMs are Pt-Pd-bismuthotellurides. Knowing that the PGMs belong to the class, the next question that should be answered is the textural association of these minerals in the tailings sample. Unfortunately, the results of the textural association of these minerals in the tailings are rather inconclusive and contradictory. One report stated that no liberated PGMs could be found in the tailings sample. In sharp contrast to this, investigations performed on the rougher and cleaner tailings indicated the presence of large quantities of liberated PGMs. The – 45µm fraction of the rougher and cleaner tailings contained respectively 33% and 15% liberated PGMs (expressed as percentages of total number of PGMs identified). The –10µm fraction of the cleaner tailings contained as much as 80 % liberated PGMs. The PGM assemblage of both the

rougher and cleaner tailings consisted mostly of Pt-Pd-Bi-Te and sperrylite. No indication was given of the number of PGMs analysed in each case (Van Wouw, 2000).

Given the inconclusive nature of the results a follow-up mineralogical investigation was conducted on the flotation tailings of Mimosa mine (Van Wouw, 2003). The following streams were subjected to the investigations: primary rougher (PRT) and cleaner tailings (PCT), secondary rougher (SRT) and cleaner tailings (SCT) and the combined recleaner tailings (RCT). The primary rougher and cleaner tailings, and the combined recleaner tailings are reground in the secondary mill, while the secondary rougher and cleaner tailings are discarded. All of these streams contained appreciable amounts of PGMs. The lowest quantity of PGE was found in the secondary rougher tailings (0.8 - 1.0 g/t PGE) while the largest concentration was found in the primary cleaner tailings (2 – 3 g/t PGE). The quantities found in the secondary rougher and cleaner tailings are indicative of the low recoveries that are obtained. Figure 3 indicates the relative amounts of PGM found in the different tailings samples (Van Wouw, 2003). Data on the liberation are discussed below.

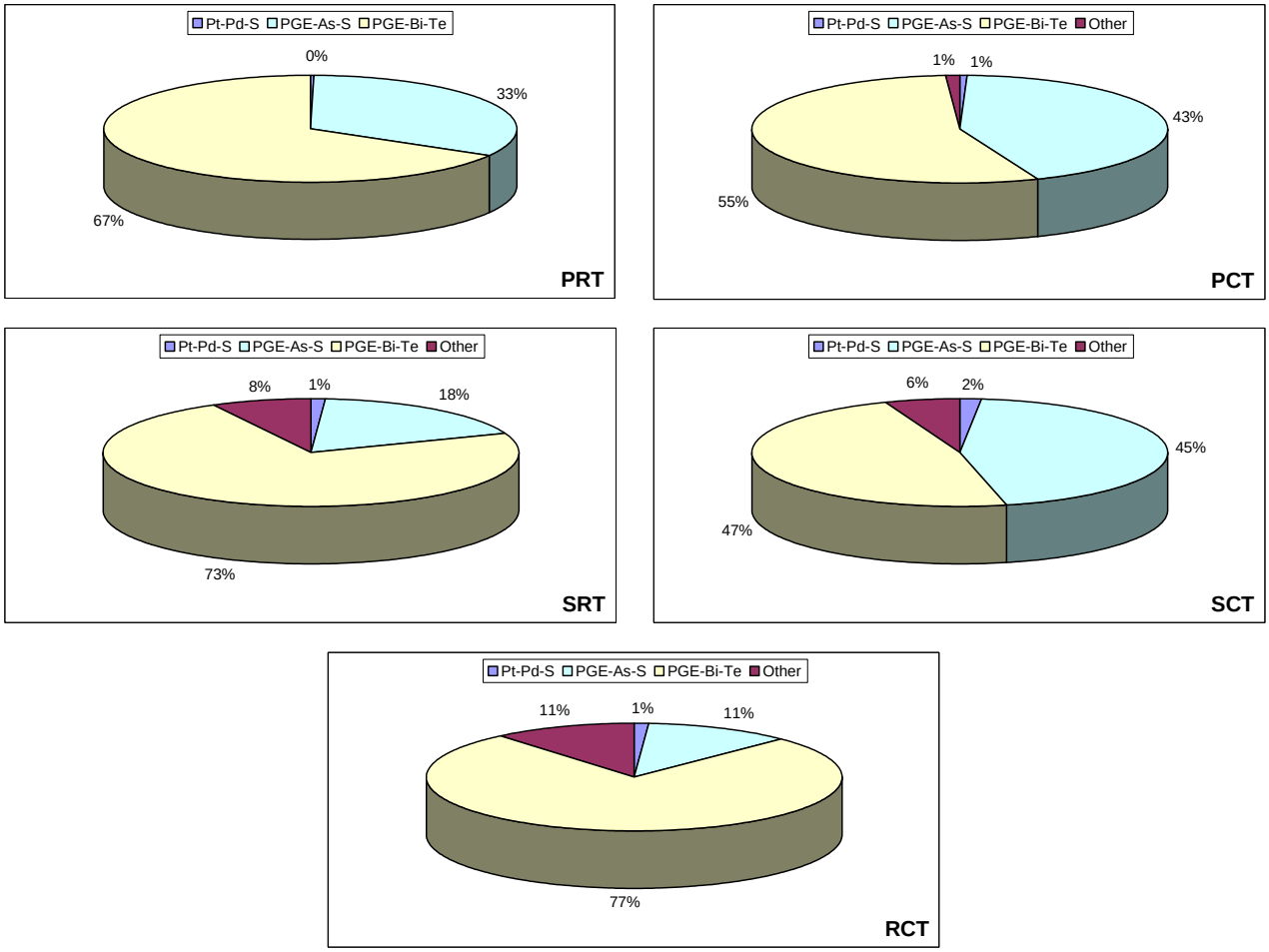

Figure 3: Relative quantities of PGMs in the tailings samples of Mimosa Mine (proportions are by number) (Van Wouw, 2003). (PRT: primary rougher tailings; PCT: primary cleaner tailings; SRT: secondary rougher tailings; SCT: secondary cleaner tailings; RCT: combined recleaner tailings; PGE-Bi-Te: PGE-bearing bismuthotellurides; PGE-As-S: PGE sulpharsenides; Pt-Pd-S: Pt-Pd sulphides)

Figure 3 indicates that the PGE-Bi-Te and PGE-As-S are by far the most representative PGM types, generally forming more than 90% of all grains found. Especially the large proportion of the Pt-Pd-Bi-Te class in all the samples investigated is noteworthy. The reason for the low flotation response of this class of mineral can be threefold:

- minerals are locked in or attached to silicates,
- minerals are liberated but are too small to be recovered
- minerals are liberated but are not responding well to the flotation stimuli.

Data on liberation are given in Figure 4, which shows the modes of occurrence of the PGMs and base metal sulphide grains. The six different modes of occurrence used in the Figure are:

- Liberated (L)
- Locked in gangue (G)
- Attached to gangue (AG)
- Associated with liberated BMS (SL)
- Associated with BMS that is locked in gangue (SAG)
- Associated with BMS that is attached to gangue (SG)

These results confirm that a large portion of the PGMs is not associated with the base metal sulphides, unlike South African ores (UG-2 and Merensky). Generally more than 70% (by volume) of the grains identified in the tailings samples occur as discrete grains (not associated with base-metal sulphide particles) (Van Wouw, 2003). This phenomenon contributes to the lower recoveries typically found in ores from the Great Dyke; small liberated PGMs are not easily recovered. Liberated PGM grains occur in all the samples, but especially the primary rougher tailings and the combined recleaner tailings contain substantial amounts of liberated PGMs. Significant association of PGMs with liberated BMS is found only in the secondary cleaner tails. These PGMs may be associated with the slow floating pyrrhotite.

The average grain size of the particles located during the search is between 3 and 4 μm in diameter (Van Wouw, 2003). The small size of these particles may be the single most important factor affecting the low recoveries of these particles; this is one of the effects studied in this project.

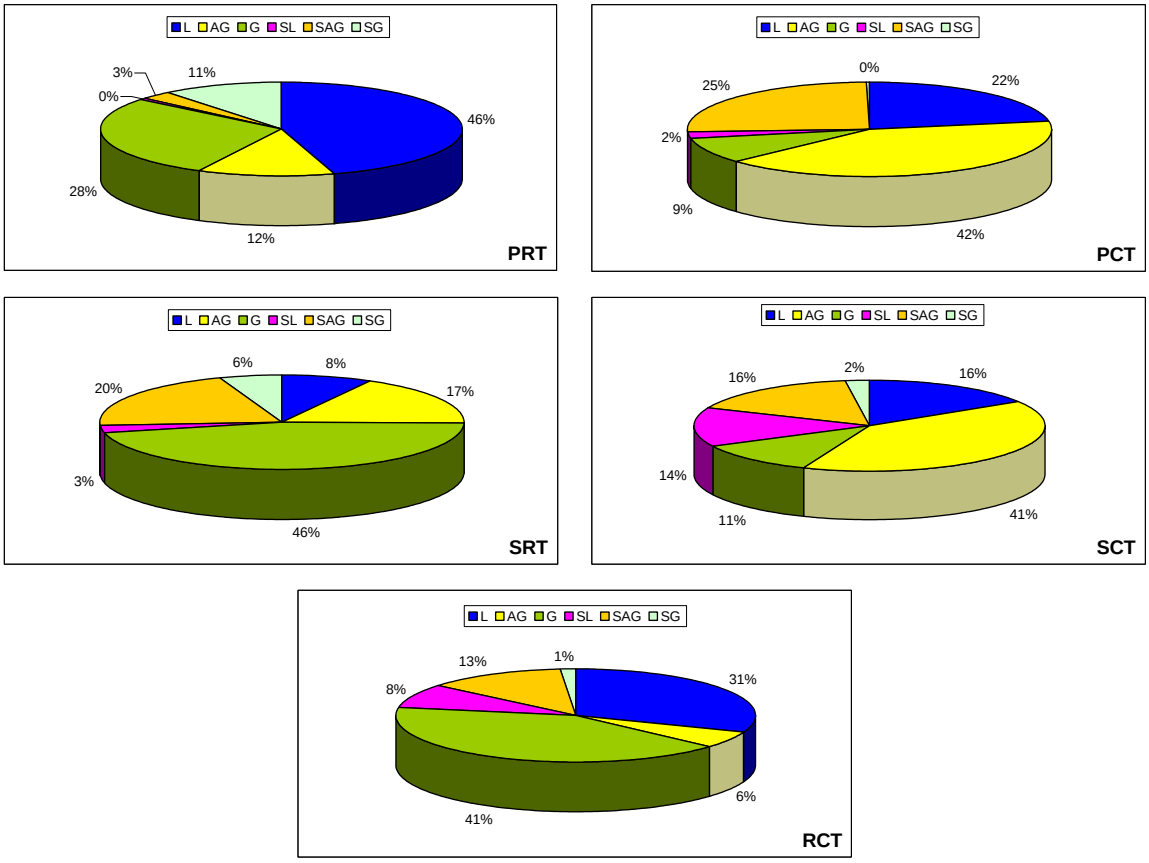

Figure 4: Modes of occurrence of PGM grains (proportions are by number) (Van Wouw, 2003) (L: liberated; G: locked in gangue; AG: attached to gangue; SL: associated with liberated BMS; SAG: associated with BMS that is locked in gangue; SG: associated with BMS that is attached to gangue).

2.1.3.2. Microprobe analysis of platinum-group minerals from Mimosa Mine (Great Dyke)

Although this has not been demonstrated, it is proposed that the Te and Bismuth contents of the Pd-Pt-Bi-Te class will affect the flotation behaviour of these particles. It is therefore important to establish the major types of PGMs in this class for the purpose of synthesis of samples used in experimental work.

Micro-probe analyses of minerals from the Great Dyke (Mimosa Mine) are shown in Figures 5-7 and in the Appendix 2. These analyses were kindly supplied by Thomas Oberthür (2002c) who has over the years studied the PGM mineralization of the Great Dyke in detail. The microprobe analyses were conducted with a Cameca Camebax

instrument (15kV, 20nA and 1μm to 2 μm spot size). Natural and synthetic standards were used for calibration.

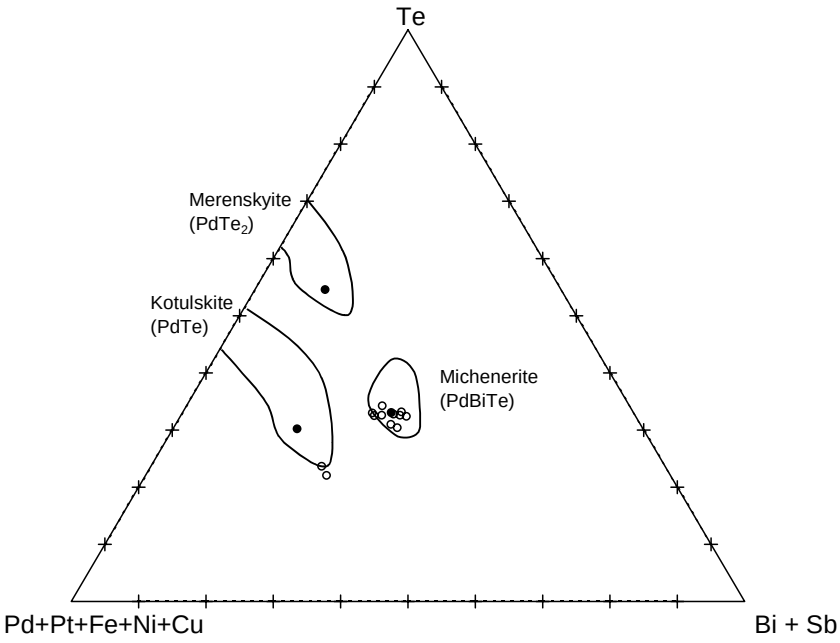

Figure 5: Composition (at %) of natural Pd-Pt-Bi-Te minerals from Mimosa Mine in the Great Dyke of Zimbabwe (Oberthür, 2002c). The curved lines enclose the compositional fields of the respective minerals reported in the literature (Wilson *et al.*, 1993).

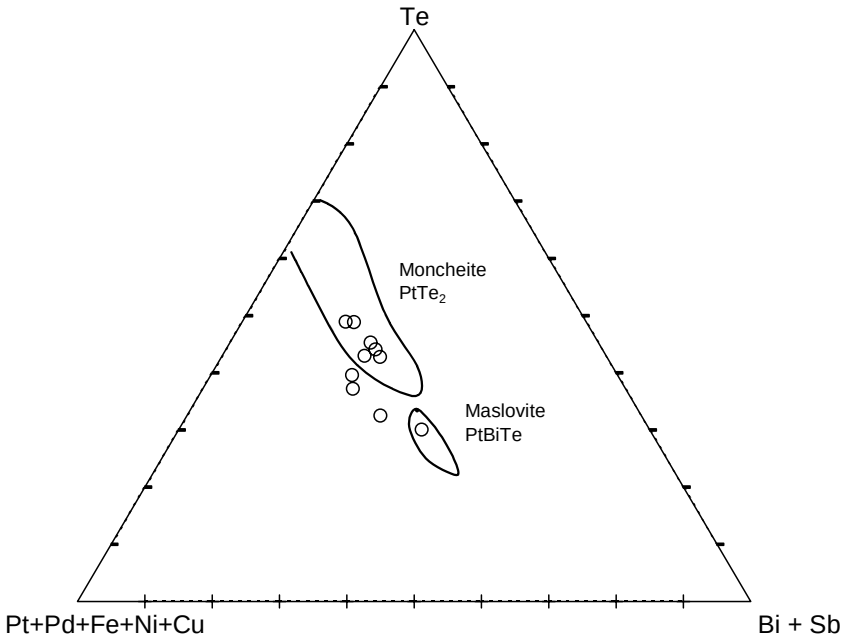

Figure 6: Composition (at %) of natural Pt-Bi-Te minerals from Mimosa Mine in the Great Dyke of Zimbabwe (Oberthür, 2002c). The curved lines enclose the compositional fields of the respective minerals reported in the literature (Wilson *et al.*, 1993).

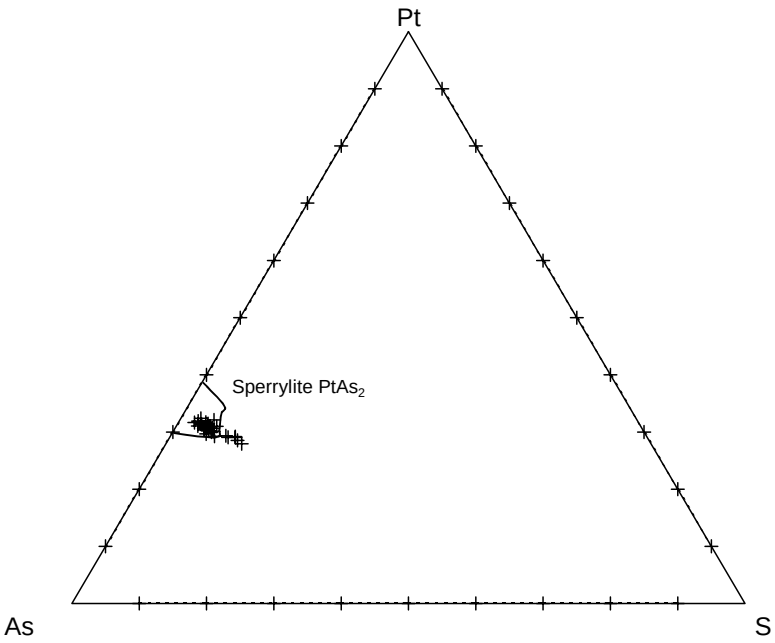

Figure 7: Composition (at%) of natural Pt-As minerals from Mimosa Mine in the Great Dyke of Zimbabwe (Oberthür, 2002c). The curved line encloses the compositional field of sperrylite reported in the literature (Wilson *et al.*, 1993).

These results clearly show that michenerite is the predominant Pd-Bi-Te mineral and moncheite the predominant Pt-Bi-Te mineral. In addition to this the microprobe results of michenerite given in Appendix 2 indicates low Pt substitution for Pd, indicating that the Pt substitution can be neglected in this instance. This simplified the synthesis procedure and the interpretation of results, which are described later in this document. In contrast to this the moncheite analysis indicate the presence of appreciable quantities of Pd (up to 6 mass percentage Pd).

2.1.3.3. Platinum-group element mineralogy of the Platreef

The PGM mineralogy of the Platreef in South Africa is very similar to that of the Great Dyke. The Platreef has recently been classified as an economically viable reef (Merkle *et al.*, 2002). Various new plants have been commissioned to exploit the reef through open pit mining. The Platreef is a variably mineralised (PGE,Ni,Cu) composite pyroxinite zone. The distribution of discrete PGMs in the Platreef tends to be erratic but by far the predominant class of PGM is the Pt-Pd-tellurides (Wilson, 1998). Unfortunately no indication of the different types of minerals

constituting the Pt-Pd-tellurides class was given. The PGE-telluride content (given as fractions of the total number of PGM grains) can vary from 80% near Drenthe in the extreme north (see map in the Appendix 3) to 90% near Tweefontein Hill, to 30% at Swartfontein (Wilson, 1998). (The map in Appendix 3 also indicates the location of future pits along the Platreef).

The three other important classes of PGMs (in order of decreasing abundance) are PGE arsenides (21%), alloys and sulphides. The PGMs are on average coarser than those found in the Merensky, UG-2 and Great Dyke ores. Interestingly enough the tellurides and arsenides are predominantly enclosed in the silicate gangue. According to Wilson (1998) up to 62% of the PGMs can be associated with the silica gangue and 38% by volume with BMSs, hence high base-metal sulphide abundances do not necessarily indicate high PGM contents. It is been found that up to 70% of the Platreef PGMs can be liberated during the milling process (Dippenaar, 2002). Given the encapsulation by silica, liberation of these particles is therefore a prerequisite for good recoveries; this confirms the importance of the flotation behaviour of the liberated minerals.

2.1.3.4. Platinum-group element mineralogy of the oxidised MSZ of the Great Dyke of Zimbabwe

Oxidised MSZ ores that occur close to the surface differ from the deeper sulphide ores in both their physical state and precious metal content. The term oxidised refers to the alteration of the pyroxinites to form hydroxy-species such as magnesium silicate hydroxides (talc) and calcium magnesium iron silicate hydroxides. The brownish colour of the ore is a result of the formation of the iron hydroxides.

The average head grade of Pt in the oxidised reserve compares well to that of the pristine (unweathered) ore. In contrast, the Pd content of the oxidised ore is significantly lower than that of the pristine ore due to the weathering of the bismuth-tellurides, which is the most important Pd-carrying PGM (Prendergast, 1990); the Pt-Pd-bismuthotellurides are susceptible to chemical dissolution. Table 4 shows the PGE distribution of the Main Sulphide Zone (MSZ) and the oxidised ores from various

localities, including the Hartley Mine, Ngezi project, Unki mine and the Old Wedza mine near Mimosa Mine (Oberthür *et al.*, 2002d).

Table 4: Summary of PGM data (Oberthür *et al.*, 2002d). The PGM proportions are by number.

	Pristine MSZ	Oxide MSZ
PGM : Number of grains → Type ↓	801	1293
(Pt,Pd)(Bi,Te) %	50.1	11.4
$PtAs_2$ (%)	19.0	57.2
(Pt,Pd,Ni)S %	8.5	28.3
Pt-Fe alloys %	2.4	3.1
PGE-sulpharsenides	11.9	-
Others %	8.7	-

In contrast to the pristine MSZ, which contains mostly (Pt,Pd)-bismuthotellurides, the oxidised reserve contains mostly of sperrylite ($PtAs_2$) grains followed by cooperite/braggite ((Pt,Pd,Ni)S). The classes of PGM found in the oxidised ore from the Great Dyke compare well with the main classes found in the typical Merensky ore. The Pt-Pd-bismuth-tellurides of the oxidised ore show incipient alteration, in contrast with the sperrylite and cooperite/braggite which show little sign of alteration (Oberthür *et al.*, 2002d): sperrylite remains the main carrier of Pt in the oxidised MSZ because it is resistant to weathering (Prendergast, 1988a). In contrast the weathering of the bismuthotellurides causes loss of palladium, resulting in a Pt/Pd ratio of 2.4 in the oxidised ore, compared with the 1.3 in the pristine ore (Oberthür *et al.*, 2002d).

The Mimosa Mine's North Hill geological complex (See Appendix 4 for a geological map) strikes over 5 km in a NNE direction at a width of about 2 km. The total ore reserves of the Far South Hill and North Hill are estimated at 14MT and 20 MT, respectively. The North Hill deposit is a well-exposed surface deposit, which dips at 3 degrees making it suitable for shallow-open cast mining with a low waste to ore ratio. Mimosa mine plans to exploit this reserve in about 2-3 years time, after the

completion of the expansion projects which are currently underway. Economic ways have to be found to exploit this reserve; there have been unsuccessful attempts previously. A thorough understanding of the mechanisms governing the flotation of the PGMs found in the oxidised reserve will be of great value to the company once it is decided to extract PGEs from this reserve.

2.2. Phases and phase relations of the platinum-group elements

PGEs frequently substitute for one another in compounds with other elements. Pt-Pd-Bi-Te minerals are no exception: 1:1 substitution between Pt and Pd (Merkle *et al.*, 1990), as well as between Te and Bi is well documented (Hoffman *et al.*, 1976). The solid solution phase fields are shown in Figures 8 and 9.

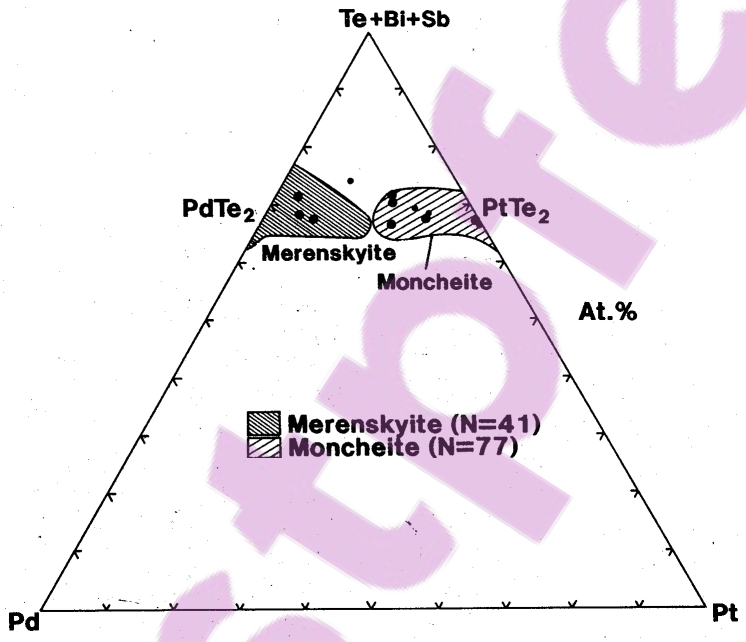

Figure 8: Pd - Pt – (Te + Bi + Sb) diagram showing the solid-solution (shaded areas) between merenskyite and moncheite (Merkle *et al.*, 1990). N represents the number of grains analysed.

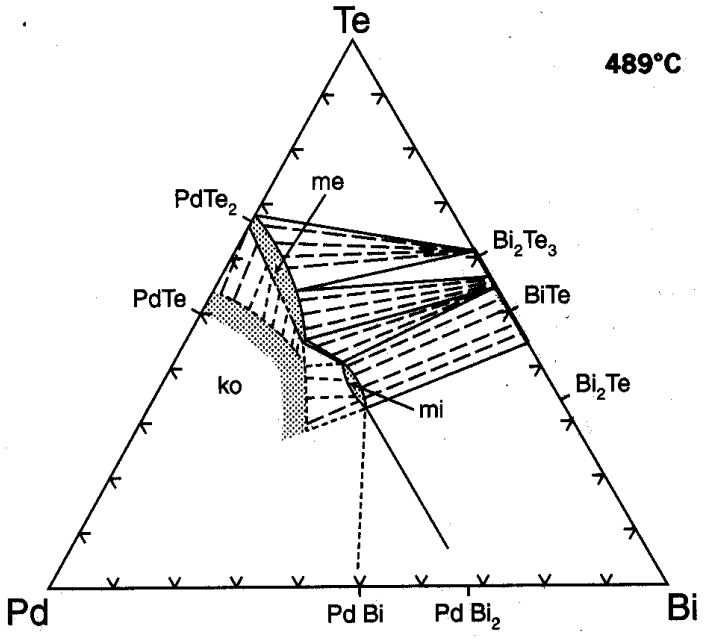

Figure 9: Synthetic phase relations (at %) in the Pd-poor portion of the system Pd-Bi-Te at 489°C. Solid solution phases are shaded; ko = kotulskite (PdTe), me = merenskyite ($PdTe_2$) and mi = michenerite (PdBiTe) (Hoffman *et al.*, 1976).

The bismuthotellurides of palladium also depart from the nominal composition: Figure 9 indicates the solid solution fields of synthetic merenskyite ($PdTe_2$) and michenerite (PdBiTe). Merenskyite shows a greater degree of Te-Bi substitution than does michenerite. The michenerite field is very narrow with the palladium content ranging from 31.3 - 33.2% (at %) (Hoffman *et al.*, 1976). Bi mainly substitutes Te in the merenskyite, but some substitution of Pd for Bi and Te is also possible. In addition to this, Pt can also substitute for Pd on a 1:1 basis. Figure 10 shows the solid solution fields of merenskyite, moncheite, michenerite and sperrylite as determined by microprobe analysis of natural minerals (Evans *et al.*, 1994) (N represents the number of analysis performed). The solid solution field of merenskyite as shown in Figure 10 (for natural minerals) is larger than that shown in Figure 9 (for synthetic minerals), in length (Bi substitution) and width (Pd or Pt substitution). Contaminants (Fe, S and Ni) are possibly responsible for the discrepancy in the width (Pd or Pt substitution) of the stability field. Cabri *et al.*(1979) suggested, albeit a quarter of a century ago, that all Pd-Te data in the literature require major revision. However, in the absence of other data the diagrams shown in Figure 10 were used to determine the alloy compositions for the work presented here.

This work concentrated on michenerite, as this is the most prevalent Pd-bearing in many of the Great Dyke deposits and prominent in the Platreef, and on sperrylite as the second most prevalent mineral class of the Great Dyke deposits

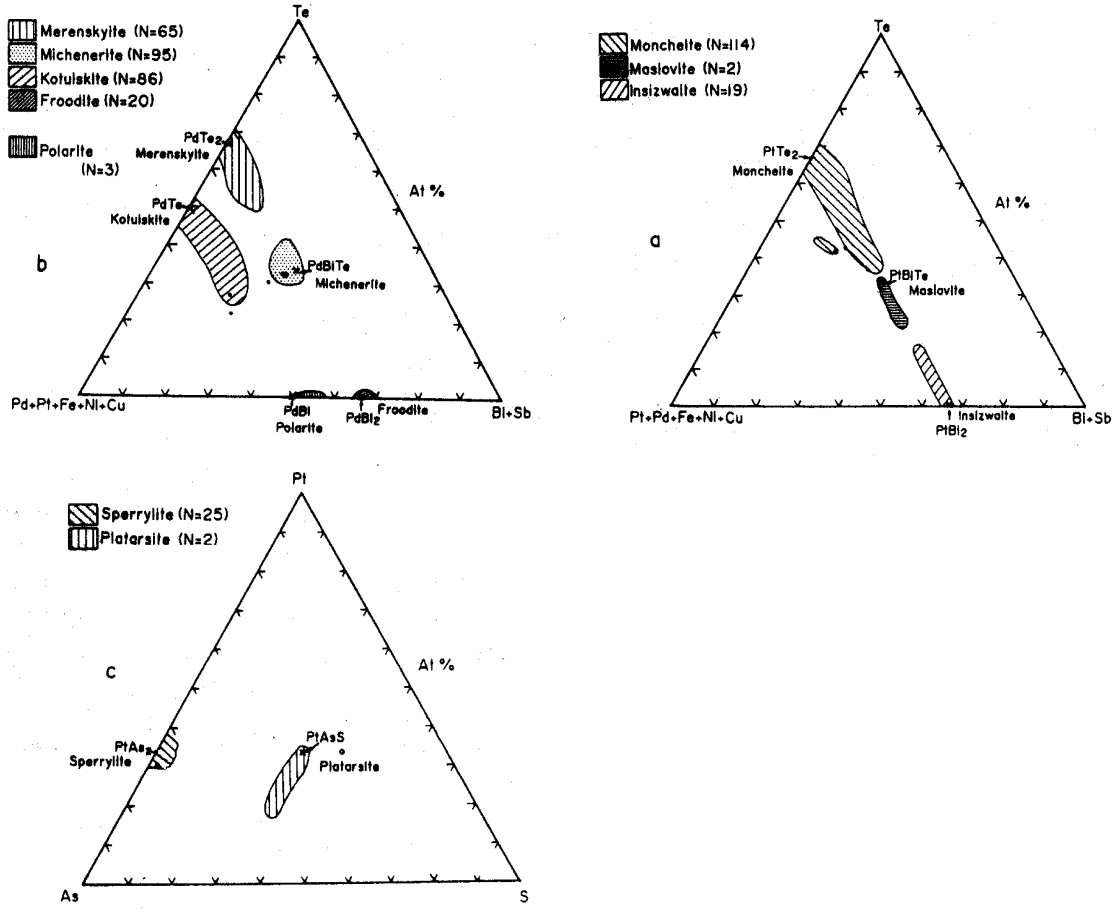

Figure 10. Ternary diagrams showing compositions of PGM phases based on the analyses of natural minerals (Wilson *et al.*, 1993).

2.3. Flotation behaviour of platinum-group minerals

Research on the flotation behaviour of selected platinum-group minerals is very limited. Volyanskii *et al.* (1985) investigated the reactions of two sulfhydryl collectors, namely potassium butyl xanthate (KX) and sodium dibutyl dithiophosphate (DTP), with sperrylite. The sperrylite contained 73.12% Pt, 0.11 % Ni, 0.04% Cu, 0.02% Fe and the balance As (in mass %). This composition of this "alloy" does not

correspond with the chemical composition of stoichiometric sperrylite, which contains 57% Pt by weight. No indication was given on whether this "sperrylite" was synthetically prepared or whether a natural sample was used. Nevertheless, the mass (1g) and particle size (+ 0.074 –0.44 mm) suggest that a synthetic sperrylite sample was employed.

The investigations were performed by employing electrochemical and spectrophotometric techniques. The organic species were extracted from the liquid phase of the pulp and were washed off the solid surface using n-hexane. The potassium butyl xanthate and sodium dibutyl dithiophosphate distribution mass balance are shown in Table 5.

Table 5: Potassium butyl xanthate and sodium dibutyl dithiophosphate distribution mass balance (Volyanskii *et al.*, 1985) (KX: potassium butyl xanthate; DTP: sodium dibutyl dithiophosphate; DTP-dithiolate: oxidised species of DTP; M[C]n: metal xanthate species; solid phase: mineral sample; liquid phase : solution containing the collector).

System	pH	Initial amount of collector (mg)		Amount (mg)								Total Sum (mg)
				Liquid phase				Solid phase				
		KX	DTP	KX	DTP	X_2	DTP-dithiolate	M[C]n	DTP	X_2	DTP-dithiolate	
Sperrylite + KX	6.9	1.03	-	0.83	-	0.03	-	0.05	-	0.12	-	1.03
	8.0	1.03	-	0.80	-	0.03	-	0.04	-	0.16	-	1.03
	10.0	1.03	-	0.63	-	0.13	-	0.06	-	0.21	-	1.03
Sperrylite + DTP	6.9	-	1.05	-	0.90	-	0.03	0.01	0.04		0.05	1.03
	8.0	-	1.05	-	0.89	-	0.03	0.01	0.04		0.05	1.03
	10.0	-	1.05	-	0.79	-	0.03	0.01	0.14		0.06	1.03

The significance of these results is that they are consistent with the formation of dixanthogen on the surface of the "sperrylite". Dixanthogen can only form if the mineral surface attains a mixed potential higher than the xanthate-dixanthogen

equilibrium value. From the results given in Table 5 it appears that the metal xanthate species (M[C]n) can also exist on the surface of the "sperrylite". The authors of this study also mentioned the formation of platinum xanthate species as a result of the interaction of the "sperrylite" with the collector. Table 5 shows further that the pH has a definite effect of adsorption properties of the dixanthogen (more alkaline pH being favourable for X_2 formation). While these are interesting results, there are several discrepancies in the paper, including apparently erroneous interpretation of UV spectra. It hence seems warranted to re-investigate the flotation behaviour of sperrylite.

Penberthy *et al.* (2000) conducted a comprehensive study on the recovery of platinum-group elements from UG-2 chromite from the Bushveld Igneous Complex. As mentioned earlier, the platinum-group mineral assemblage of the UG-2 chromite consists mainly of PGE-sulphides (predominantly, cooperite, braggite, malanite and laurite) and a significant component of alloys (such as Pt-Fe alloy) or various tellurides. The PGMs were mainly associated with the base metal sulphides (>74 %), occurring either within or at the sulphide-gangue grain boundary. Fifty percent of the PGMs were liberated during milling. Most of the PGMs associated with the sulphides reported to the concentrate during flotation, while PGMs associated with the silicates were not recovered. The response of the liberated PGMs to the flotation stimulus was difficult to investigate due to their small size (< 10 μm). Most of the liberated grains did float, albeit at a lower rate than the base metal sulphides. In general the ranking of the PGM flotation rate was in decreasing order braggite, cooperite, malanite, ferroplatinum and laurite (See Figure 11). No indication was given of the rate at which sperrylite and (Pt,Pd)-bismuthotellurides float.

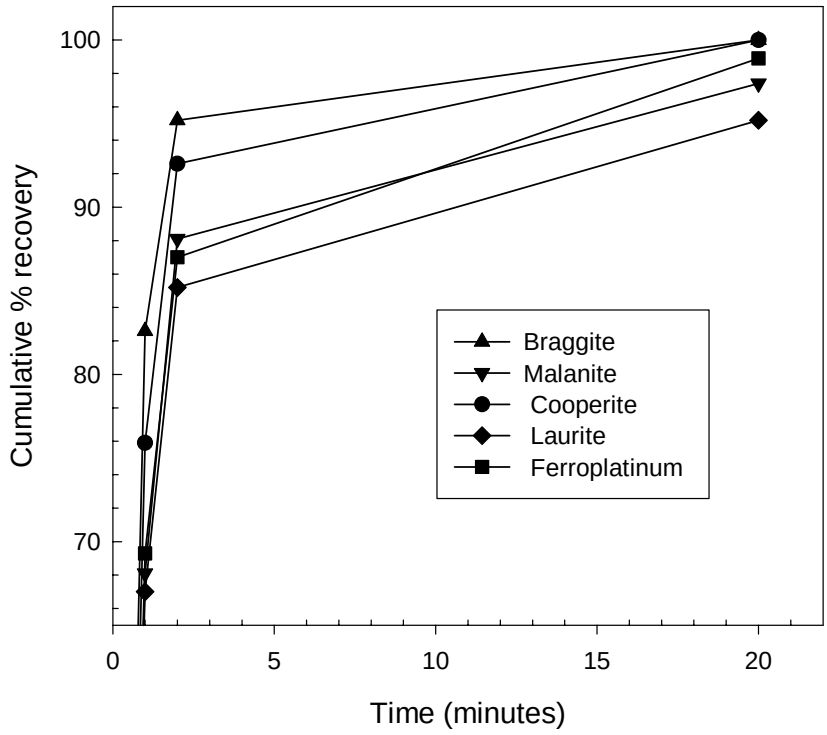

Figure 11: The recovery for selected liberated PGMs (redrawn from Penberthy *et al.*, 2000) in batch flotation tests.

According to staff of the Anglo Platinum Research Centre (ARC) (ARC, 2002), based on their experience, some physical characteristics and the recovery of the different classes of PGM can be summarised as follows:

Table 6: Some physical characteristics and the recovery behaviour of different classes of PGM (ARC, 2002).

Class	Size	Density	Gravity recovery	Flotation recovery
Sulphides	Often coarse	High	Good	Good
Tellurides	Variable	Low	Poor	Poor
Arsenides	Variable	Medium	Good	Good
Alloys	Often coarse	Very high	Excellent	Variable
Oxides	Fine	Low	Very poor	Very poor

The inherent assumption of Table 6 is that all the minerals are liberated. This table underlines the importance of a good understanding of the flotation behaviour of the tellurides with the main aim to optimise the recovery of these minerals.

2.3.1. Platinum-group element recovery from the oxidised MSZ of the Great Dyke of Zimbabwe

Sperrylite is the principal platinum carrier in the oxidised MSZ of Mimosa mine (formerly known as Wedza mine) and previous attempts, which included flotation and gravity concentration, did not achieve better than 50% Pt recovery (Prendergast, 1988b). Metallurgical test work performed by Zimplats on the their oxidised ores only achieved recoveries of between 15-30% (Oberthür *et al.*, 2002d). Evans (1994) reported that PGE-bearing minerals in the weathered ore are predominantly platinum-iron alloys of variable composition containing variable amounts of bismuth, palladium and tellurium. Evans *et al.* (1994) suggested that the bismuthotellurides and Pt-Pd-sulphides have been altered *in situ* by the leaching of the sulphur, tellurium and bismuth. This hypothesis was not supported by Stribrny *et al*. (2000). However, Oberthür *et al.* (2002d) have shown the existence of ill defined "PGE-oxides or hydroxides " around altered (Pt,Pd)-bismuthotellurides. Preliminary results show the loss of Te and Bi and the increase in Pt and Pd contents from the oxides or hydroxides. The fact that these phases contain oxygen was verified by micro-probe analysis and corresponds to the work published by Evans *et al.* (2000). In addition to the formation of these PGE oxides or hydroxides, it was suggested by Stribrny *et al.* (2000) and Oberthür (2002d) that the PGEs are dispersed in the iron hydroxides or smectites. The weathering of the sulphides to goethite or limonite minerals, and the alteration of the pyroxenites, prevent the efficient concentration of precious metals by sulphide flotation (Prendergast, 1990). The textural association of the PGMs with the altered sulphides is not well known at this stage, but electron micro-probe investigations have revealed that the PGMs in the oxidised deposit are located at the goethite-limonite patches after the interstitial sulphides (Evans *et al.*, 1994; Oberthür, 2002b).

The possibility of applying an oxidic float to recover the altered sulphides is currently being tested at General Metallurgical Research and Services (GMRS). Prendergast

(1988) proposed the recovery of the PGM by fine grinding and flotation by altering the flotation conditions.

2.4. Chemical stability of Michenerite

All three elements in Michenerite (PdBiTe) are fairly noble, concerning the considerable overlap of their stability areas with that of water (See Figures 12 - 14) (Pourbaix, 1974). All the relevant reaction equations can be found in Pourbaix (1974). Palladium is thermodynamically stable in the presence of aqueous solutions free from strongly oxidising conditions at low pH values. Both Te and Bi oxidise in the bismuth-telluride minerals despite the fact that these elements do not oxidise readily, in their pure state, in air. Aerated water attacks bismuth to form Bi_2O_3, which is in turn very soluble in dilute acids. TeO_2 is formed in aerated water and forms a non-protective film if the TeO_2 is freshly precipitated. The kinetics of the oxidation in solution is not very well understood, but if oxidation proceeds at a high enough rate, oxidation could impact negatively on the flotation process.

The majority of sulphide flotation plants operate at pulp potentials (using air as carrier gas) between 200 mV (SHE) and 300 mV (SHE) (Ralston, 1991). Ores from the Merensky and UG2 reefs have a natural buffer capacity ensuring pH levels between 8 and 9 (Buswell *et al*., 2002; Ekmekçi et al., 2003). Considering the typical values of the pulp potential and pH (assuming the same values for the Great Dyke of Zimbabwe) Te and Bi are likely to be oxidised in industrial flotation circuits if the oxidation proceeds at a higher rate than competing reactions (possibly the oxidation of the collector).

Elvy *et al.* (1996) reported the incongruent oxidation (the migration of some metal atoms to the surface to form an overlayer of a metal-oxygen species) of minerals in the Pd-Te-Bi system leading to the formation of layer of tellurium and/or bismuth oxide covering the palladium-rich substrate The reactivity of the minerals increased in the order of: PdTe < PdTeBi < PdBi. This is in the same order as the reactivities of Pd, Te and Bi in the pure form. This implies that merenskyite should be more resistant

to oxidation than michenerite, since merenskyite has the higher tellurium content and lower bismuth content.

Figures 12, 13 and 14 represent the potential-pH diagrams respectively of bismuth, palladium and tellurium in water.

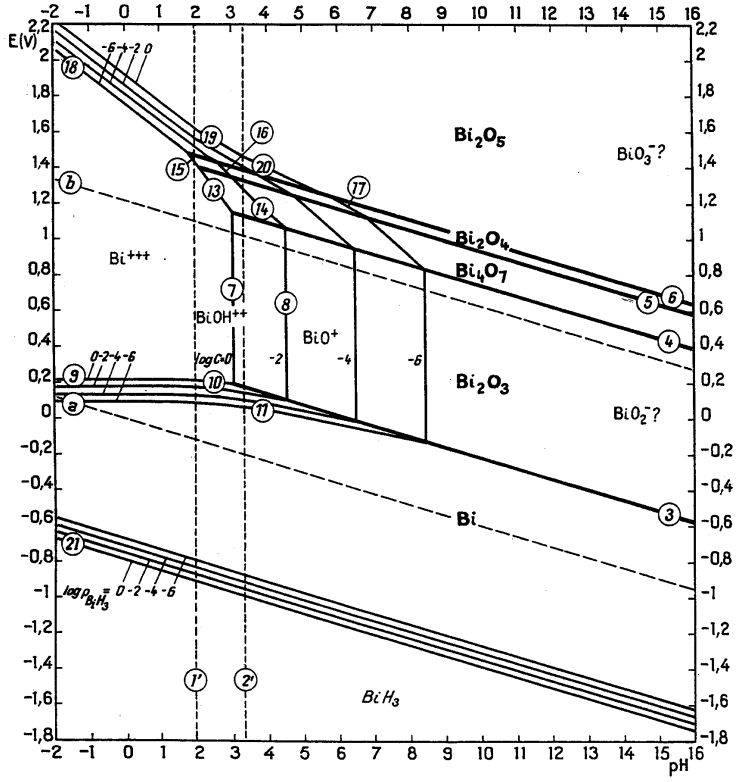

Figure 12: Potential-pH equilibrium diagram for the system bismuth-water for molar concentrations of dissolved species of 1M, 10^{-2}M, 10^{-4}M and 10^{-6}M, at 25°C (Pourbaix, 1974).

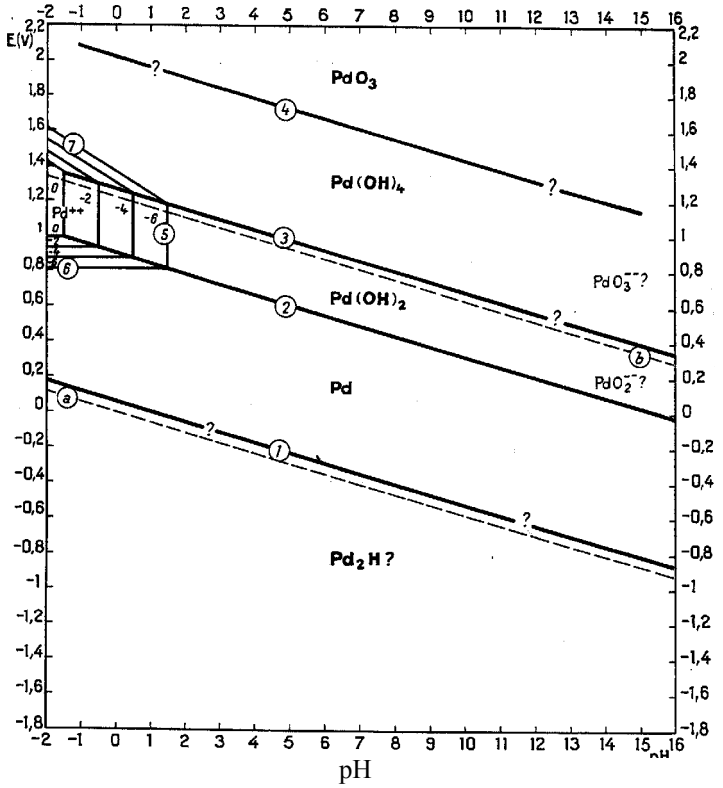

Figure 13: Potential-pH equilibrium diagram for the system palladium-water for molar concentrations of dissolved species of 1M, 10^{-2}M, 10^{-4}M and 10^{-6}M, at 25°C (Pourbaix, 1974).

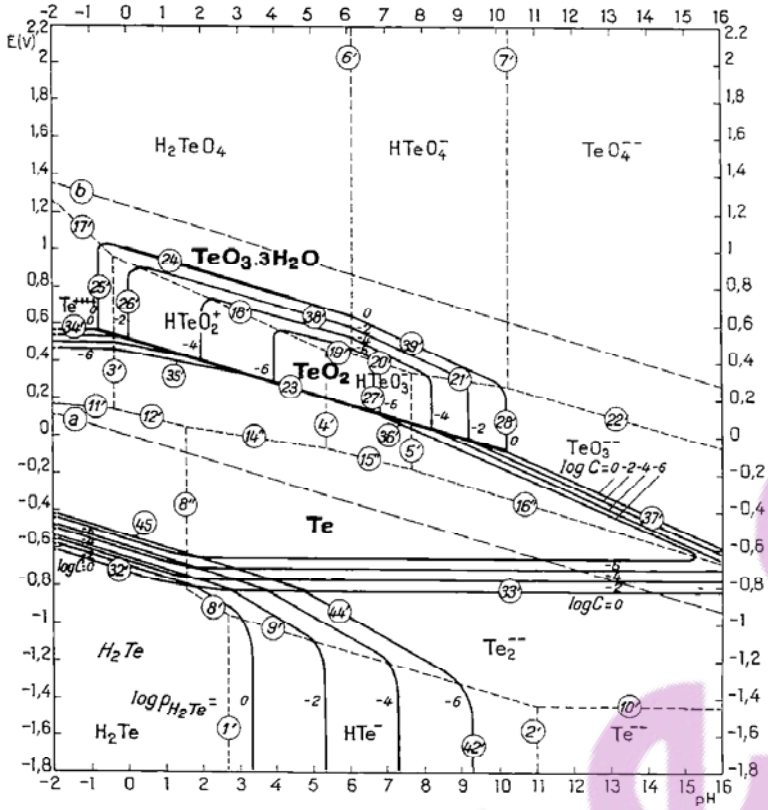

Figure 14: Potential-pH equilibrium diagram for the system tellurium-water for molar concentrations of dissolved species of 1M, 10^{-2}M, 10^{-4}M and 10^{-6}M, at 25°C (Pourbaix, 1974).

Investigations performed by Peyerl (1983) on the mode of occurrence of platinum-group minerals in the Merensky reef and UG-2 chromitite, revealed bismuthotellurides to be the PGM which was least resistant to chemical attack by HNO_3. None of braggitte, cooperite, sperrylite, laurite or platinum-iron alloys showed any chemical attack after been exposed to diluted and concentrated boiling HNO_3 for 10 hours. The bismuthotellurides showed dissolution behaviour similar to that of the base metal sulphides. The issue on the stability of bismuthotellurides in aqueous solutions must be investigated in order to predict their response in milling and flotation circuits. This issue was not studied in any detail in the present work, which concentrated on unoxidised samples.

2.5. Interaction of Thiols with metals

It was proposed that the interaction of thiols with metals (platinum, gold and copper) involves an electrochemical mechanism, with anodic oxidation of the collector supported by a cathodic (reduction) reaction (e.g. reduction of oxygen) (Woods *et al.*, 1974):

$$2X^- = X_2 + 2e^- \quad (1)$$

$$0.5O_{2(ads)} + H_2O + 2e^- = 2OH^- \quad (2)$$

In these equations X^- indicates the xanthate ion and X_2 dixanthogen. Woods *et al.* (1974) further proposed that reaction 1 proceeds via an initial chemisorption step and that the multi-layers of dixanthogen product are bound to the chemisorbed monolayer xanthate by the interaction of the hydrocarbon parts of the molecule. The main experimental advantage of the electrochemical nature of these reactions is that the reactions can be tracked by electrochemical techniques (potentiodynamic measurements and impedance measurements).

The possible oxidation of dithiocarbonate collectors was hence studied through potentiodynamic measurements in the present work; anodic and cathodic polarization diagrams were drawn for synthetic Pd-Bi-Te and $PtAs_2$ working electrodes, to investigate the anodic oxidation and oxygen reduction reactions. The possibility of the formation of a surface layer of the collector was determined through impedance measurements. Impedance measurements allow *in situ* detection of the formation of surface layers (of collector), by a decrease in the circuit capacitance.

Impedance measurements are based on the modelling of an electrode in solution as an electronic circuit containing resistors, capacitors and inductors. A simplified version of such a circuit is shown in Figure 15. The equivalent circuit contains a resistor in series with a parallel circuit containing a capacitor and resistor.

The capacitance effect is a result of the double layer charging effect (C_D) and possible surface layers (C_s). The electrode capacitance is the series combination of the two effects as shown below

$$\frac{1}{C} = \frac{1}{C_D} + \frac{1}{C_s} \qquad (3)$$

As shown by equation (3), formation of a surface layer (with a non-zero value of C_s) will cause the electrode capacitance to decrease. In this way, the formation of surface layers can be detected when the mineral is anodically polarized in the presence of xanthate ions.

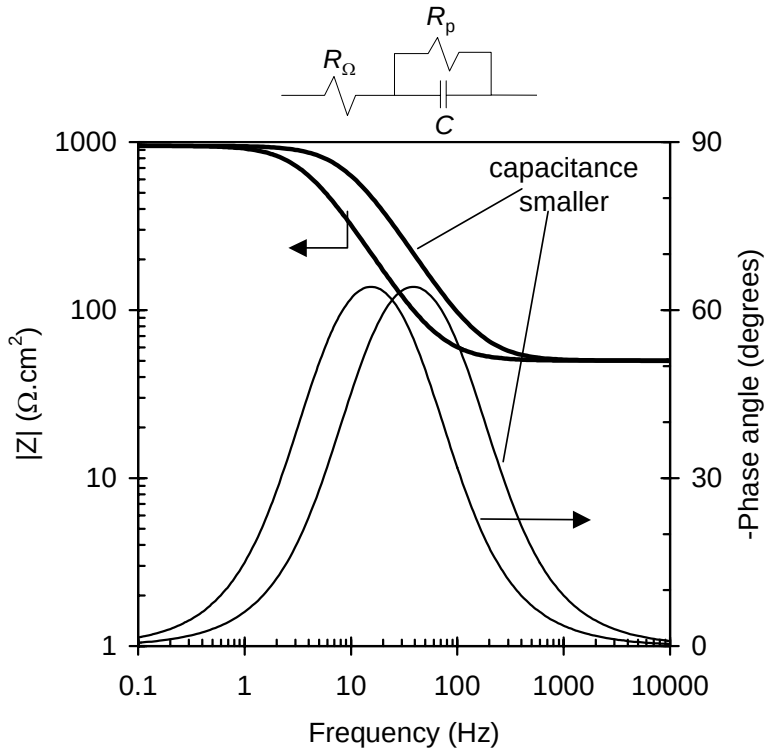

Figure 15: Bode plot of the impedance of a metallic electrode in a solution (with an equivalent circuit as shown). The effect of a decrease in capacitance is shown in the Bode plot. Drawn for R_Ω = 50 Ω.cm^2, R_p = 900Ω.cm^2 and C = 50 μF/cm^2 or 20 μF/cm^2.

3. Research Problem and Objectives

As stated in Chapter 2, the Great Dyke platinum reserve (in Zimbabwe) and the Platreef (in the Bushveld Complex in South Africa) have recently become major sources of platinum-group minerals (PGMs). These platinum reserves are altered, and difficult to process, requiring innovative beneficiation technologies to recover PGMs. As a result of weathering these ores contain high levels of talc (typical levels above 10% for the Great Dyke compared to less than 1% for the Merensky reef) and serpentine (typical levels of 60% for the Platreef). High reagent consumption and lower recoveries – compared with ores from the Merensky and UG-2 reefs – result. In addition, the Great Dyke and Platreef show poorer association of PGMs with base metal sulphides; larger portions of the PGMs belong to the Pd-Pt-Bi-Te, PGE-S-As and PGE-alloy classes (Van Wouw, 2003). Mineralogical investigations (QemSCAN) on all effluent flotation streams of Mimosa mine (located along the Great Dyke) indicated the presence of appreciable amounts of unrecovered platinum group minerals (PGMs) (Van Wouw, 2003). Most of the liberated PGMs found in the effluent streams belonged to the Pt-Pd-Bi-Te class. There are similar practical indications of poor recovery of PGE-bismuth tellurides from the Platreef (Dippenaar, 2002).

The idea which was tested in the experimental work was that poor recovery of liberated PGE bismuthotellurides could be caused by surface chemical effects (lack of interaction with the collector), or physical effects (lack of collision with or attachement to bubbles, or poor stability of attachment). The experimental work hence had the following specific aims:

- To determine the electrochemical interaction of ethyl xanthate with synthetic Pd-Bi-Te and $PtAs_2$ minerals, with impedance measurements, and voltammetry.
- To identify species on the surface by employing *in situ* Raman spectroscopy.
- To determine the potential dependence of the hydrophobicity of the mineral surface with electrochemically controlled contact angle measurements.
- To compare the collector interaction results of $PtAs_2$ (typical fast floater and very abundant in platinum ores) with that of Pd-Bi-Te.

- To quantify the actual flotation rate of synthetic Pd-Bi-Te by performing microflotation tests.
- To predict the possible effect of particle size on the flotation rate constant of Pd-Bi-Te.

4. Experimental procedure

This chapter gives brief descriptions of the experimental methods which were used in the present study.

4.1. X-ray diffraction and Scanning Electron Microscopy

A Siemens D-501 X-ray diffraction (XRD) instrument was used to identify the crystalline phases in the synthetically prepared minerals (Pd-Bi-Te and $PtAs_2$) and the natural minerals (pyrrhotite, chalcopyrite and pyrite). Each sample was milled for 10 minutes in a swing mill and subsequently pressed into Siemens sample holders (1 – 2 grams of sample) using a glass slide. The specifications on the XRD instrument and settings are shown in Table 7.

Table 7: Instrument and data collection parameters.

Instrument	Siemens D-501
Radiation	Cu *K*α
Temperature	25°C
Specimen	Flat-plate rotating (30 rpm)
Power setting	40 kV, 40 mA
Soller slits	2° (diffracted beam side)
Divergence slits	1°
Receiving slits	0.05°
Monochromator	Secondary, graphite
Detector	Scintillation counter
Range of 2θ	5 – 80° 2θ
Step width	0.04 ° 2θ
Time per step	1.5s

The microstructures of the synthetic and natural mineral samples and samples from flotation concentrates were investigated by employing a scanning electron microscope

(SEM) (JSM-6300). All the mineral and flotation concentrate samples were polished using a 0.05μm Micropolish Alumina-B suspension and chemically analysed by EDX (energy dispersive X-ray analysis). The non-metallic samples were mounted in epoxy resin (impregnated under vacuum) and gold coated by sputtering. The different phases were identified by examining the sample with back-scattered electron imaging using a Centaurus back-scatter detector. The analyses were performed using a Voyager analysis system using a Si (Li) (lithium-drifted silicon) detector with a Norvar window analysing X-rays produced at 25kV acceleration voltage with a working distance of 10mm, using 100 seconds of analysis time.

4.2. Synthesis of selected platinum group minerals

In any fundamental study of a surface the starting material must be clearly defined and as free from impurities as possible. The draw-back of using synthetic materials is the uncertainty about the correspondence between the synthetic crystal and the natural mineral. This is a concern for especially the PGMs considering the host of impurities found in PGMs such as Fe, Ni and Cu. However, the very small size (less than 10 μm in the case of the Great Dyke) and scarcity of individual grains contribute to the complexity of studying fundamental interactions. It was therefore decided to perform fundamental work (electrochemical investigation, *in situ* Raman spectroscopy and electrochemically-controlled contact angle measurements) on synthetic minerals. Contact angle measurements (using Equilibrium Capillary Pressure techniques) could be possible on natural grains, but too many hand-picked grains would be required to form a packed bed. The main advantage of synthesizing these minerals in bulk is the possibility of performing microflotation tests to evaluate the performance of different reagent suites. The minimum particle size was fixed by the constraints of contact angle measurements, which required mineral particles with exposed diameters of 6-10 mm. (Smaller diameters would have been sufficient for electrochemical and Raman investigations, but the same working electrodes – large enough for contact angle measurements – were used in all three types of tests.)

Sperrylite ($PtAs_2$), and Pd-bearing bismuthotelluride (michenerite) were synthetically prepared since – as discussed in Chapter 2 – these are the most abundant PGMs in the orebody which is the subject of the current study.
Each material was synthesised by reacting stoichiometric quantities (accurately weighed to 3 decimal places) of its constituent elements (total about 1g) in an evacuated silica tube. Palladium wire (diameter 0.5mm, 99.99+%), platinum wire (diameter 1.0 mm, 99.99+%), tellurium lump (99.999+%), bismuth rod (99.997%) and arsenic lump (99.9999%) were used. All these constituents were supplied by Goodfellow.

The michinerite (equimolar mixtures of Pd, Bi and Te) was heated to a sufficiently high temperature (700^{o}C) to melt the Bi and Te and to dissolve the Pd before the final heat treatment in the muffle furnace was applied. In the first step, the Pd-Bi-Te was held at 700^{o}C for 20 hours followed by slow cooling over 6 hours. Despite using the same procedure as been described by Evans *et al.* (1996), homogeneity of the synthetically prepared sample was not achieved. Back-scattered electron images showed the presence of three phases. Energy dispersive X-ray analysis (EDS) performed on the phases indicated the presence of a Bi-rich phase, Pd-rich phase and that of a phase with a composition approximating that of the target phase (that is, equimolar Pd-Bi-Te). The same heat treatment was repeated on the same sample in an attempt to produce a single solid solution phase. The microstructure that was obtained resembles that of the previous back-scattered electron image (three phases were present). It was concluded that a peritectic transformation reaction had to take place to consume the Bi-rich (liquid) and Pd-rich (solid) phases. The rate of this reaction will be greatly enhanced if a very fine microstructure is obtained before the onset of the final heat treatment stage at 480^{o}C. This was accomplished by heating the sample to the required melting temperature followed by cooling in still air for a few seconds before being subjected to heat treatment at 480^{o}C.

It can clearly be seen from the back-scattered electron image shown in Figure 16 that the microstructure after the 480^{o}C heat treatment is much more homogeneous with only two phases clearly visible. EDS analysis performed on the light phase indicated this phase to be rich in bismuth. Following the positive outcome of this heat treatment the sample was treated for another 100 hours at 480^{o}C to ensure phase integrity and

homogeneity. A fully homogeneous microstructure was only obtained by employing the heat treatment at 480°C for up to 60 days. The electron back-scattered image and XRD spectra of the microstructure are shown in Figure 17 and in Appendices 5 and 6. To summarise, samples used for the microflotation tests were treated for 60 days at 480°C, while the samples for the rest of the test work were treated for 100 hours at the same temperature.

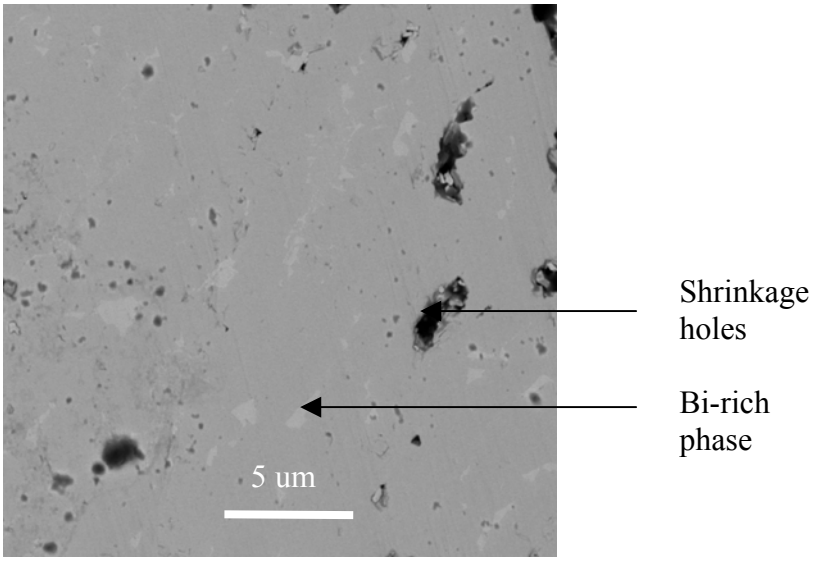

Figure 16: Back-scattered electron micrograph showing the two most prominent phases of the synthetically prepared michenerite (Pd-Bi-Te) heated to 700°C, followed by cooling in still air and heat treatment at 480°C for 100 hours. Accelerating voltage 25kV.

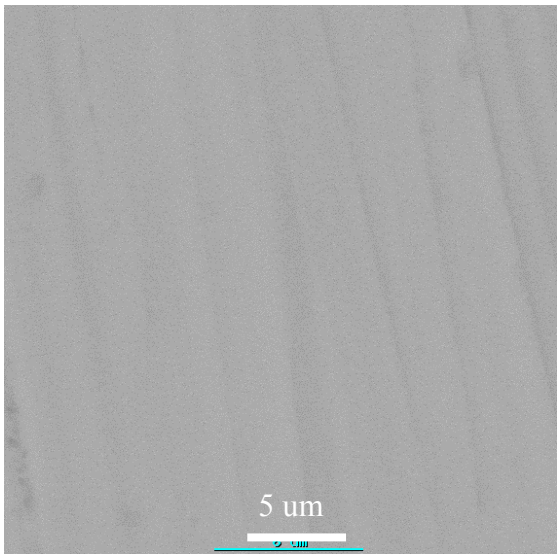

Figure 17: Back-scattered electron micrograph of the synthetically prepared michenerite (Pd-Bi-Te) heat-treated at 480°C for 60 days. Accelerating voltage 25kV.

Sperrylite ($PtAs_2$) was prepared by heating stoichiometric amounts of the constituents to 800°C in a sealed silica ampoule (1 gram total sample mass). The ampoule could not be heated to a high enough temperature to melt the contents because of concern around elevated partial pressure of arsenic at high temperatures. (The melting point of pure arsenic is 817°C [at 28 atm] and the sublimation point is 613°C [Weast, 1982]). The constituents were held for 6 hours at 800°C before being slowly cooled to room temperature over a period of 5 hours. The synthetic sperrylite was subsequently investigated by electron-back scattering and XRD analysis to verify the integrity and identity of the phase sought. A back-scattered electron image and XRD pattern of the synthetic sperrylite are shown in Figure 18 and Appendix 7, respectively. These examinations provided no evidence of minor concentrations of other phases.

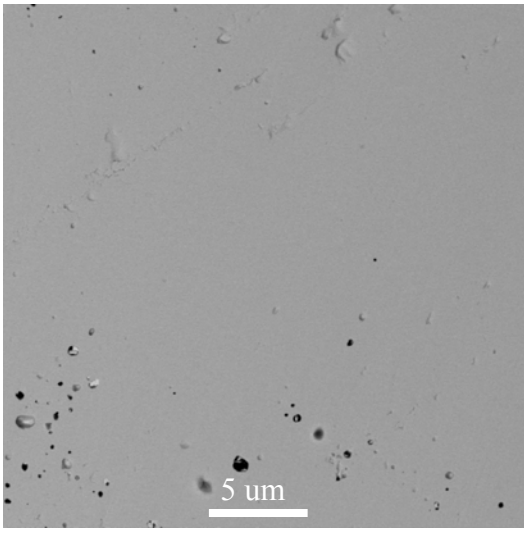

Figure 18: Back-scattered electron micrograph showing the single solution phase of the synthetically prepared sperrylite. Accelerating voltage 25kV.

4.3. Electrochemical measurements

A conventional electrochemical cell with a three-electrode system was used. Potentials were measured against a Ag/AgCl reference electrode filled with saturated KCl, which has a potential of +0.20V against the standard hydrogen electrode. The PGM crystals were mounted in resin and electrical contact was achieved between the contactor shaft and the mineral by employing a spring. The surface area of the Pd-Bi-Te and the $PtAs_2$ sample was 0.12 cm^2 and 0.14 cm^2, respectively. Two platinum wire electrodes (10 cm in length) were placed in glass tubes closed with porous glass discs at their ends to serve as counter electrodes. The platinum counter electrodes were placed at equal distances (3 centimetres) from the working electrode. The voltammograms were constructed with a Schlumberger 1287 potentiostat and the potentiostat was interfaced with a Schlumberger 1260 frequency response analyzer for the impedance measurements. All experiments were conducted at 25°C (± 1°C). Sodium borate at a concentration of 0.05M $Na_2B_4O_7$ was used to buffer the solution at a pH value of 9.3.

A large ohmic resistance between the working and reference electrode is undesirable because it masks the effective overpotential applied to the system. As a result the *IR* effects need to be evaluated to determine whether they affect the polarisation

measurements. High-frequency impedance spectroscopy (see Chapter 5 for more detail) was used to calculate the solution resistance whereas low-frequency impedance measurements resulted in the sum of the solution and polarisation resistances. The solution resistance was subtracted from the impedance value obtained at the low frequency measurements yielding the polarisation resistance of the system. A typical solution resistance of 200Ω.cm^2 was measured for a Pd-Bi-Te electrode polarised at 0.3V (SHE) in a 0.05 M $Na_2B_4O_7$ solution containing 1 x 10^{-3} M potassium ethyl xanthate (see figure 25); the relatively low value of the solution resistance should not affect the polarisation measurements significantly since this value is much lower than the polarisation resistance (> 10^4 Ω.cm^2).

Distilled water with a final resistivity of 18MΩ.cm was used to prepare solutions. Prior to measurements, the solution was de-aerated for 2 hours with argon gas (99.999%), from which oxygen was removed by passing the gas over zirconia turnings at 600^{o}C. The solution was replaced between experimental runs to avoid contamination. Purified potassium ethyl xanthate (KEX) was used in all the experiments. The xanthate was purified on a regular basis by dissolving in acetone, filtering the solids and subsequent evaporation of the acetone in a vacuum (De Wet *et al*., 1996). The xanthate solutions were prepared minutes prior to the commencement of the experimental run to avoid decomposition. The PGM working electrode was freshly prepared before each experiment by wet grinding to 2400 grit silicon carbide paper followed by wet polishing using a 0.05μm Micropolish Alumina-B suspension. Distilled water with a final resistivity of 18MΩ.cm was used to make up the polishing suspension. This polishing treatment gave reproducible results. After polishing the samples were thoroughly washed with distilled water and immediately transferred to the electrochemical cell for measurements.

Figure 19 shows the reduction halfcycles on a Pt-electrode after different gas purging times, when using de-aerated argon gas for oxygen removal. Clearly a longer de-aeration period results in lower oxygen reduction currents, which is the desired effect when performing anodic polarisation measurements. This effect of the de-aeration period on the anodic polarisation measurement was confirmed by measurements on Pd-Bi-Te for the dearation periods shown in figure 19.

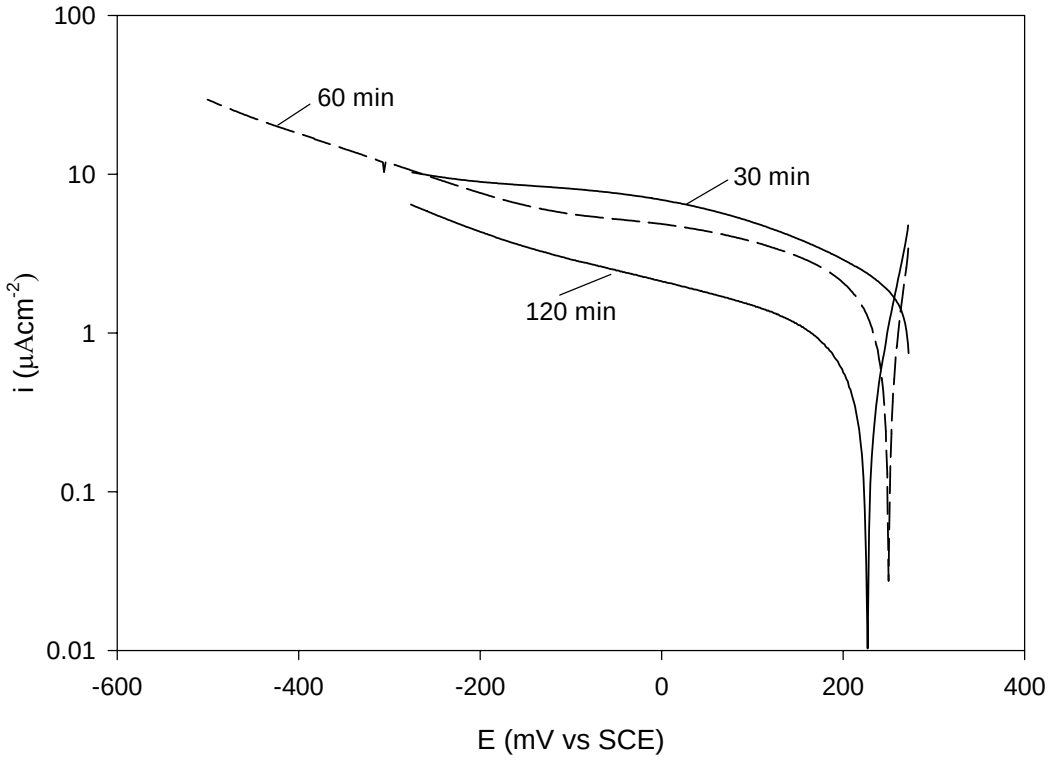

Figure 19: Reduction of oxygen on platinum for different de-aeration periods in a 0.05 M $Na_2B_4O_7$ solution at 25°C. Potential sweep carried out at 1mV/s.

The anodic polarization curve for the 120-minute de-aeration period showed the most detail (the least interference from cathodic reactions), and hence all solutions were de-aerated for 2 hours before electrochemical measurements.

4.4. Raman spectroscopy

4.4.1. Introduction

In 1928, Professor C.V. Raman discovered the inelastic scattering of light by which a molecule scatters a single photon which loses energy in the process. The difference between the higher energy state produced by the incident beam and the photon of lower energy released corresponds to the vibrational energy of the molecule of interest (Woods *et al.*, 2000). The vibrational energy is a unique characteristic of the species of interest.

The quantised vibrational changes that are associated with the scattering of the light are similar to those of the IR absorption spectrum, but there are enough differences between the two techniques to make the techniques complementary. The Raman microprobe is capable of achieving a spatial resolution 10 times better than that of IR microprobes, because the spatial resolution is proportional to the wavelength of the incident beam. The spatial resolution is typical of the order of a 1μm (Woods *et al.*, 2000). In contrast to the IR microprobe samples for the Raman microprobe do not have to be dry. In addition to this Raman spectroscopy has the advantage that the incident and scattered beams can have wavelengths in the region not strongly absorbed by water molecules (Woods *et al.*, 2000). This makes the technique ideal to perform *in situ* investigations in an aqueous medium using glass or – preferably - silica windows.

A major limitation of the Raman technique is that it has a lower sensitivity than most systems which stems from the fact that only one photon out of 10^8 photons from the incident flux will undergo scattering (Woods *et al.*, 2000). However, the Raman technique can provide valuable information on organic and inorganic species on the surface of many minerals, mineral identity, and species in aqueous solution.

Surface enhancement Raman scattering spectroscopy (SERS) involves the enhancement of the scattering intensity of species, which are adsorbed onto or are close to a roughened surface. The intensity is enhanced by a factor of some 10^4 to 10^5.

Because of this extremely high surface sensitivity monolayers and sub-monolayers can be investigated making it an indispensable tool for the studying of collector interactions with surfaces. Especially the potential dependency of the collector adsorption on the metal of interest is of great importance to fundamental research. Unfortunately only three noble metals (Au, Ag and Cu) provide large enhancement. However roughening techniques performed on metals (Pt, Pd, Cr and Fe) can generate SERS on these metals with an enhancement factor between 1 and 4 orders in magnitude (Zhong-Qun *et al.*, 2002). The roughening technique involves oxidation-reduction cycles (by variation of the potential) in a chloride or sulphate medium.

4.4.2. Experimental

The Raman measurements were taken with an XY Raman spectrometer from Dilor, using the λ = 514.5 nm laser line of a Coherent Innova 90 Ar^+-laser as exciting line. The spectra were recorded in a backscattering configuration with a long working distance 50x objective of an Olympus microscope attached to the instrument. The instrument is equipped with a nitrogen cooled CCD detector and the spectral resolution was at least 2 cm^{-1} for all the measurements. A low laser power of 50-100 mW was used for all measurements to avoid decomposition of species on the sample surface.

As for electrochemical measurements, sodium borate at a concentration of 0.05 M $Na_2B_4O_7$ was used to buffer the solution at pH value of 9.3. The solution was de-aerated for 2 hours with Argon gas (99.999%), from which traces of oxygen were removed by passing the gas over zirconia turnings heated at 600^oC. The PGM working electrode was freshly prepared between experimental runs by wet abrasion using a 0.05 μm Micropolish Alumina-B suspension. The electrode was subsequently washed by double distilled water and quickly transferred to the electrochemical cell for measurements. The system was flushed thoroughly with the de-aerated argon to prevent oxidation of the minerals once the mineral was positioned in the electrochemical cell. Once flushed the system was sealed (using rubber plugs) and kept at a positive pressure to avoid the ingress of air.

All experiments were conducted at 25^{o}C (± 1^{o}C) by immersing the electrolyte reservoir (700 ml in volume) in a water bath. The liquid phase was pumped at a constant rate of 100 ml/min over the working electrode by employing a peristaltic pump. The electrochemical cell (8cm long and wide and 2cm deep) consisted of a quartz window (2mm thick) at the top, two platinum counter electrodes, and the Luggin tube. The platinum wire counter electrodes (1.5 cm long and 0.5mm in diameter) were placed at equal distances (1cm) from the working electrode. The working electrode was placed close to the quartz window (approximate distance of 3mm) to facilitate easier focusing. The surface potential was controlled using a Schlumberger 1287 potentiostat while measuring the current as a function of time. The surface of the mineral was reduced at – 0.4V (SHE) for about 5 minutes before the commencement of the experiments

The laser beam was focused on the sample by means of an optical microscope fitted with a video camera. The continuous radiation of a laser focused for extended periods on one spot can lead to the decomposition of surfactants. The decomposition of the surfactants is very sensitive to the surface properties of the mineral: both pure tellurium and pure bismuth showed interaction with the laser in the presence of xanthate even at low radiation powers, but the interaction of the laser with the surfactants on the Pd-Bi-Te was not nearly as evident. Because of the possibility of laser-induced surface changes each Raman spectrum (recording time of about 120 seconds) was taken at a site away from the previous site (but remaining in the same general area) to prevent the gradual decomposition of the surfactants by continuous radiation.

The electrochemical cell employed for Raman spectroscopy is shown in Figure 20.

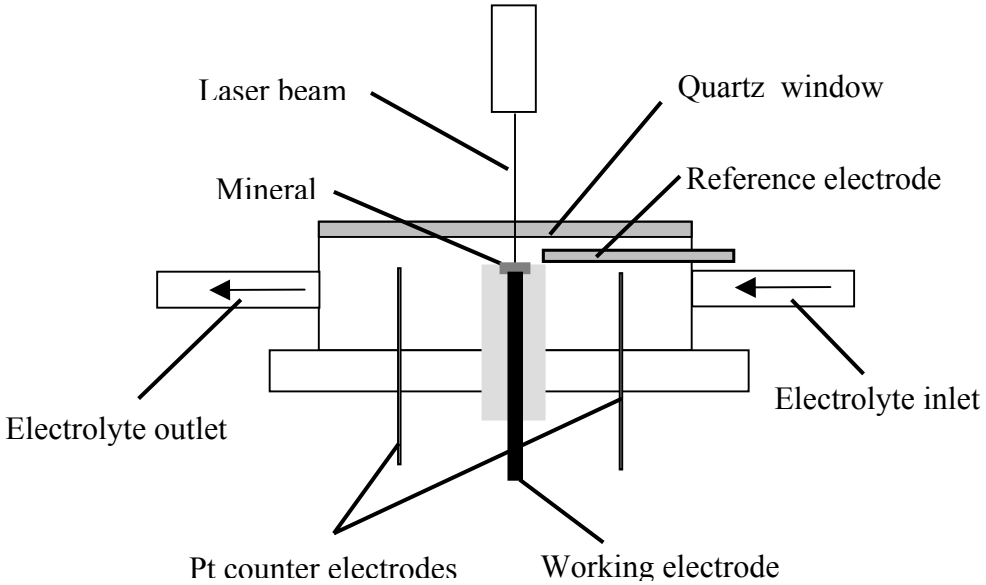

Figure 20: Schematic of the *in situ* electrochemical cell used for Raman spectroscopy.

Figure 21 shows the laser focused on the mineral placed in the *in situ* electrochemical cell.

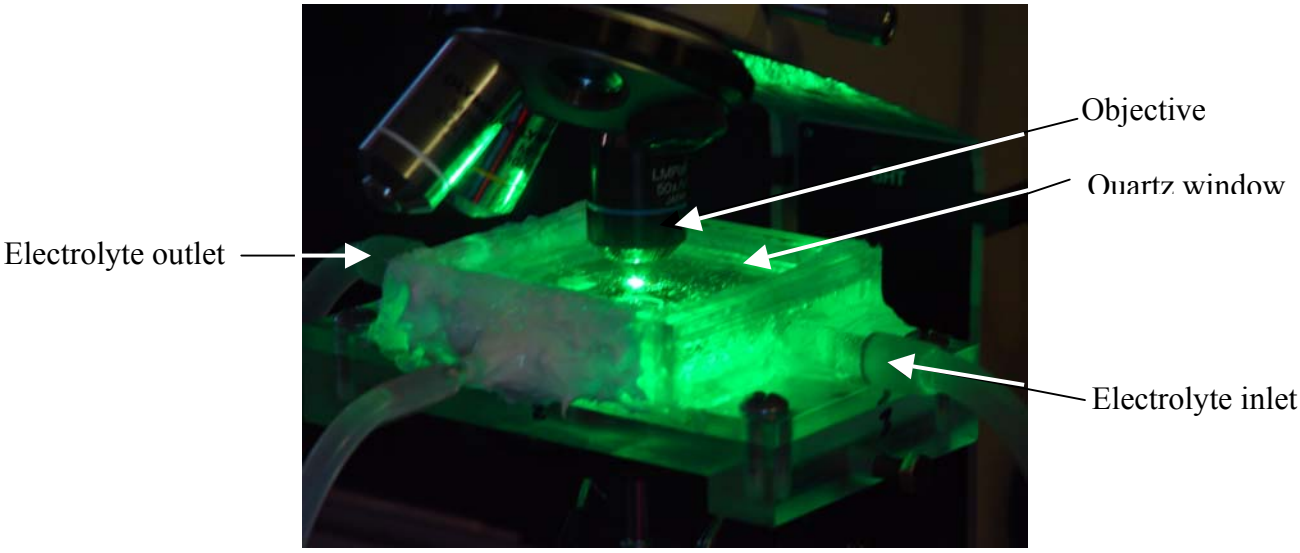

Figure 21. Optical image of the laser focused on mineral while the Raman spectrum is recorded.

4.5. Contact angle measurements

A modified electrochemical cell with two parallel plate windows was used to perform contact angle measurements under potentiostatic control. The same polishing procedure was used as described earlier. The electrochemically controlled contact angle measurements were performed under the same conditions as mentioned in the section on electrochemical measurements. The electrochemical cell was placed on the optical bench of the Ramé-Hart contact angle goniometer (Model: 100-00-230) and the captive bubble arrangement (The nitrogen bubble was introduced to the down-ward facing mineral surface in the electrolyte).

Woods *et al.* (1977) showed that residual polishing agents and any form of organic contamination have a serious effect on the contact angle measurements (for example: washing of a polished gold electrode with ethanol and distilled water produced a contact angle of 70^{o} instead of the expected 0^{o}). As a result care had to be taken during this investigation to avoid any form of contamination when performing contact angle measurements. Organic contamination of the distilled water was minimised by using the Simplicity^{TM} water system of Millipore. The water system employs purification media and an UV lamp to produce distilled water with extremely low levels of organic contamination (< 15 ppb) and a final resistivity of 18MΩ.cm.

A glass capillary with a very small opening was used to place the small nitrogen bubbles (approximately 0.5mm in diameter) on the mineral surface. The contact angle measurement procedure involved stepping the potential to the required value for 5 minutes. The contact angle was measured directly after polarization was terminated, measuring contact angles on both sides of the bubble. At least 5 bubbles were placed as quickly as possible on the surface from which contact angles were measured. The electrode was subsequently withdrawn form the cell and a new surface was generated, by employing the same polishing routine as mentioned above. The contact angle measurements were subsequently repeated at the same potential. A standard deviation and 95% confidence interval were determined from the measurements of the two runs. For cases where zero contact angles were found (indicating no attachment), a bubble protruding from the glass capillary was placed on the surface and then slowly

withdrawn from the surface, to test whether attachment was indeed absent. Lack of attachment characterizes a zero contact angle. Latex gloves were worn throughout the experiments to avoid the contamination of the mineral surfaces. After the completion of the contact angle measurements the glassware was thoroughly washed using purified distilled water and placed in drying oven to prevent organic contamination.

4.6. Microflotation measurements

4.6.1. Natural and synthetic minerals

The most abundant base metal sulphides found in Merensky ore are pyrrhotite (approximately 45%), pentlandite (approximately 32%), chalcopyrite (approximately 16%) and pyrite (approximately 2-4%) (Feng and Aldrich, 1999), and hence the flotation of some of these common sulphides was compared with that of the palladium bismuth telluride. Massive crystals of pentlandite (a typical fast-floating mineral) could not be sourced, but natural pyrrhotite and pyrite samples were obtained from the Wards Natural Science Company, and natural chalcopyrite was obtained from the hand-picked mineral collection of the Department of Geology, University of Pretoria. X-ray diffraction (XRD) analysis confirmed the phase composition of the natural samples and identified the monoclinic crystal structure of pyrrhotite (see Appendices 8-10 for XRD spectra).

Pd-bearing bismutho-telluride (michenerite, representative of the most abundant PGM found in the flotation feed) was prepared synthetically. The synthesis procedure is given in paragraph 4.2. The Pd-Bi-Te mineral samples were stored under purified argon once removed from the evacuated, sealed quartz tubes.

4.6.2. Flotation

A microflotation cell (capacity of 250 ml) as described before (Bradshaw and O'Connor, 1996) was used to determine the flotation response of the selected minerals. The microflotation cell consists of a cylindrical tube with a lower conical (tapered) section with air introduced through a needle valve located at the base of the cell. During the study flotation tests were carried out at a constant gas flow rate of 3.5

cm^3/min. The pulp was kept in suspension and circulated by employing a peristaltic pump. A cone at the top of the flotation cell deflects the mineral-loaded bubbles whereupon the bubbles burst, resulting in the collection of the mineral in the concentrate launder.

Purified sodium isobutyl xanthate (SIBX) was obtained from SENMIN. Other chemicals were of analytical grade quality. It was decided to use sodium isobutyl xanthate as collector instead of potassium ethyl xanthate since the former is used in industry and the aim of the microflotation experiments was to keep as many variables as close as possible to plant conditions in order to establish the true flotation response of the Pd-Bi-Te minerals. The potassium ethyl xanthate (at a concentration of 10^{-3} M) is most frequently used in fundamental studies involving functional groups and surfaces, hence the selection for the fundamental work of this thesis (see sections 4.3, 4.4 and 4.5).

All mineral samples (initial mass of around 3.5 grams) were freshly ground in an agate mortar prior to each experiment. The crushed products were screened to produce a particle size distribution of +38 μm-106 μm for microflotation tests. Microflotation experiments were carried out on a 2 gram single mineral sample added to 250 cm^3 of solution. Sodium carbonate (0.1 M) and hydrochloric acid (0.1 M) were used for pH adjustments prior to the flotation tests. Microflotation tests were performed in synthetic water containing the major ions found in plant process water (Mg^{2+} 80 ppm, Ca^{2+} 80 ppm, Na^{+} 135 ppm, Cl^{-} 270 ppm, SO_4^{2-} 250 ppm, NO_3^{-} 135 ppm, NO_2^{-} 40 ppm and CO_3^{2-} 40 ppm). The mineral samples were conditioned for 1 minute in the synthetic water followed by SIBX addition (giving a 5×10^{-5} M concentration) and conditioning for a further 3 minutes. During subsequent batch flotation the concentrates were collected at total times of 3, 6, 10 and 20 minutes. The concentrates and non-floated fraction were allowed to air-dry and were weighed. All flotation tests, except on the Pd-Bi-Te, were performed in triplicate to ascertain the repeatability of the microflotation test procedure.

5. Results and discussion

5.1. Electrochemical and contact angle results

5.1.1. Pd-Bi-Te

The variation of the current as a function of potential, obtained by changing the potential linearly with time between – 0.2V (SHE) and 0.3V (SHE) at a scan rate of 1mV/s, is shown in Figure 22. (These current-potential curves were measured in triplicate). A small anodic current is evident in the region > 0V in the absence of the collector and is possibly due to the oxidation of the mineral surface. There is a significant anodic current at potentials > 0.2V (SHE) in the presence of potassium ethyl xantante. Two cathodic peaks appear on the return cathodic sweep. These two peaks are due to the reduction of the products of the anodic oxidation. One of the peaks can reflect to reduction of dixanthogen to xanthate, whilst the other may indicate reduction of metal oxides. The potential for equilibrium between ethyl xanthate (10^{-3} M concentration) and pure diethyl dixanthogen is 0.121V (SHE) (Woods *et al*., 1974); this potential is shown in Figures 22 and 28. The section on the Raman investigation (section 5.2.2.) will shed more light on the nature of the reduction reactions.

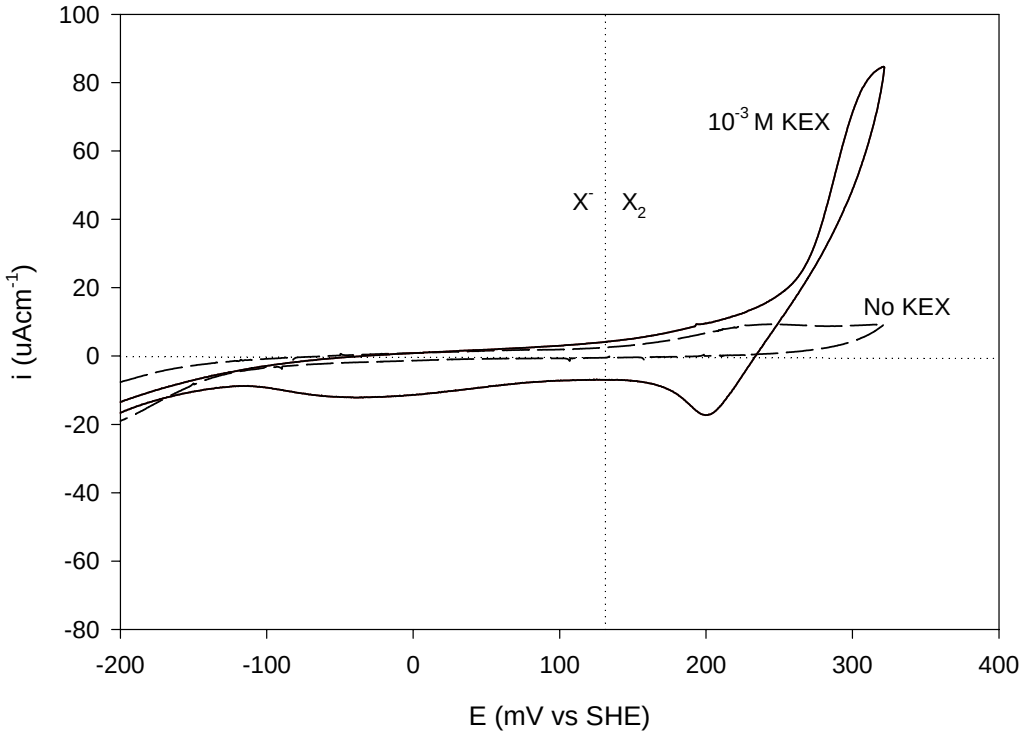

Figure 22: Current-potential curves for a Pd-Bi-Te electrode in a 0.05 M $Na_2B_4O_7$ solution at 25°C in the absence and presence (10^{-3} M KEX) of xanthate collector. Potential sweep carried out at 1mV/s. Starting potential of – 0.2 V (SHE) and positive initial sweep direction.

More detail of the anodic reactions are shown in Figure 23, obtained by changing the potential linearly with time between 0.1 (SHE) and 0.4V (SHE) at a scan rate of 1mV/s. The figure clearly indicates the enhanced anodic activity in the presence of xanthate. In addition to this the figure shows that some oxidation of the mineral occurs in the absence of xanthate, at potentials more positive than 300mV. This anodic current does not originate from adsorption of oxygen only (or from other side reactions). Although anodic current from oxygen adsorption is observed on – for example – pure platinum in this potential range, the charge associated such oxygen adsorption on platinum is in the range 120-400 μC/cm^2 (as found in sulphuric acid (Zolfaghari *et al.*, 2002), potassium hydroxide (Damjanovic *et al.*, 1987) and borate buffer solutions (Woods, 1971), much less than the total anodic charge of 5.8 mC/cm^2 for the mineral in Figure 23.

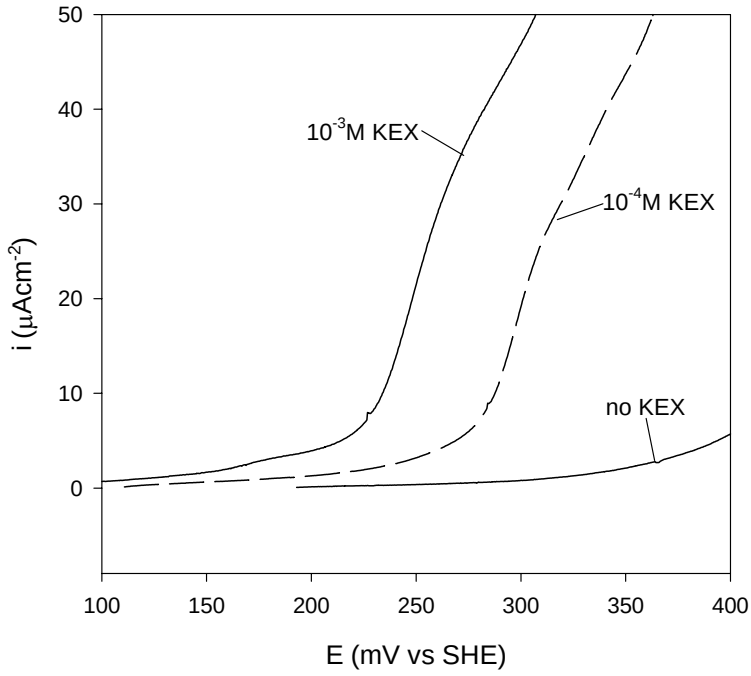

Figure 23: The influence of KEX on the anodic activity for Pd-Bi-Te. Current-potential curves for a Pd-Bi-Te electrode in a 0.05 M $Na_2B_4O_7$ solution at 25°C in the absence and presence of potassium ethyl xanthate. Potential sweep carried out at 1mV/s.

As mentioned earlier, Elvy *et al.* (1994) investigated the incongruent oxidation (in air) of minerals in the Pd-Te-Bi system leading to the formation of layer of tellurium and/or bismuth oxide covering the palladium-rich substrate. It was found that the reactivity of the minerals increased in the order of: PdTe < PdTeBi < PdBi. This is in the same order as the reactivities of Pd, Te and Bi in the pure form. To test whether the same ranking holds in the borate buffer solution, the anodic polarisation behaviour of the pure elements and the Pd-Bi-Te was measured. Figure 24 shows the anodic polarization curves of Bi, Pd, Te and Pd-Bi-Te in a deoxygenated solution containing 0.05 M $Na_2B_4O_7$.

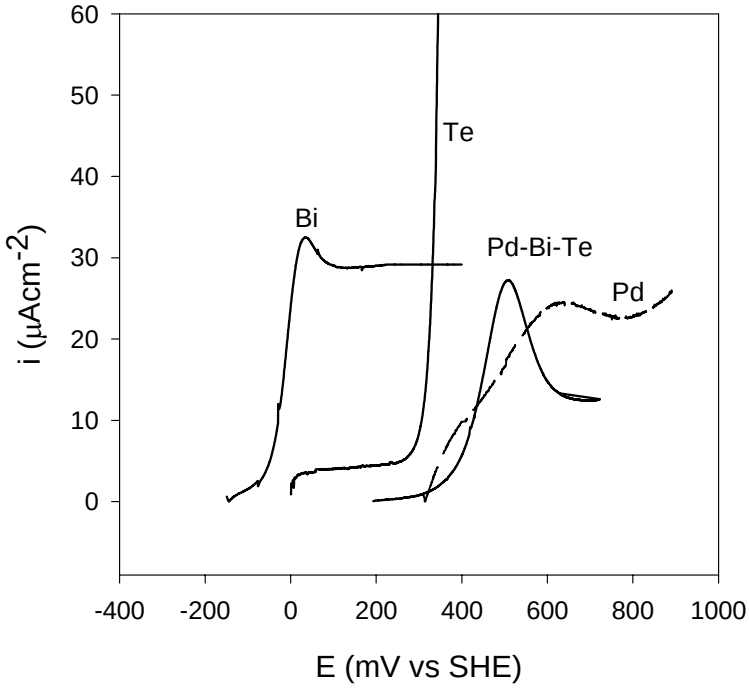

Figure 24: Anodic behaviour of selected metals and alloys in a de-oxygenated solution containing 0.05 M $Na_2B_4O_7$.

Figure 24 clearly shows that Bi is more reactive than Te at potentials lower than 300mV. It is thus expected that minerals containing higher levels of Bi should be more susceptible to oxidation, in agreement with Elvy *et al*. (1994). Although the reactive Bi and Te constitute 66.6 percent (mole basis) of the Pd-Bi-Te mineral, the reactivity of the mineral is much lower than that of the pure constituents. The low palladium activity apparently accounts for the low reactivity of the mineral: as shown in figure 24, the anodic behaviour of michenerite is very similar to that of pure palladium.

In order to investigate the formation of possible surface layers of collector, the Pd-Bi-Te electrode was polarized for 20 minutes at 0.3V (SHE) in a 0.05 M $Na_2B_4O_7$ solution with or without 1 x 10^{-3} M potassium ethyl xanthate, following which impedance measurements were performed. The results of this experiment are shown in Figure 25.

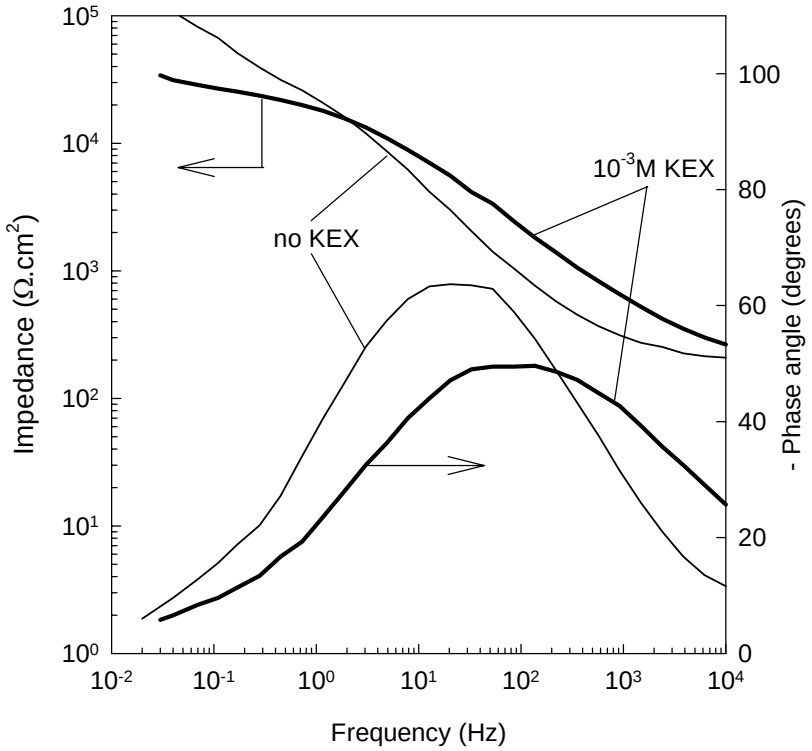

Figure 25: Bode plots for a Pd-Bi-Te electrode after anodic polarisation for 20 min at 0.3V (SHE) in a 0.05 M $Na_2B_4O_7$ solution containing zero and 1 x 10^{-3} M potassium ethyl xanthate.

The contribution of the capacitance value to the impedance is a maximum at intermediate frequencies i.e. where the phase angle is a maximum. The difference in the impedance values (with and without the collector) at intermediate frequencies, see Figure 25, is significant. The fact that a change in the impedance values was observed indicates a change in the capacitance due to the formation of a continuous layer on the surface. The formation of such a layer would tend to decrease the capacitance (see equation 3).

These surface layers can possibly be multi-layers of dixanthogen. Dixanthogen can only form if the mineral surface attains a potential higher than the equilibrium potential of the xanthate-dixanthogen couple. The reversible potential for the oxidation of ethyl xanthate to diethyl dixanthogen is 0.121V (SHE) at a collector concentration of 10^{-3}M KEX (Woods *et al.*, 1974). Efficient cathodic reactions (for

example the reduction of oxygen on the surface of the mineral) would tend to increase the mixed potential. To test whether the potential will be high enough to allow oxidation of xanthate to dixanthogen, cathodic polarisation behaviour and open-circuit potentials were measured. The cathodic polarization diagram showing the reduction of oxygen on the surface, in a borate-only solution, is given in Figure 26.

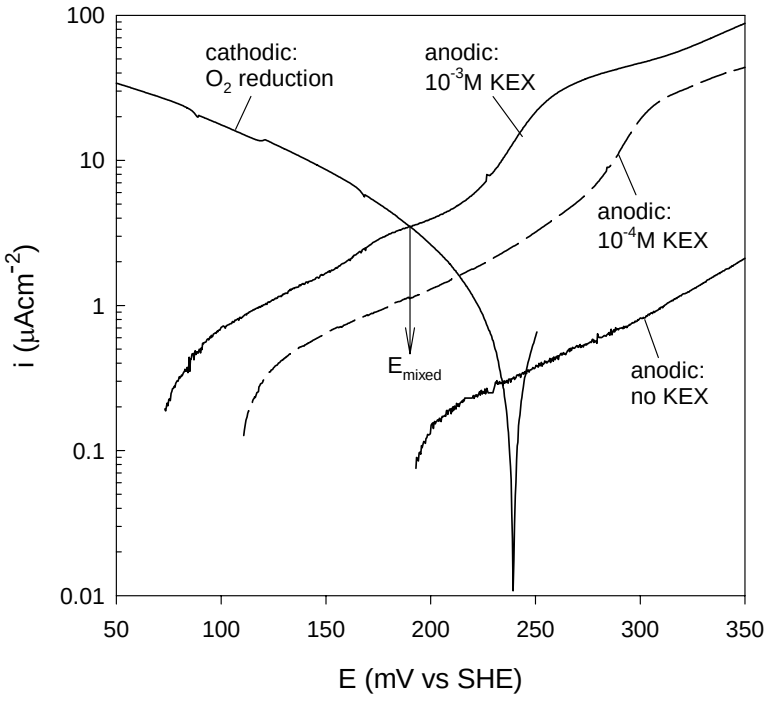

Figure 26: Current-potential curves for a Pd-Bi-Te electrode in a 0.05 M $Na_2B_4O_7$ solution at 25°C in the absence and presence of potassium ethyl xanthate. The anodic polarisation diagrams were measured in deaerated solutions. The cathodic polarisation diagram was constructed in an oxygen-saturated 0.05 M $Na_2B_4O_7$ solution. Potential sweeps carried out at 1mV/s.

The intersection of the cathodic and anodic polarization diagram (for 10^{-3} M KEX) in Figure 26, gives an estimate of the mixed potential (E_{mixed}) for this system. The actual measured mixed potential of the electrode in an oxygen-saturated solution containing 10^{-3} M KEX, is shown in Figure 27.

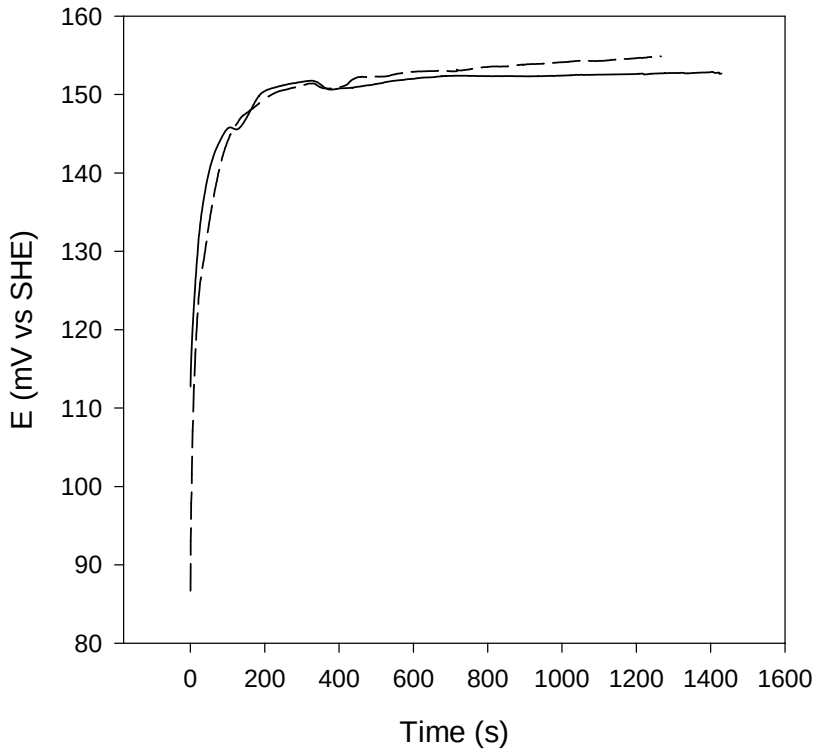

Figure 27: Mixed potential (for two runs) for Pd-Bi-Te in an oxygenated solution containing 10^{-3} M KEX, at a pH value of 9.2.

The mixed potential was measured after freshly preparing the Pd-Bi-Te electrode by grinding and polishing according to the method described in Chapter 4. The borate solution was firstly aerated for 2 hours with oxygen gas whereafter the xanthate was added to obtain a concentration of 10^{-3} M KEX. The electrode was subsequently washed with double distilled water and quickly transferred to the electrochemical cell for measurements. The potential readings commenced the moment the electrode was immersed in the solution (t = 0 s). The true mixed potential (see Figure 27) compares well (difference is less than 30mV) with the value predicted from individual anodic and cathodic polarisation diagrams (see Figure 26). This clearly demonstrates that the mixed potential of the system is higher than the equilibrium potential of the xanthate-dixanthogen couple. It is thus possible for dixanthogen to form on the surface of Pd-Bi-Te.

Contact angle measurements are consistent with the formation of the hydrophobic species (presumed to be dixanthogen) at potentials above the xanthate-dixanthogen

equilibrium potential. Figure 28b shows that, in the presence of ethyl-xanthate, a zero contact angle was observed at those potentials which yielded negligible anodic currents on the voltammograms (for example, 0.1 V in Figure 28a). When the potential was increased to more positive values the contact angle increased strongly. The potential where non-zero contact angles were first observed corresponds well with commencement of xanthate oxidation to dixanthogen. The maximum angle measured was 63 degrees. The contact angle measurements demonstrate that the mineral surface is hydrophobic at high potentials. This hydrophobicity will result in the flotation of the particle if sufficient quantities of the surfactant are present and successful bubble attachment is achieved. This suggests that the poor flotation recovery of the Pd-Bi-Te minerals from flotation feeds cannot be attributed to a lack of interaction between the collector and the mineral surface.

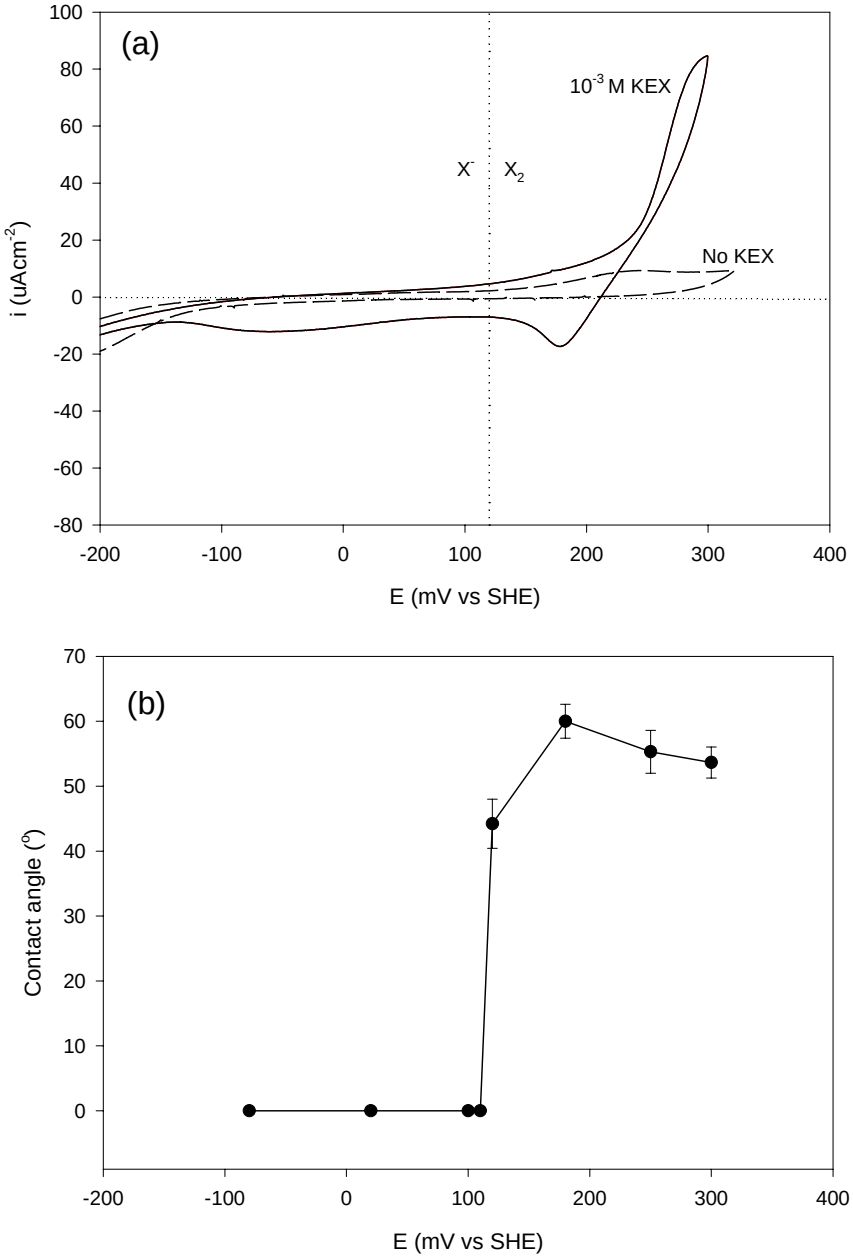

Figure 28: (a) Current-potential curves for a Pd-Bi-Te electrode in a 0.05 M $Na_2B_4O_7$ solution at 25°C in the absence and presence (10^{-3} M KEX) of xanthate collector (data of Figure 22). The equilibrium potential for the oxidation of xanthate to dixanthogen is indicated on the graph. (b) Contact angles for Pd-Bi-Te electrode in a 0.05 M $Na_2B_4O_7$ solution at 25°C in the presence of 10^{-3} M KEX after 300s of polarisation at the relevant potential.

5.1.2. $PtAs_2$

Similar measurements of cathodic and anodic polarisation behaviour and contact angles were performed for sperrylite. Figure 29 shows the cathodic polarisation diagram (measured in oxygen-saturated borate buffer without xanthate), and the anodic polarisation diagram (measured in oxygen-free borate buffer with and without xanthate). Cyclic voltammograms are shown in Figure 30a. Similar to Pd-Bi-Te, the anodic current increases strongly at more positive potentials, in the presence of xanthate. However, for sperrylite the potential where the current starts to increase strongly (0.25 V [SHE]) is significantly more positive than the reversible potential of the xanthate - diethyl dixanthogen equilibrium.

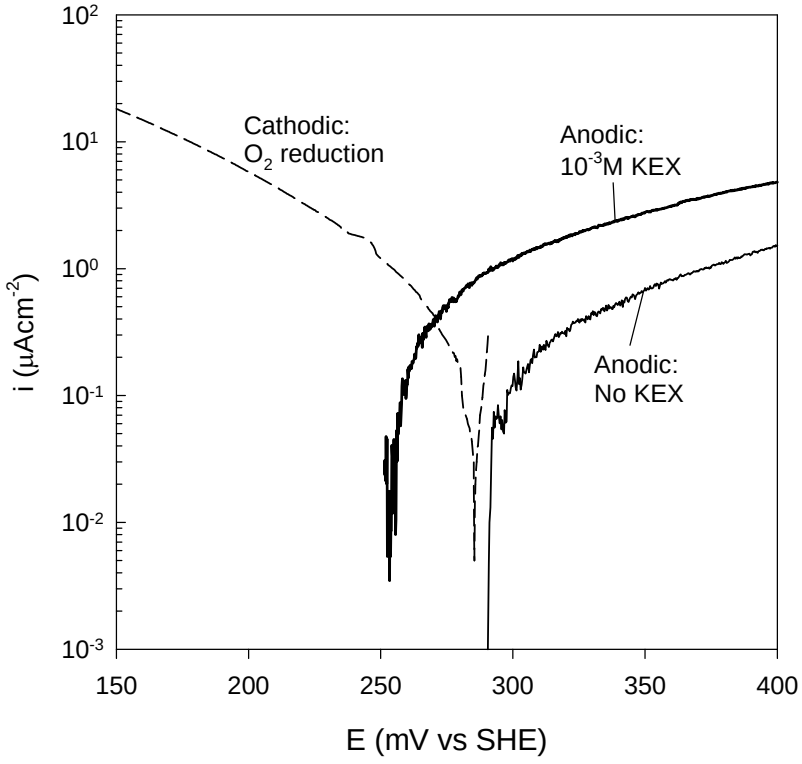

Figure 29: Current-potential curves for a $PtAs_2$ electrode in a 0.05 M $Na_2B_4O_7$ solution at 25°C in the absence and presence of potassium ethyl xanthate. The anodic polarisation diagrams were measured in deaerated solutions. The cathodic polarisation diagram was constructed in an oxygen-saturated 0.05 M $Na_2B_4O_7$ solution. Potential sweeps carried out at 1mV/s.

Figure 30b shows that $PtAs_2$ is hydrophilic at low potentials, with zero contact angles. When the potential was increased to more anodic values the contact angle increased strongly. The maximum angle measured was 54 degrees. The potential where non-zero contact angles were first observed is some 100mV more positive than the xanthate-dixanthogen equilibrium potential, but does correspond to the lowest potential (some 250mV [SHE]) where significant anodic current was measured (see Figures 29 and 30a).

Woods *et al.* (1974) indicated that a maximum contact angle was observed for multilayer surfactant formation, whilst fractional coverages of the surfactant gave rise to smaller angles. The measured contact angles should therefore also depend on the charge transferred during polarisation and not only on the applied potential. This is indeed shown in Figure 31, which shows the dependence of the contact angle on the charge passed (integrated anodic current) in the presence of xanthate (A similar plot cannot be shown for michenerite because currents passed during contact angle measurements were not recorded). Error bands on the charge indicate 95% confidence intervals for at least 2 runs at the same applied potential. Figure 31 shows that the contact angle is independent of the charge transferred for values higher than 50 $mC.cm^{-2}$. Significant contact angles were observed for as low as 8 $mC.cm^{-2}$ charge transferred. The measurement technique used did not allow establishment of the minimum required amount of charge to establish a hydrophobic surface. Woods *et al.* (1974) indicated that a monolayer of dixanthogen is equivalent to a charge of 50 $\mu C.cm^{-2}$. This equivalent charge was calculated based on the assumption that chain length does not affect the packing density of dixanthogen. However Woods *et al.* (1990) showed that efficient flotation recovery occurs with less than a monolayer of collector on the surface.

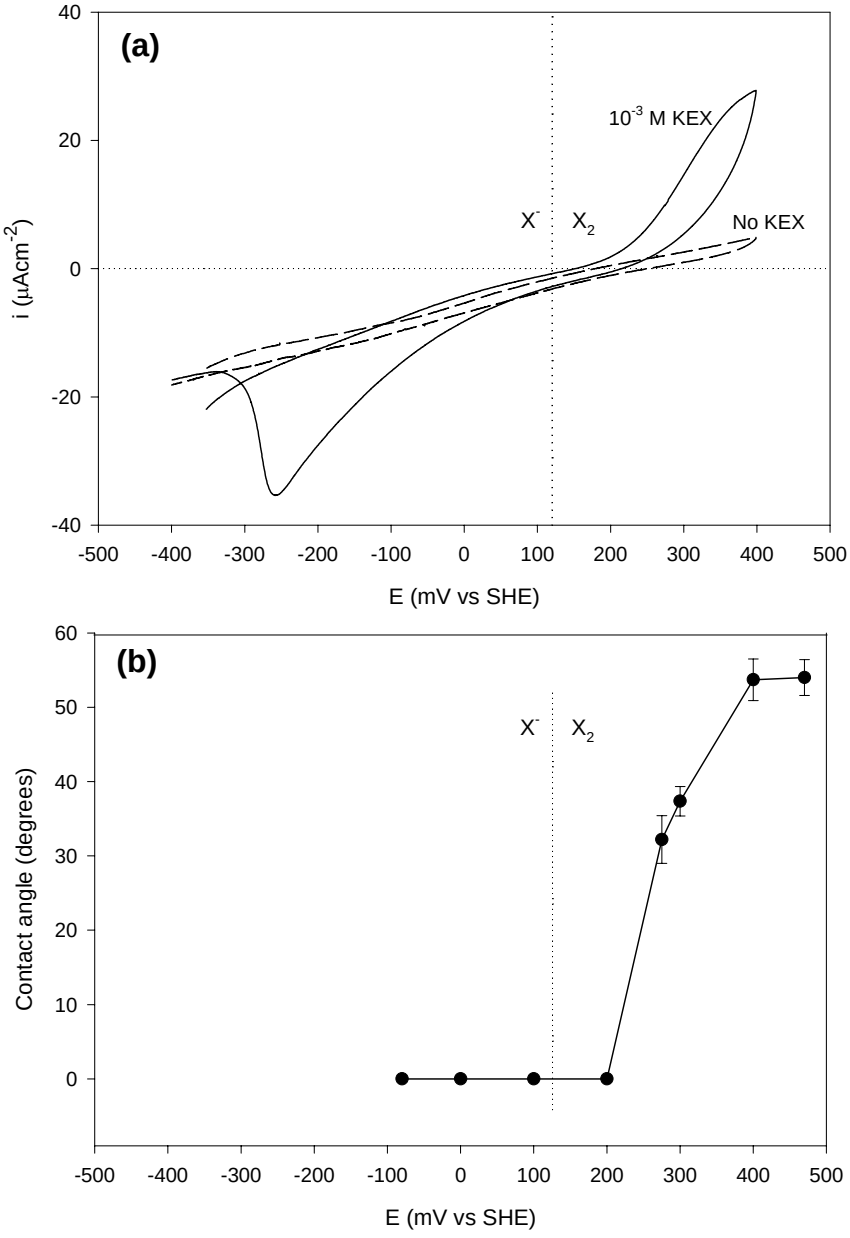

Figure 30: (a) Current-potential curves for a $PtAs_2$ electrode in a 0.05 M borate buffer solution at 25°C in the absence and presence (10^{-3}M KEX) of xanthate collector. Potential sweep carried out at 1mV/s. Starting potential of – 0.4V (SHE) and positive initial sweep direction. The equilibrium potential for the oxidation of xanthate to dixanthogen is indicated on the graph. (b) Contact angles for $PtAs_2$ electrode in a 0.05M $Na_2B_4O_7$ solution at 25°C in the presence of 10^{-3}M KEX after 300s of polarisation at the relevant potential.

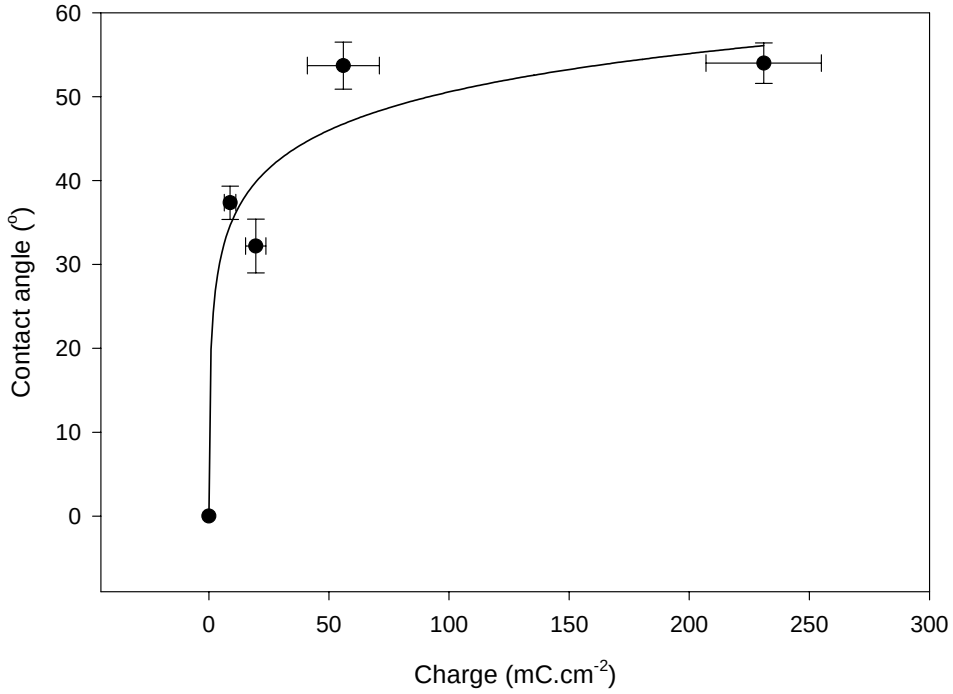

Figure 31: Dependence of contact angle on the charged transferred during anodic polarisation (for the measurements reported in Figure 30) of sperrylite in the presence of 10^{-3}M KEX. Error bands on the charge measured indicate 95% confidence intervals for at least 2 measurements.

5.2. Characteristic peaks in Raman spectra

5.2.1. Collector and oxidised collector

Figure 32 shows the Raman spectra obtained from freshly synthesized potassium ethyl xanthate and diethyl dixanthogen, for reference. The comparative Raman bands of potassium ethyl xanthate and of diethyl dixanthogen are shown in Table 7; the bands are in close agreement with those published by Buckley *et al.* (1997) and Woods *et al.* (1998).

Table 7: The comparative Raman bands of potassium ethyl xanthate and of diethyl dixanthogen. Assignment of the bands of the xanthate compounds was based on the work published by Woods *et al.* (1998).

	Wave number (cm^{-1})			
	Woods *et al* (1998)		This work	
Vibration	KEX (aq)	EX_2 (l)	KEX (aq)	EX_2 (l)
CS_2 antisymmetric stretch	1046	1041	1046	1041
CCOC stretch	864	845	864	844
CS_2 symmetric stretch *trans*	660	695	659	694
CS_2 symmetric stretch *gauche*	615	646	614	646
OCS_2 out of plane *wag*	556	528	-	-
SS stretch	n.a.	498	n.a.	498
COC deformation *gauche*	493	473	493	-
COC deformation *trans*	449	427	448	428
OCC deformation	399	378	401	378

n.a. not applicable

5.2.2. Results of Raman spectroscopy on Pd-Bi-Te

An *in situ* Raman spectrum from a Pd-Bi-Te electrode polarized for 1 hour at 0.3V (SHE) in 0.05 molar sodium tetraborate solution containing 1 x 10^{-3} molar potassium ethyl xanthate is also shown in Figure 32. The 498 cm^{-1} band from the S-S stretching vibration (in dixanthogen) was used to identify dixanthogen on the surface of the minerals (see Table 7). As illustrated by Figure 32, the 498 cm^{-1} Raman band was identified on the Pd-Bi-Te, as were clear bands at 444 and 399 cm^{-1} (slightly shifted from the 448 and 401cm^{-1} bands which are characteristic of xanthate). The small band shift approaches the spectral resolution of the instrument. Nevertheless, a small shift can possibly be attributed to compound formation. It has been shown that the formation of the AuEX radical can be responsible for a shift of 18 cm^{-1} in case of the COC deformation *trans* band (Woods *et al.*, 1998).

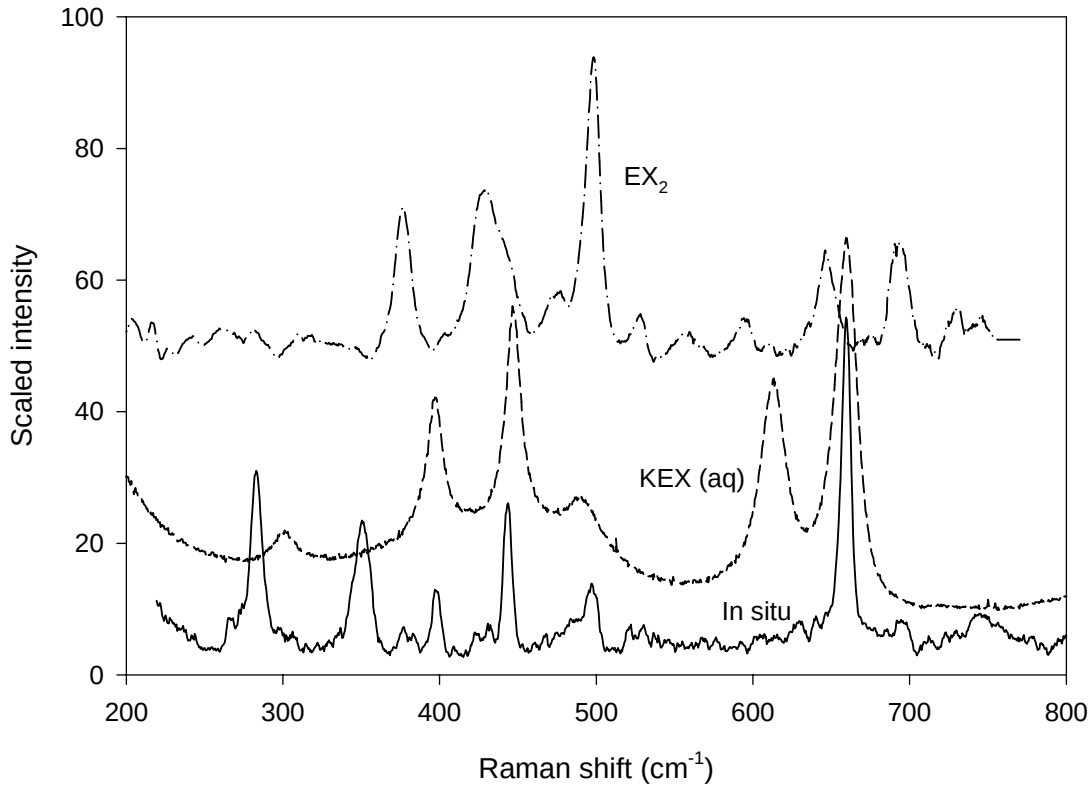

Figure 32: Raman spectra of freshly synthesized potassium ethyl xanthate, diethyl dixanthogen and the *in situ* spectrum of the surface of Pd-Bi-Te anodically polarized in the presence of xanthate for one hour. Laser power rating of 100mW and recording time of 120 seconds.

Extended polarization (at 0.2V [SHE]) of the Pd-Bi-Te electrode for approximately 1 hour in the solution containing 10^{-3}M xanthate caused the formation of visible droplets on the mineral surface. An *in situ* Raman spectrum from these droplets is shown in Figure 33. The spectrum unambiguously shows that ethyl xanthate is oxidized to diethyl dixanthogen on the mineral surface.

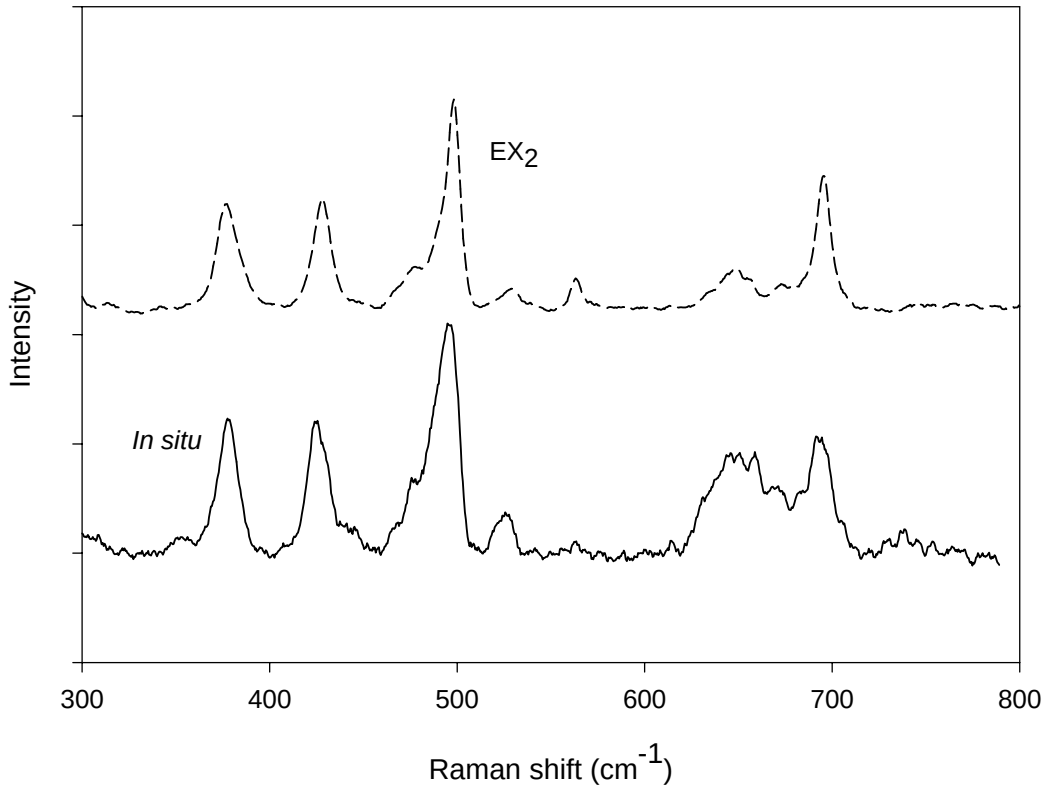

Figure 33: Raman spectra of freshly synthesized diethyl dixanthogen and of droplets on the surface of the Pd-Bi-Te electrode polarized for an hour at 0.2V (SHE) in a 0.05 M $Na_2B_4O_7$ solution containing 1 x 10^{-3} M potassium ethyl xanthate. Laser power rating of 100mW and recording time of 120 seconds.

More detail on the development of the Raman spectrum with polarization time is given in Figure 34, which shows *in situ* Raman spectra from the Pd-Bi-Te electrode polarised at 0.3V (SHE) in a 0.05 M $Na_2B_4O_7$ solution containing 1 x 10^{-3} M potassium ethyl xanthate for different time intervals. Before the start of anodic polarisation, the sample was held at – 0.4V (SHE), where no dixanthogen formation is possible. The spectrum recorded at this potential is labelled with 't=0 s' in Figure 34. It can be seen from Figure 34 that no Raman peak other than the weak and broad 743cm^{-1} band was observed in the spectrum. After anodic polarisation for 120s or longer, xanthate itself is present on the mineral surface: the Raman spectra in Figures 32 and 34 exhibit clear bands at 659 cm^{-1}, which represents a small shift of about 1cm^{-1} from the CS_2 symmetric stretch of xanthate. Notwithstanding this small shift in band

position, the Raman spectra clearly confirm that ethyl xanthate retains its molecular integrity when it adsorbs on the surface of the mineral. Chemisorbed xanthate is the first species to be identified on the mineral surface, with adsorption faster than can be measured by this method (since spectra take 120 seconds to record). Dixanthogen could only be identified on the surface after long exposure times i.e. 1600 seconds in Figure 34. The band that arises from the S-S stretching vibration of dixanthogen at 498cm^{-1} is present in both Figures 32 and 34 (see times from 1600 seconds onwards). This clearly demonstrates that the anodic current recorded in Figure 28a can be attributed to the formation of this compound. Unlike the results for copper and silver Figure 28a does not exhibit any prewave indicative of chemisorption of xanthate (Woods *et al.,* 1998). The absence of the prewave suggests that chemisorption takes place in the same potential region as dixanthogen formation. Woods *et al.* (1998) showed that xanthate chemisorbs at underpotentials on gold, silver and copper. While these results suggest that underpotential deposition does not take place on Pd-Bi-Te, further experiments would be required to resolve this.

The clear bands obtained after even short periods of anodic polarisation indicates that surface enhancement of the Raman bands could have occurred. The phenomenon of surface enhanced Raman scattering (SERS) has been used extensively to characterize surface layers at sub-monolayer coverages (Woods *et al.*, 1998; Buckley *et al.*, 1997; Woods *et al.*, 2000). This phenomenon is surface sensitive and also does not enhance the bands equally; it has been observed on copper, silver and gold (Woods *et al.*, 2000). For the present results - as in the case of gold - the 660 cm^{-1} (xanthate) band shows a greater intensity despite the fact that much more dixanthogen than xanthate should be present on the surface given the relative large overpotential (0.18V) applied. However the anodic oxidation of ethyl xanthate on gold occurs before the formation of the metal xanthate resulting in a potential region (between – 0.057 V and –0.035V) where only dixanthogen is formed on the surface. An *in situ* SERS spectrum taken at a potential within this region showed the presence of a chemisorbed monolayer and dixanthogen (Woods *et al.*, 1998). The hypothesis states that only a monolayer of xanthate is deposited on the mineral with multi-layers of dixanthogen depositing on top of the xanthate layer (Woods *et al.*, 1998). Sustained anodic polarisation at this potential therefore continues the deposition of the dixanthogen, without increasing xanthate coverage. It is believed that the difference in Raman peak

intensities reflect differences in attachment of the two species to the surface (Woods *et al*, 1998). It is postulated that the covalent chemisorbed xanthate gives more signal enhancement than the covalently-bonded dixanthogen. Palladium, however, shows only a small enhancement factor (SERS does occur with palladium under very specific conditions which was probably not the case in this study [Zhong-Qun *et al.*, 2002]) compared to the copper, silver and gold and the presence of a xanthate peak at 660 cm^{-1} should not only be attributed to the formation of the monolayer. The formation of bulk metal xanthate is dependant on the reversible potential of the xanthate-metal xanthate equilibrium potential; this is not known for the metals used in the study. For the gold system, however, at extended polarisation at high potentials dixanthogen and gold xanathate are formed (Woods, 1972). It is, therefore, suggested that a metal xanthate, most probably bismuth xanthate is the major interaction product of the collector with Pd-Bi-Te.

Raman spectroscopy performed on pure Bi and Te electrodes polarized at 0.2V (SHE) in a 0.05 M $Na_2B_4O_7$ solution containing 1 x 10^{-3} M potassium ethyl xanthate for 1 hour did indicate the formation of dixanthogen. However, because of the reactivity of both elements under laser illumination, lower laser power had to be used, to the detriment of the response signal.

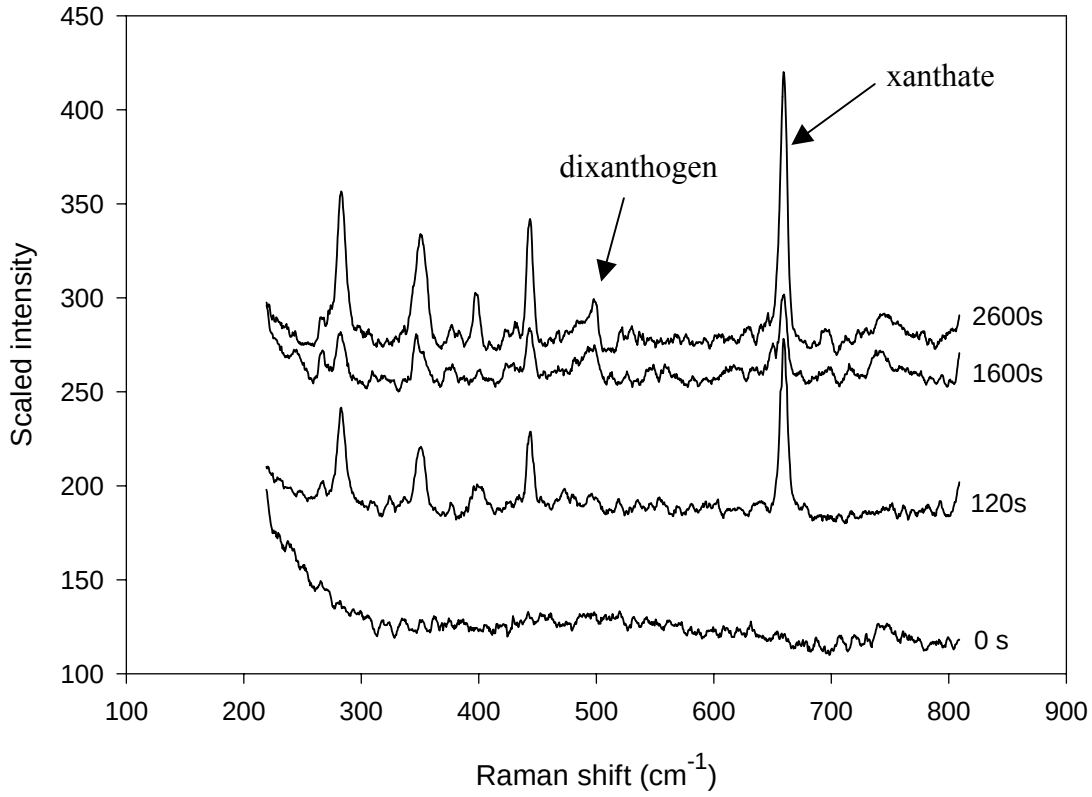

Figure 34: Raman spectra of Pd-Bi-Te electrode polarized for different lengths of time at 0.3 V (SHE) in 0.05M $Na_2B_4O_7$ solution containing 1 x 10^{-3} M potassium ethyl xanthate. Laser power of 100mW and recording time of 120 seconds. Arrows indicate the Raman peaks to be characteristic of xanthate and dixanthogen.

The surface roughness of the mineral plays a vital role in the enhancement of the Raman signal. Figure 35 indicates local variability in the signal strength (which was not the result of differences in focusing; care was taken to focus the beam well in all cases). Despite the variability, general trends can be observed by plotting the ratio of the intensity of the specific band (peak heights) to that of a reference band (see Appendix 11 for spectra and summary of results). The time-lag measurements of which summarised results are shown in Figure 35 were each taken at a new site in close proximity to the previous measurement site. Figure 35 shows the intensity ratio of the 498 cm^{-1} band, corresponding to the S-S stretch or dixanthogen, to that of the reference band. The measurements were grouped in intervals of a 1000s to be able to calculate averages and corresponding standard deviations.

The reference band was the 743 cm^{-1} band. As discussed later the origin of this band is not clear, but the band intensity is relatively insensitive to anodic polarization (see Figure 38 and Table 8).

Table 8: The integrated area of the 743 cm^{-1} band (integrated from 727 cm^{-1} to 760 cm^{-1}) as a function of the anodic polarization time. The Pd-Bi-Te electrode was polarized for different lengths of time at 0.3 V (SHE) in 0.05M $Na_2B_4O_7$ solution containing 1 x 10^{-3} M potassium ethyl xanthate. Laser power of 100mW and recording time of 120 seconds were used.

Polarization time (s)	Area (counts.cm^{-1})
0	197.2
840	188.9
1800	183.6
3000	190.3

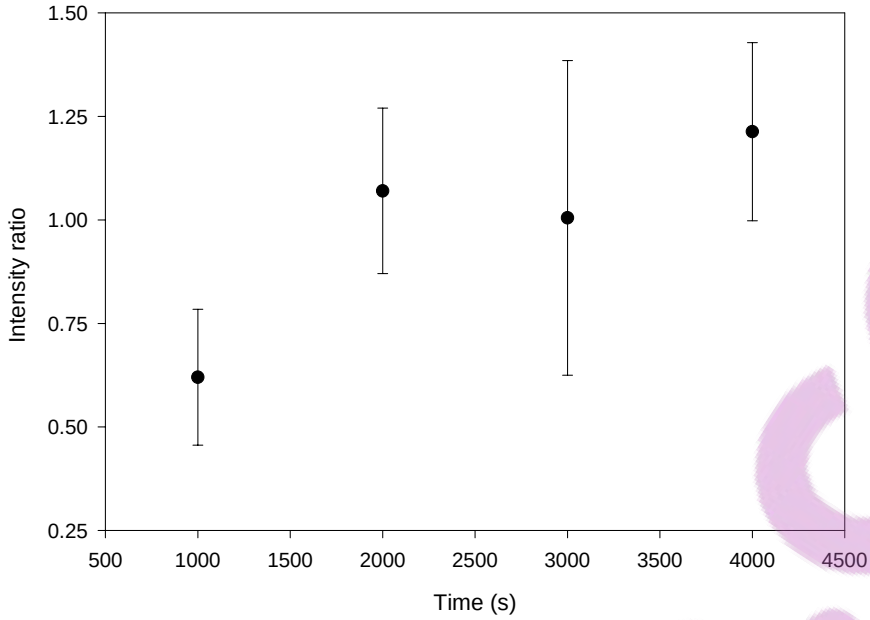

Figure 35: Intensity ratio of 498 cm^{-1} band (indicative of dixanthogen) to that of the 743 cm^{-1} band as a function of the anodic polarization time. Anodic polarization was carried out at 0.3V (SHE) in a 0.05 M $Na_2B_4O_7$ solution containing 1 x 10^{-3} M potassium ethyl xanthate. Error bands indicate 95% confidence intervals for a single run, with around 5 measurements for each 1000s of polarisation time.

These results are in line with the hypothesis that multi-layers of diethyl dixanthogen deposit when the mineral surface is polarized at potentials more anodic than the minimum potential required for dixanthogen formation (Woods *et al.*, 1998). The deposition of the multi-layers over time results in the increase of the amount of dixanthogen as indicated in Figure 35. Figure 36 plots the intensity ratio of the 660 cm^{-1} band (characteristic of xanthate) relative to the 743 cm^{-1} reference band, for the same time intervals as shown in Figure 35. While rather scattered, these results show a constant xanthate peak height (irrespective the presence of xanthate in the form of the chemisorbed layer or the metal xanthate).

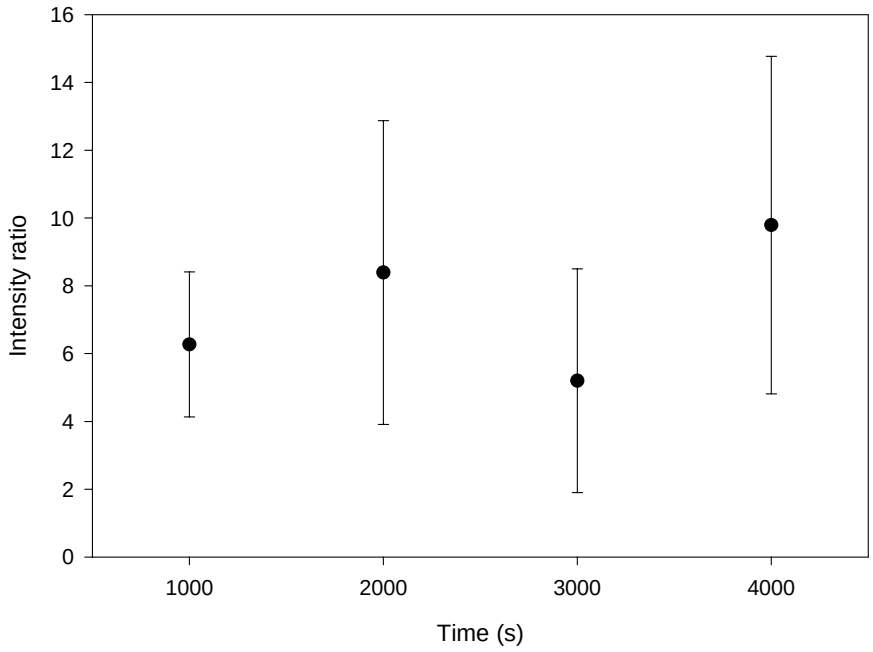

Figure 36: Intensity ratio of 660 cm^{-1} band (indicative of xanthate) to that of the 743 cm^{-1} band as a function of the anodic polarization time. Anodic polarization was carried out at 0.2V (SHE) in a 0.05 M $Na_2B_4O_7$ solution containing 1 x 10^{-3} M potassium ethyl xanthate. Error bands indicate 95% confidence intervals for a single run, with around 5 measurements for each 1000s of polarisation time.

Although the formation of dixanthogen is evident from the results, it has been shown that chemisorption of xanthate or the formation of metal xanthate itself establishes a non-zero contact angle resulting in a hydrophobic surface (Woods *et al.*, 2000). The fact that xanthate could be identified within 120 seconds, indicates that the interaction of the collector with the mineral should yield a hydrophobic surface even after short conditioning time.

Raman spectroscopy elucidated the nature of the reduction reactions of the cathodic leg of the cyclic voltammograms. When, after anodic polarization, the potential of the Pd-Bi-Te was decreased to 0.1V (which is in the region of the higher-potential cathodic peak – see figure 22 – and is below the xanthate-dixanthogen equilibrium potential) the band at 498 cm^{-1} was no longer observed. Figure 37 shows the Raman spectrum observed for a Pd-Bi-Te electrode held at 0.1V (SHE) in a 10^{-3} M KEX

solution at pH of 9.2 (see middle spectrum) after being polarized at 0.2V (SHE) (bottom spectrum). It is important to note that the cathodic peak in the higher potential region is more positive than the xanthate-dixanthogen equilibrium potential. Thus, the cathodic peak (see Figure 28a) in the higher potential region cannot be the result of the reduction of the bulk phase (i.e. dixanthogen) only and may involve the reduction of metal oxides which formed during anodic polarisation (for instance bismuth oxide). When the sample was subsequently held at – 0.2V for extended periods (6000s) the intensity of the 660 cm^{-1} band (xanthate) decreased relative to the 743 cm^{-1} band for the same recording conditions. It hence appears that the cathodic peak in the lower potential region arises from the reduction of the xanthate (either present as a monolayer or metal xanthate) and the dixanthogen.

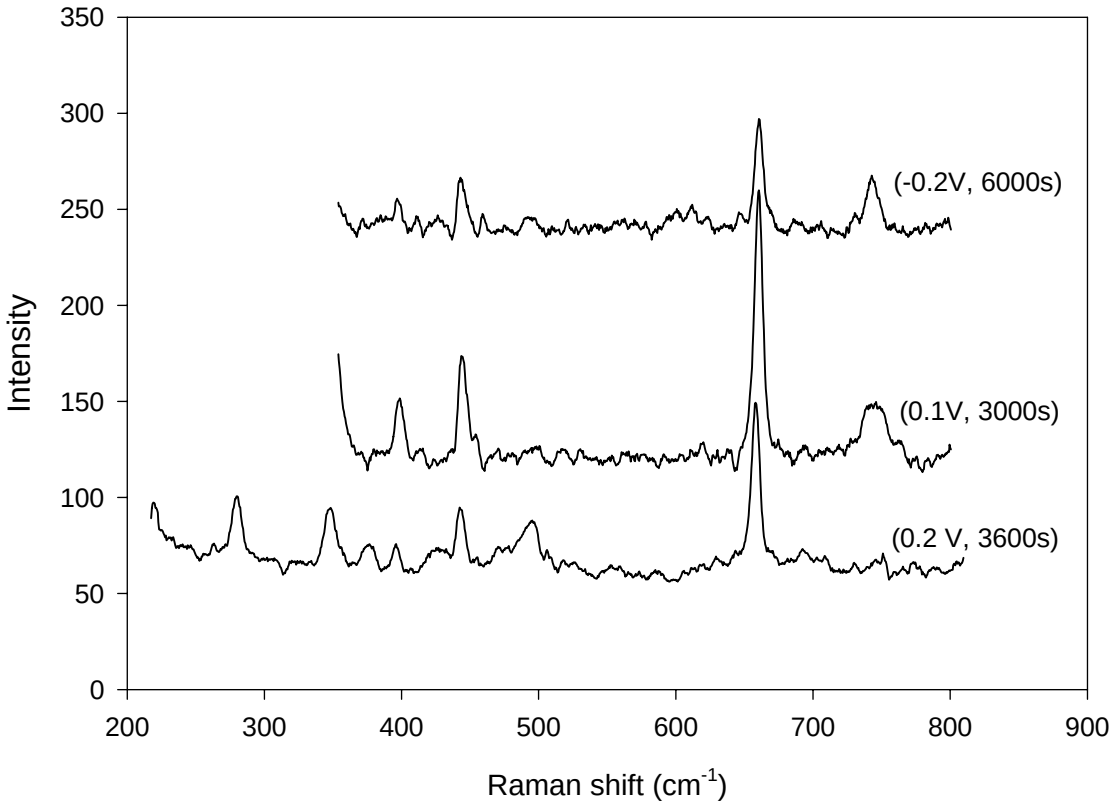

Figure 37: Raman spectra of Pd-Bi-Te electrode polarised at 0.2 V for 3600s, and subsequently at 0.1V and –0.2V (SHE) in 0.05 M $Na_2B_4O_7$ solution containing 10^{-3} M potassium ethyl xanthate. Laser power of 100mW and recording time of 120 seconds.

5.2.3. Oxidation of Pd-Bi-Te

The comparatively weak bands located at 283 cm^{-1}, 350 cm^{-1} and 743 cm^{-1} (see the *in situ* spectrum in Figure 32) could not be related to either ethyl xanthate or diethyl dixanthogen. The band at 743 cm^{-1} shows considerable broadening, perhaps indicative of poor crystallinity of the related phase. The peaks could not be identified from literature data: palladium and tellurium sulphides have strong bands at 401cm^{-1} and between 229-264 cm^{-1}, respectively (van der Maas *et al.*, 1987). No data could be found in relation to bismuth.

Figure 28a shows that a net anodic current arises when the Pd-Bi-Te electrode is polarized at 0.3V in a 0.05 M $Na_2B_4O_7$ containing solution. The absence of xanthate indicates that the anodic current is a result of background processes involving the mineral itself i.e. oxidation of the mineral. The possibility that the 743 cm-1 band originates from a mineral oxidation product was investigated.

The nature and dynamics of this band were investigated by polarizing the Pd-Bi-Te surface at 0.3V in the 0.05 M $Na_2B_4O_7$ solution whilst recording Raman spectra over time (see results in Figure 38). The figure clearly indicates that no marked increases in the intensities of the 743 cm^{-1} bands (shaded in Figure 38) relative to the background could be identified over time. This constancy makes this band a useful point of comparison for the xanthate and dixanthogen bands, as discussed earlier.

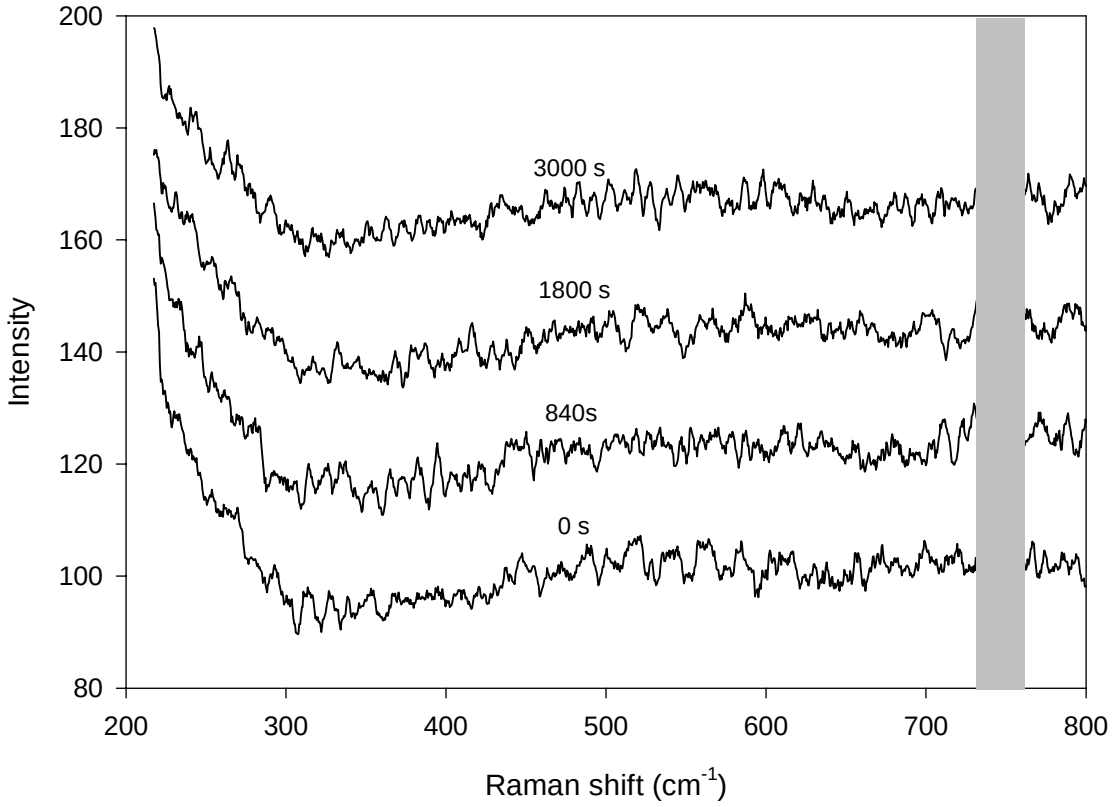

Figure 38: Raman spectra recorded of the surface of the Pd-Bi-Te electrode polarised at 0.3V (SHE) in a 0.05 M $Na_2B_4O_7$ solution containing no xanthate. Laser power rating of 100mW and recording time of 120 seconds. The 743 cm^{-1} band is highlighted.

To test the possible origins of the 743 cm^{-1} band, various pretreatments were applied to the Pd-Bi-Te sample, followed by the measurement of the Raman spectra. In all cases, the sample was first ground and polished (according to the procedure listed in Chapter 4), followed by immersion in the borate buffer solution polarised at 0.3 V (SHE), or drying in a stream of purified argon for 5 minutes (sample was kept in argon during measurements), or exposure to air (10 minutes were allowed for air to diffuse into the cell previously filled with purified argon). The resulting Raman spectra are shown in Figure 39, together with a reference spectrum for a concentrate buffer solution and a spectrum for the Pd-Bi-Te after anodic polarisation [0.3 V (SHE) for one hour in a $1x10^{-3}$ M potassium ethyl xanthate solution]. The spectrum of the concentrated buffer solution was recorded in a glass macro cell hence the peak

between 300 cm^{-1} and 500 cm^{-1} (see $Na_2B_4O_7$ (aq) spectrum in figure 39) reflects the absorbance of the glass.

Figure 39 clearly indicates that the oxidation of the mineral in air causes a band at 743 cm^{-1}, which corresponds to the spectrum measured after anodic oxidation in borate. Exposure of the mineral to purified argon gas did not cause a band to appear at this position, indicating that the band formed in air is a result of the interaction of the laser with the surface in the presence of oxygen. However, the results are somewhat ambiguous: the borate buffer solution does give a peak around 750 cm^{-1} and – as shown later – a peak was also found at this position for sperrylite in borate buffer. It hence cannot be stated with certainty whether the peak originates only from a mineral oxidation product or only the borate buffer. Nevertheless, the consistent height of this peak during polarisation did make this a useful reference band.

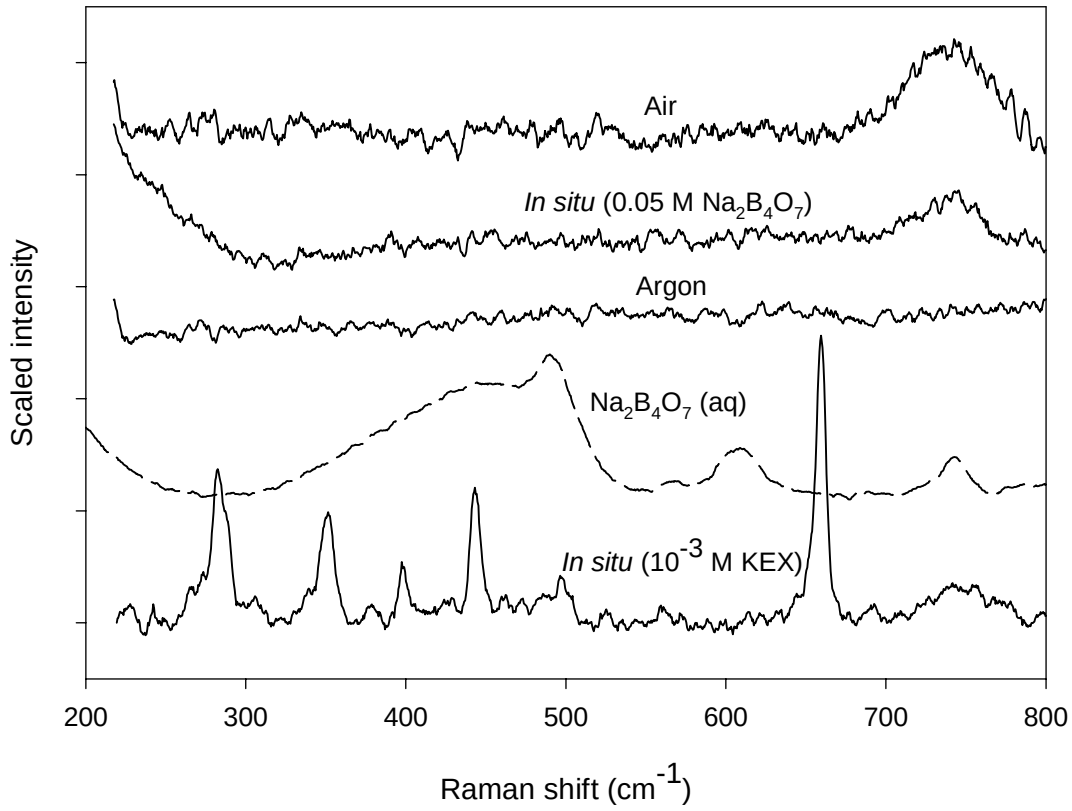

Figure 39: *In situ* Raman spectra recorded of Pd-Bi-Te in the presence of KEX, argon, borate and air, respectively (*In situ* spectrum: Pd-Bi-Te electrode polarised at 0.3 V (SHE) for 3600s in 0.05 M $Na_2B_4O_7$ solution containing 1 x 10^{-3} M potassium ethyl xanthate; $Na_2B_4O_7$ (aq) spectrum: glass macro cell containing saturated borate solution; argon spectrum: sampled dried in purified argon for 5 minutes; *In situ* 0.05 M $Na_2B_4O_7$ spectrum: Pd-Bi-Te electrode polarised at 0.3 V (SHE) for 3600s in a 0.05 M $Na_2B_4O_7$-containing solution; air spectrum: spectrum taken in air). Laser power rating of 100 mW and recording time of 120 seconds.

5.2.4. Results of Raman spectroscopy on $PtAs_2$

Similar Raman measurements were performed with the synthetic sperrylite sample. An *in situ* Raman spectrum from a $PtAs_2$ electrode polarized for 2600s at 0.3V (SHE) in 0.5 molar sodium tetraborate solution containing 1 x 10^{-3} molar potassium ethyl xanthate is shown in Figure 40. Figure 40 also shows the Raman spectra obtained from freshly synthesized potassium ethyl xanthate and diethyl dixanthogen. Table 9 shows the energies of some of the characteristic bands in the Raman spectrum of the $PtAs_2$ measured in the presence of xanthate at 0.3V (SHE) and corresponding bands of synthesized potassium ethyl xanthate and diethyl dixanthogen.

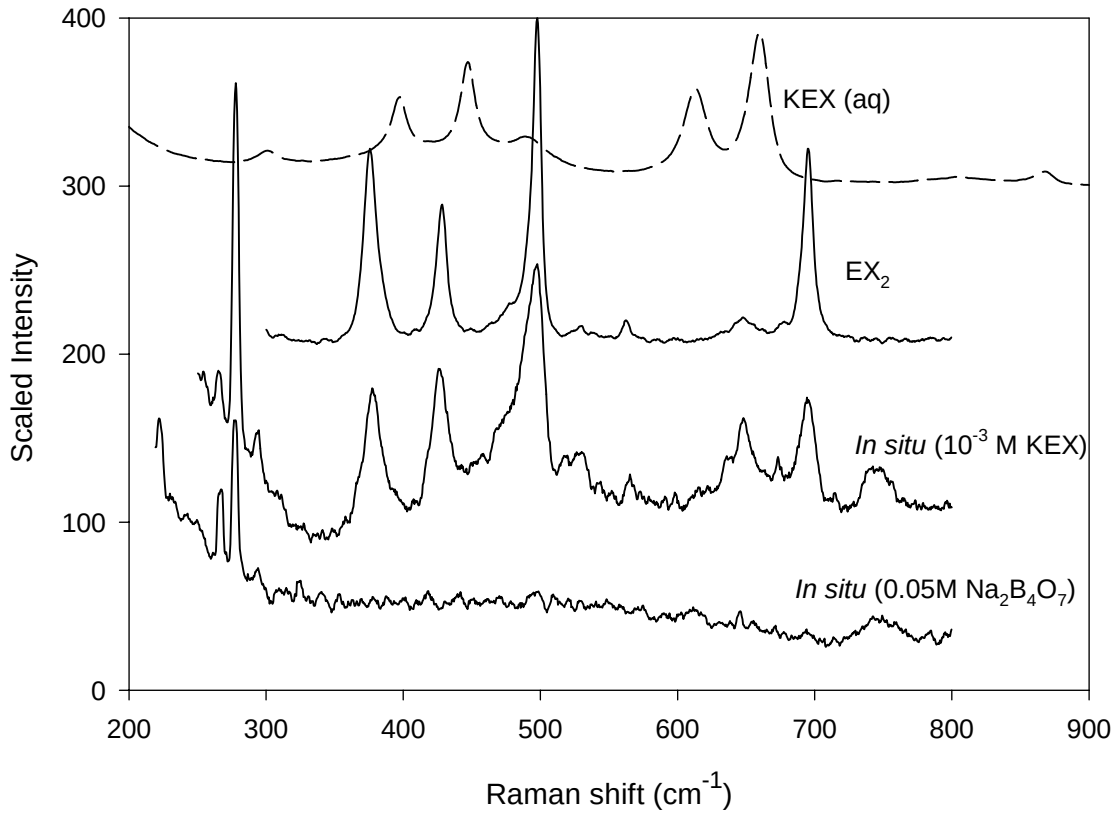

Figure 40: Raman spectra recorded of freshly synthesized potassium ethyl xanthate, diethyl dixanthogen and the *in situ* spectrum of the surface of $PtAs_2$ after polarization at 0.3V (SHE) in a 0.05 M $Na_2B_4O_7$ solution for 2600s in the presence (1 x 10^{-3} M potassium ethyl xanthate) and absence of xanthate. Laser power rating of 100mW and recording time of 120 seconds.

Table 9: Characteristic Raman bands of xanthate compounds and of $PtAs_2$, which was anodically polarised in the presence of ethyl xanthate. Assignment of the bands of the xanthate compounds was based on the work published by Woods *et al.* (1998).

Vibration	KEX (aq)	EX_2 (l)	*In situ* 300 mV
CS_2 antisymmetric stretch	1046	1041	1041
CCOC stretch	864	845	846
CS_2 symmetric stretch *trans*	660	695	695
CS_2 symmetric stretch *gauche*	615	646	647
OCS_2 out of plane *wag*	556	528	527
SS stretch	n.a.	498	498
COC deformation *gauche*	493	473	-
COC deformation *trans*	449	427	427
OCC deformation	399	378	377

n.a. not applicable

The bands located at 278 cm^{-1} and 745 cm^{-1} (see the in situ spectra) could not be related to either ethyl xanthate nor diethyl dixanthogen. The Raman spectrum of pure platinum and arsenic taken in air are also shown in Figure 41. The Pt-Pt bond only shows bands in the region of 180-195 cm^{-1}, in close agreement with published data (van der Maas *et al.*, 1987). The band located at 743 cm^{-1} was found for both electrodes studied (see Figures 32, 34 and 41) and can probably be assigned to the buffer solution, even though the results in Figure 39 indicate an additional contribution from oxidation of the Pd-Bi-Te electrode.

Figure 40 displays a band at 498 cm^{-1}, which demonstrates the presence of dixanthogen on the surface. The anodic peak shown in Figure 30a hence reflects oxidation of xanthate to dixanthogen. In contrast to the spectra observed on the Pd-Bi-Te no clear bands could be found from chemisorbed xanthate on the surface of the mineral. However, the formation of dixanthogen on the surface could be detected after short polarisation times as shown in Figure 41. When compared with Pd-Bi-Te, the kinetics of the formation of dixanthogen is much faster on the $PtAs_2$. The presence of a chemisorbed xanthate layer on sperrylite cannot be ruled out – the layer may

simply be undetected because of poor enhancement of the Raman signal. Although the phenomenon of SERS is not fully understood, it is known that not all substrates facilitate SERS.

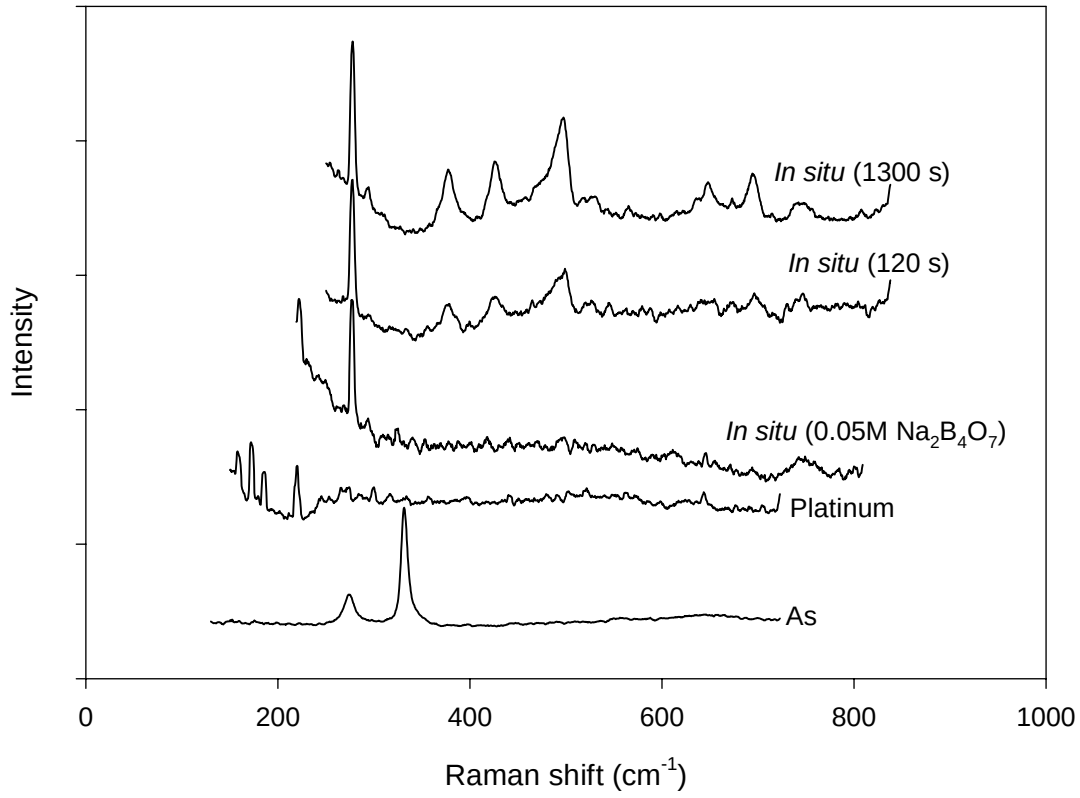

Figure 41: Raman spectra of $PtAs_2$ electrode polarised at 0.3 V (SHE) in 0.05M $Na_2B_4O_7$ solution containing 1 x 10^{-3} M potassium ethyl xanthate for different times (see top two plots). Spectra of $PtAs_2$ in 0.05M $Na_2B_4O_7$ solution (third plot) and of pure platinum and arsenic taken in air (second from bottom and bottom, respectively). Laser power of 100mW and recording time of 120 seconds.

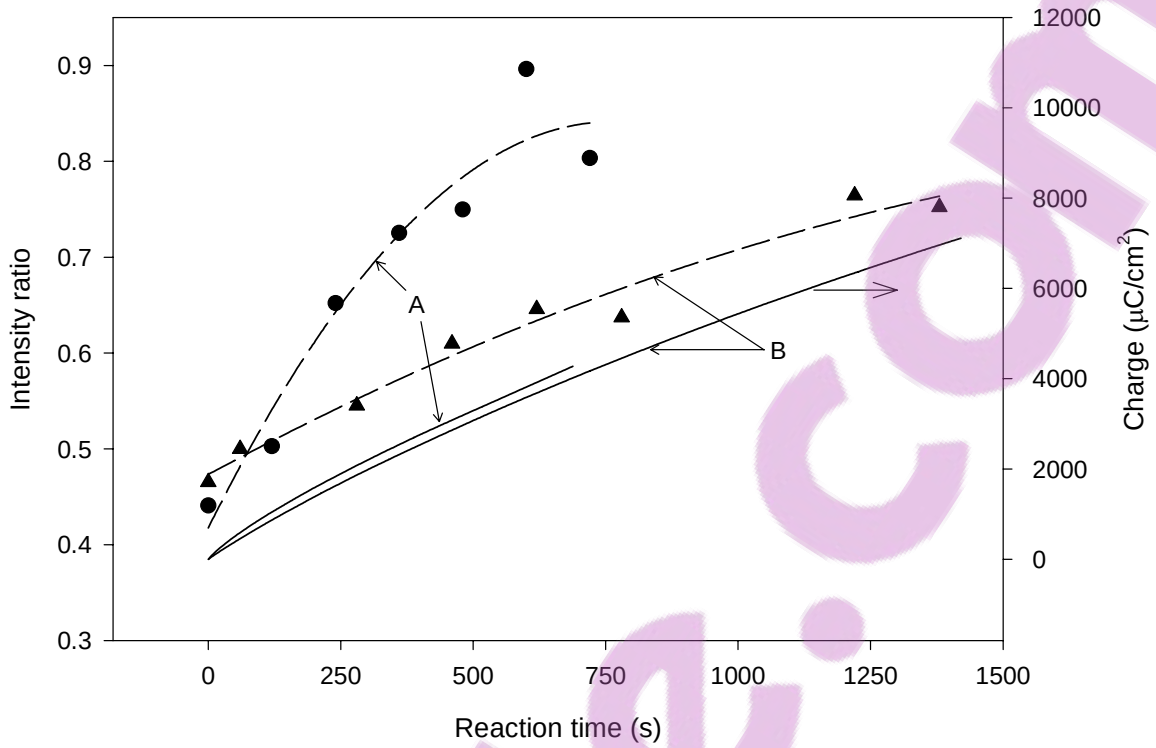

Figure 42: Intensity ratio of 498 cm^{-1} (dixanthogen) band relative to that of the 275 cm^{-1} (sperrylite) band as a function of the anodic polarization time (data points and broken lines). Anodic polarization of sperrylite was carried out at 0.3V (SHE) in a 0.05 M $Na_2B_4O_7$ solution containing 1 x 10^{-3} M potassium ethyl xanthate. The total anodic charge passed during polarization is also shown (full lines). "A" and "B" are data sets from two different sets of measurements.

Figure 42 plots the intensity ratio of the 498 cm^{-1} band (dixanthogen) relative to the 275 cm^{-1} band (sperrylite base-line) and the associated measured anodic charge transfer for two different sets of measurements, A and B, as functions of reaction time. It is unlikely that the conditions for the *in situ* measurements, for example fluid flow patterns over the electrode, were the same for every run, hence the difference in measured anodic current is not surprising. Nevertheless, Figure 42 clearly indicates that larger anodic charges can be related to increased amounts of dixanthogen on the mineral surface.

5.3. Flotation kinetics of Pd-Bi-Te

5.3.1. Introduction

The flotation behaviour of the liberated PGMs is mostly affected by the type of PGM and grain size. The previous sections of this chapter investigated the electrochemically interaction of ethyl xanthate with synthetic Pd-Bi-Te and $PtAs_2$ by employing impedance measurements, voltammetry, Raman spectroscopy and electrochemically controlled contact angle measurements.

To summarise the results for Pd-Bi-Te: Impedance measurements on Pd-Bi-Te which had been anodically polarised in the presence of ethyl xanthate for prolonged times indicated the formation of a continuous surface layer. The mixed (open-circuit) potential of the mineral is more positive than the xanthate-dixanthogen couple, indicating the possibility of forming dixanthogen on the mineral surface. Electrochemically controlled contact angle measurements showed maximum contact angles of 63°, underlining the hydrophobic nature of the surface. Raman spectroscopy confirmed the co-presence of xanthate with dixanthogen on the mineral surface.

From these measurements it is clear that the poor flotation response is not caused by an absence of interaction between the collector and the mineral surface. However, the (static) contact angle measurements do not characterise flotation behaviour directly, because of the kinetic resistance to bubble-particle attachment (Nguyen *et al*., 1998): the induction time (which is extensively used in bubble-particle attachment modelling) better describes the flotation collection. As a result smaller particles show slower flotation rates compared to larger particles. Penberthy *et al.* (1999) found that small liberated platinum-group minerals did float albeit at lower rates. In that work, the average measured particle diameter of the liberated particles in the UG-2 concentrates in the fast- (first-minute concentrate), medium- (second-minute concentrate) and slow-floating concentrates (after 20 minutes) was 8µm, 4µm and 2µm, respectively. The average particle size of the liberated platinum-group minerals found in the rougher tailings of Mimosa Mine was between 3 µm and 4 µm (Van Wouw, 2000). Indeed, the probable reason for loss of the Pd-Bi-Te minerals to tailings is poor flotation kinetics, which in turn may be related to particle size effects.

This study investigated the flotation kinetics with micro-flotation tests. The flotation response of synthetically prepared Pd-Bi-Te minerals was compared with that of typical minerals found in platinum ores, including chalcopyrite (a typical fast-floating mineral) and pyrrhotite (a typical slow-floating mineral). The particle size range was the same in all cases, namely 38 – 106 μm.

5.3.2. Results and discussion

Figure 43 compares the cumulative mass recovery for selected natural minerals with that of synthetic Pd-Bi-Te. The error bars refer to the standard deviation of the triplicate tests.

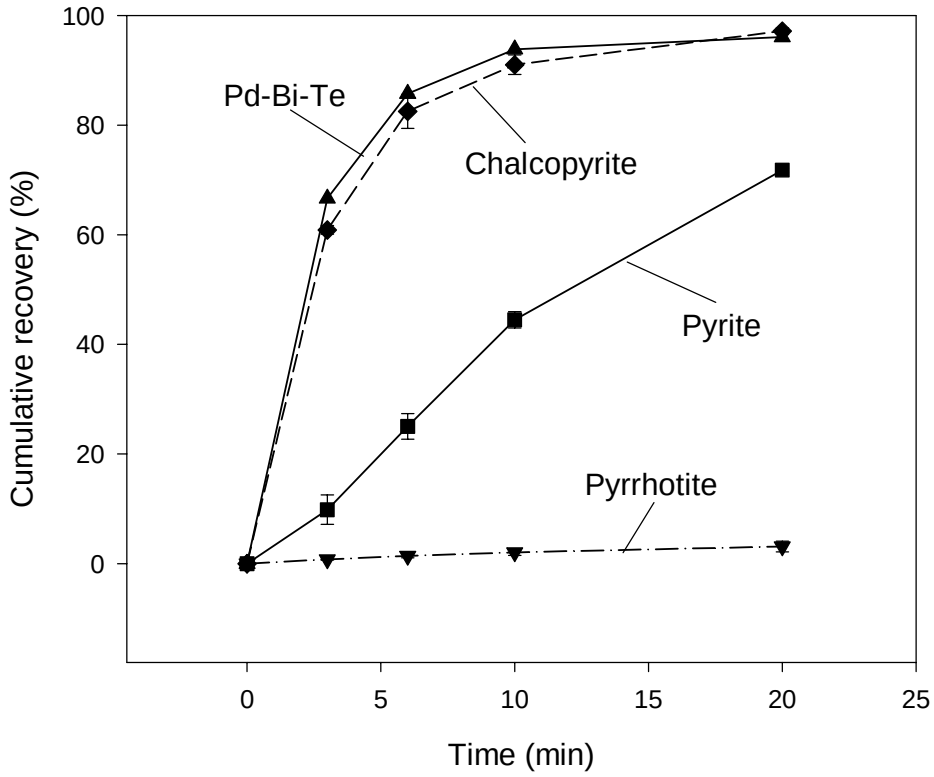

Figure 43: Recovery-time curves during microflotation of selected natural and synthetic minerals in a synthetic solution containing 5×10^{-5} M sodium isobutyl xanthate at pH 9. The particle size range: 38 – 106 μm.

The Figure 43 clearly indicates the poor flotation response of pyrrhotite at pH 9, which corresponds to literature: Senior *et al*. (1994) found that pyrrhotite was rejected at pH 9 in mixtures of pentlandite and pyrrhotite (80g/t potassium ethyl xanthate dosage, without activation). In contrast, Pd-Bi-Te shows a rapid flotation response, similar to that of chalcopyrite, which is known for its fast-floating characteristics. This similarity in the flotation kinetics is reflected by the rate constants which are summarised in Table 10; these rate constants were found by fitting the following Klimpel flotation rate equation to the batch data (Klimpel, 1984):

$$r = R\left\{1 - \left(\frac{1}{kt}\right)\left[1 - \exp(-kt)\right]\right\} \qquad (4)$$

with r = mineral recovery at time t (%)

R = infinite time recovery (%)

k = rate constant (min^{-1})

Table 10. Summary of micro-flotation rate constants of chalcopyrite and Pd-Bi-Te.

	k (min^{-1})	R (%)
Pd-Bi-Te	1.18	97.0
Chalcopyrite	0.92	98.1

In line with the electrochemical and contact-angle measurements, the microflotation work confirms that the Pd-Bi-Te should be recoverable with the regular xanthate collectors.

5.3.3.1. Particle size effects

It is proposed that the small size of the liberated PGMs might be responsible for the poor practical flotation response of these minerals: particle-bubble attachment is influenced by the particle size which affects the collision efficiency (E_c), attachment efficiency (E_a) and particle-bubble stability efficiency (E_s) (Pyke *et al*., 2003). The total collection efficiency of the process is the product of these three sub-processes.

The detailed mathematical description of these sub-processes (Duan *et al*., 2003; Pyke *et al*., 2003) was used here to estimate size effects.

This analytical model (Ralston model) yields flotation rate constants which follow the characteristic trend with particle size, with lower flotation rates for particles at the top and bottom ends of the particle size distribution. The flotation rate constants are largest for particle diameters around 40 μm and 60 μm, for chalcopyrite and quartz respectively (Duan *et al*., 2003; Pyke *et al*., 2003). In contrast, liberated PGM grains are usually much smaller, less than 10 μm in diameter: as stated earlier the average size of the liberated platinum-group minerals in the rougher tailings of Mimosa Mine was between 3μm and 4μm (Van Wouw, 2000).

For the sake of comparison, the rate constants were estimated for a 2.25 dm^3 Rushton cell, as in the previous work (Duan *et al*., 2003; Pyke *et al*., 2003). Tables 11 - 13 summarise the numerical values of the parameters in the calculations. Note in Table 12 that the contact angle on the Pd-Bi-Te is smaller than for chalcopyrite (as listed in table 13); this results in a larger value of the constant A which describes the induction time (Dai *et al*., 1999).

Table 11: Properties of the Rushton cell, as used in the model calculations (Duan *et al*., 2003). V_{cell} is the cell volume, G_{fr} the gas flow rate, v_b the bubble speed, ε the turbulent dissipation energy, and d_b the bubble diameter

V_{cell} (m^3)	G_{fr} (m^3/s)	v_b (m/s)	ε (m^2/s^3)	d_b (m)
2.25×10^{-3}	9.2×10^{-5}	0.2	14	9.70×10^{-4}

Table 12: Ore-related properties as used in model calculations.
Pd-Bi-Te (See text; values of A and B estimated from Dai *et al*., 1999):

A ($s/cm^{-0.6}$)	B (-)	ρ (kg/m^3)	ϕ (°)
0.07	0.6	8474	63

Table 13: Chalcopyrite properties (Duan *et al*.,2003):

A ($s/cm^{-0.6}$)	B (-)	ρ (kg/m^3)	ϕ (°)
0.05	0.6	4100	71

The calculated rate constants, and efficiencies of collision, attachment and stability are given in Figures 44 and 45 as functions of particle size. The lower attachment and stability efficiencies for Pd-Bi-Te result from the higher density and lower contact angle of that mineral. These give generally lower overall collection efficiencies for Pd-Bi-Te, and lower rate constants for particles larger than 20 µm. While this behaviour is not in full agreement with the experimental results in Figure 43 (note that those experimental results are for particles in the range 38-106µm), the rate constants are quite sensitive to the contact angle (and the related induction time constant *A*, which is rather scattered in the available data, Dai *et al*., 1999). The specific contact angle is also dependent on the xanthate species which is present on the mineral surface. For example, for 10 ppm collector concentration, Woods (1974) reported maximum contact angles on platinum of 70^o for diethyl xanthate, and 85^o for dibutyl xanthate. Hence the main conclusion from these predicted rate constants is that these are similar for chalcopyrite and Pd-Bi-Te, and especially so for the small particles, although the rate constant for larger Pd-Bi-Te particles is significant smaller.

This finding is consistent with the slow flotation response of small hydrophobic PGMs as found by Penberthy *et al*. (2000) for UG-2 chromite: small PGMs do float, but at a significantly lower rate.

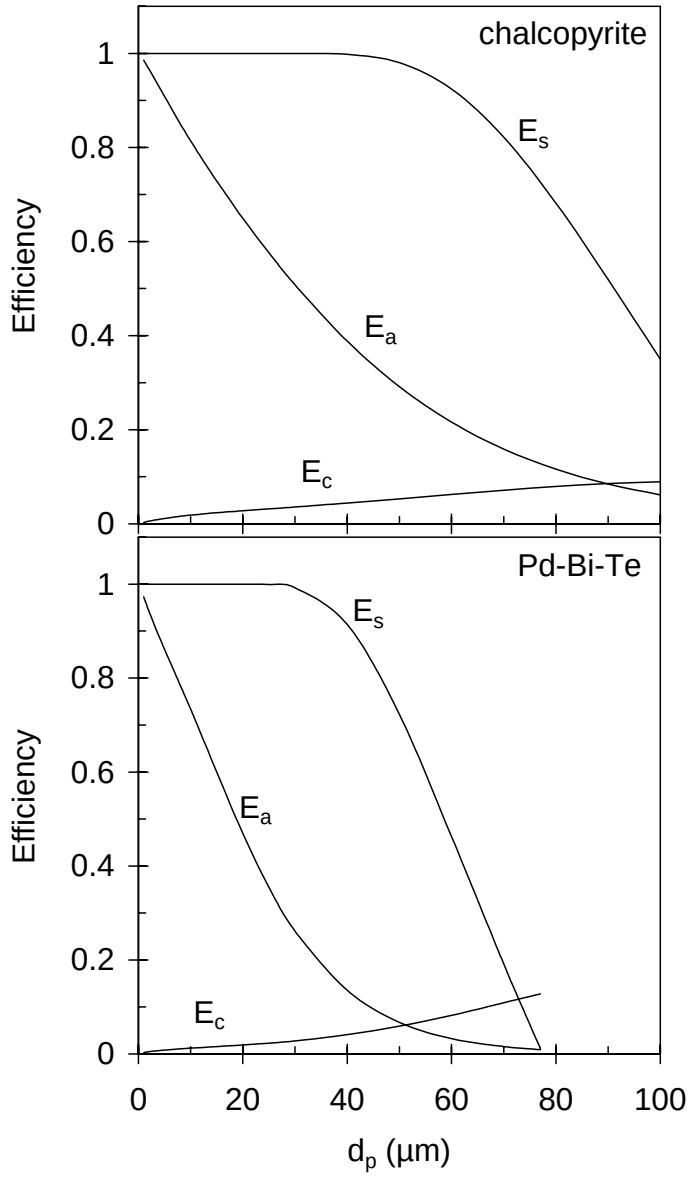

Figure 44. Calculated efficiencies of collision (E_c), attachment (E_a) and stability (E_s) at different particle sizes, for chalcopyrite (upper graph), and Pd-Bi-Te (lower graph).

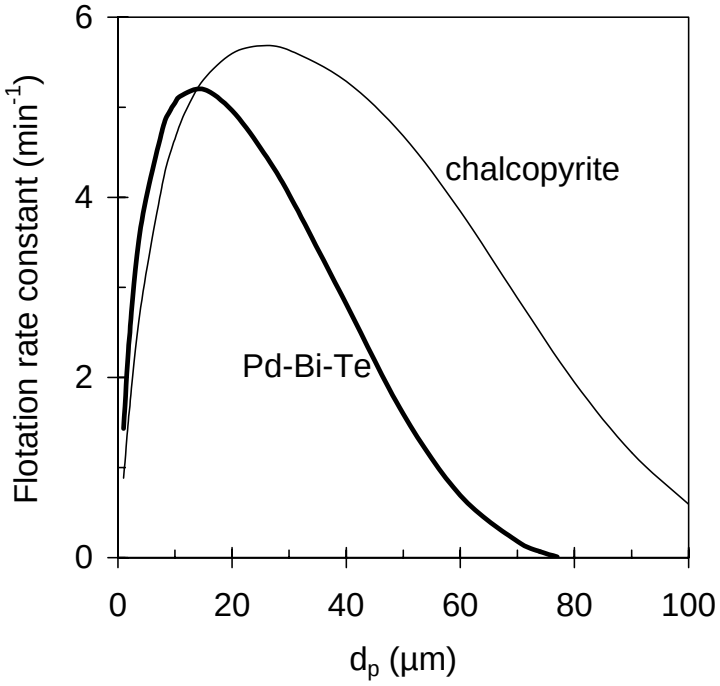

Figure 45. Calculated flotation rate constants at different particle sizes, for chalcopyrite (lighter line), and Pd-Bi-Te (heavier line).

6. Conclusions

The adsorption of ethyl xanthate on Pd-Bi-Te and $PtAs_2$ has been studied using voltammetry, impedance measurements and Raman spectroscopy. Pd-Bi-Te and $PtAs_2$ electrodes show strong anodic currents when polarized at 0.3V(SHE) in a 0.05 M $Na_2B_4O_7$ solution containing 1 x 10^{-3} M potassium ethyl xanthate. No chemisorption prewave could be identified. Pd-Bi-Te shows very strong anodic activity when polarized at potentials > 0.2V (SHE) in the presence of potassium ethyl xantante. Prolonged exposure (20 minutes) of Pd-Bi-Te at this potential resulted in lower capacitance values. The lowering of the capacitance is a result of the formation of a continuous surface layer. Cathodic and anodic polarization curves predicted a mixed potential higher than that of the equilibrium xanthate-dixanthogen couple. As a result the increased anodic activity and the formation of the layer are likely to reflect the formation of diethyl dixanthogen on the surface.

Raman spectroscopy has confirmed that the strong anodic currents found on both minerals reflect the oxidation of xanthate to dixanthogen. Furthermore, Raman spectroscopy has confirmed the co-presence of xanthate with dixanthogen indicating that xanthate retains its molecular integrity when it adsorbs on the surface of the Pd-Bi-Te. The identification of both species on the surface of the Pd-Bi-Te suggests that SERS occurs on Pd-Bi-Te. However, this phenomenon could not be identified on the $PtAs_2$. The formation of dixanthogen on the surface of the $PtAs_2$ is "instantaneous" (meaning that it occurs within the 120s required to measure a Raman spectrum) whilst dixanthogen could only be identified on the Pd-Bi-Te after longer periods of polarization. However, chemisorbed xanthate could be identified on the surface of the Pd-Bi-Te within 120 seconds; this yields a hydrophobic surface as indicated by electrochemically-controlled contact angle measurements. Maximum contact angles of 63^{o} were measured in the case of Pd-Bi-Te. The presence of xanthate and dixanthogen on the surface and the fact that the surface is hydrophobic suggest that the poor flotation recovery of the Pd-Bi-Te minerals from flotation feeds cannot be attributed to a lack of interaction of the collector with the surface.

The flotation kinetics of Pd-Bi-Te has been studied and compared with that of natural copper and iron sulphides by performing single mineral microflotation tests. The microflotation tests showed that Pd-Bi-Te floats rapidly, with rates slightly exceeding that of (fast-floating) chalcopyrite. This supports the previous electrochemical results, which showed xanthate oxidation (to dixanthogen) at the mineral surface. The Ralston model predicts a sharp drop-off in flotation rate constants for small (<5 μm diameter) Pd-Bi-Te particles. The conclusion is that small particle size is a probable cause for the low recoveries of Pd-Bi-Te at platinum concentrators along the Great Dyke of Zimbabwe.

7. Recommendations for future work

Investigations on natural grains and industrial conditions

The very small size and scarcity of individual grains contribute to the complexity of studying fundamental interactions, which necessitates the use of synthetic minerals. The main advantage of synthesizing these minerals in bulk is the ability of performing microflotation tests to evaluate the flotation kinetics of the minerals. However, natural grains contain minor impurities as Sb, Fe, Ni and S, which may impact on the flotation response. To evaluate the validity of using synthetic grains, single natural grains must be subjected to electrochemical investigations and *in situ* Raman spectroscopy in future work.

Multi-components systems are known for the very complex nature of the interactions between the gangue, minerals and the solution. It is, therefore, crucial to investigate the effect of competing reactions in the pulp solutions on the flotation recovery of Pd-Bi-Te. The oxidation behaviour of the minerals forms an integral part in the full comprehension of the flotation behaviour of this class of PGMs. The oxidation behaviour will dictate the necessity of adding collectors to the mill to avoid excessive oxidation or maybe opting for the utilisation of nitrogen as carrier gas.

The Ralston flotation models have proven to be very useful in the prediction of the flotation rate constants from fundamental relationships, however the fluid velocity and energy dissipation of industrial flotation cells are not known, limiting the usefulness of this model. The cell design can impact greatly on the recoverability of the PGMs and this effect needs to be quantified.

Bubble size

The latest trend in the recovery of liberated particles from tails is to increase the power rating of the flotation cell and as a result increasing the turbulent conditions to enable more effective particle-bubble contact. It is also believed that smaller bubbles are required to float small particles more efficiently (Tortorelli *et al.*, 1997). The

predicted effect of bubble size on the recovery of the Pd-Bi-Te particles is shown in Figure 46 (see Tables 11 and 12; all other parameters were kept constant and only the bubble size was changed). These results clearly indicate that – for smaller bubbles - the rate constant for fine particle flotation increases significantly whilst the rate constant of the larger particles is sharply lower. Hence the bubble flotation will only be beneficial to the process if the liberated particles are extremely fine as in the case of liberated PGMs from the Great Dyke.

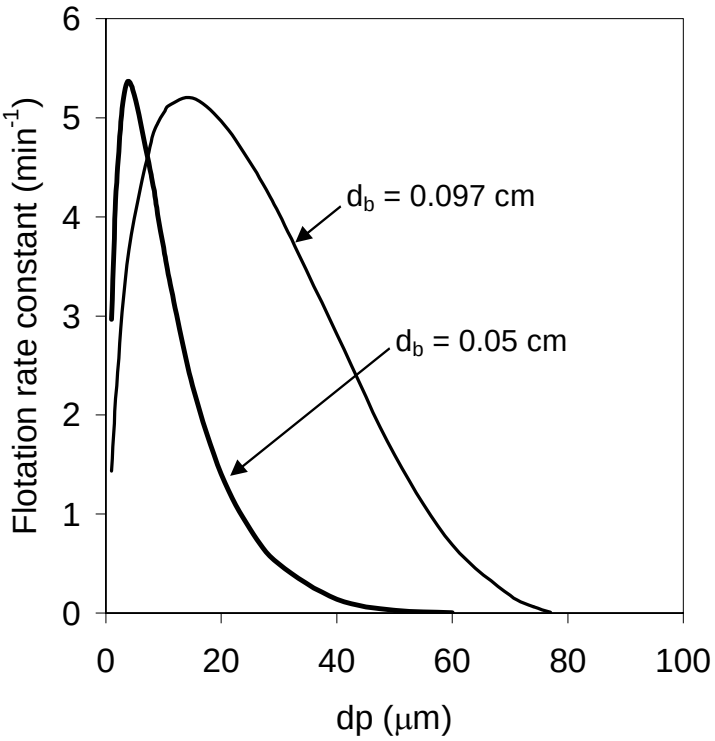

Figure 46. Calculated flotation rate constants at different particle sizes, for two bubble sizes.

Two-phase system

Recent advances in the research of aqueous two-phase systems have indicated the possibility to extract very small particles by employing this separation step. Aqueous two-phase extraction employs two polymer-rich aqueous phases which are immiscible in each other, and with different physicochemical interactions with respect to inorganic particles, to achieve selective separation (Osseo-Asare, 1994; Zeng *et al.*, 2001). The basic principle of extraction involves the selective partitioning of

inorganic particles due to physicochemical interactions (for example the interaction of hydrophobic particles with organic polymers) between the surface particles and one of the aqueous phases. The particles can then be selectively removed from the system through the separation of the two aqueous phases. The surface chemistry of the inorganic particles can thus be exploited to concentrate the particles preferentially in one of the two phases.

Aqueous two-phase extraction is very attractive for the separation of very fine particles (even in the nanoparticle range) since two liquids are employed, similar to liquid-liquid extraction processes; there is no limit on the lower-end of the particle size range (Osseo-Asare, 1994; Zeng *et al.*, 2001).

This technology opens up the possibility of the extraction of very small liberated particles, which are not readily recoverable in conventional flotation circuits because of the effect of particle size. Knowing the surface chemistry of the poorly recoverable PGMs an aqueous two-phase system can be engineered to target and recover these particles. However, the complexity associated with industrial pulps will pose many challenges to employing this process on an industrial scale and as a result extensive research in this field is still required

8. References

ARC, 2002, *Personal communication*.

Bradshaw, D.J., and O'Connor, C.T., 1996, *Measurement of the sub-process of bubble loading in flotation*, Minerals engineering, vol. 9, pp. 443-448.

Buckley, A.N., Parks, T.J., Vassallo, A.M., and Woods, R., 1997, V*erification by surface-enhanced Raman spectroscopy of the integrity of xanthate chemisorbed on silver*, International Journal of Minerals Processing, vol 51, pp 303-313.

Buswell, A.M., Bradshaw, D.J., Harris, P.J., and Ekmeci, Z., 2002, *The use of electrochemical measurements in the flotation of platinum-group mineral (PGM) bearing ore*, Minerals Engineering, vol. 15, pp. 395-404.

Cabri, L.J., 1981,. *Platinum-Group Elements: Mineralogy, Geology and Recovery,* Canadian Institute of Metallurgy, Special volume, vol 23, pp 267.

Cabri, L.J., 1988, *New developments in determinaion of the distribution of precious metals in ore deposits*, Proceedings of the Seventh Quadrennial IAGOD Symposium, pp 149-154.

Cabri, L.J., 1992, *The distribution of trace precious metals in minerals and mineral products*, Mineralogical Magazine, vol 56, pp 289-308.

Cabri, L.J., 1994, *Current status of determination of mineralogical balances for platinum-group element bearing ores*, Transactions of the Institution of Mining and Metallurgy (Section B: Applied Earth Science), vol 103, pp B3-B9.

Cabri, L.J., Rowlan, J.F., Laflamme, J.H.G., and Steward, J.M., 1979, *Keitconnite, telluropalladinite and other Pd-Pt tellurides from the Stillwater Complex, Montana*, Canadian Mineralogist, vol 17, pp 589-594.

Dai, Z., Fornasiero, D., and Ralston, J., 1999, *Particle-bubble attachment in mineral flotation*, Journal of colloid and interface science, vol. 217, pp 70-76.

Damjanovic, A., Yeh, L-S. R., and Wolf, J.F., 1982, *Formation of thin oxides at platinum anodes in alkaline solutions. III pH dependence*. Journal of the Electrochemical Society, vol. 129, pp 55-61.

De Wet, J.R., Pistorius, P.C., and Sandenbergh, R.F., 1997, *The influence of cyanide on pyrite flotation from gold leach residues with sodium isobutyl xanthate*, International Journal of Minerals Processing, vol 49, pp 149-169.

Dippenaar, J., 2002, *Personal communication.*

Duan, J., Fornasiero, D., and Ralston, J., 2003, *Calculation of the flotation rate constant of chalcopyrite particles in an ore*, International journal of mineral processing, vol. 72, pp 227-237.

Ekmekçi, Z., Bradshaw, D.J., Allison, S.A., and Harris, P.J., *Effects of frother type and froth height on the flotation behaviour of chromite in UG2 ore*, Minerals Engineering, vol. 16, pp. 941-949.

Elvy, S.B., Williams, P.A., and Buckley, A.N., 1996, *XPS evidence for the incongruent surface oxidation of minerals in the Pd-Te-Bi system*, Surface and interface analysis, vol. 24, pp 641-646.

Evans, D.M., Buchanan, D.L., and Hall, G.E.M., 1994, *Dispersion of platinum, palladium and gold from the Main Sulphide Zone, Great Dyke, Zimbabwe*, Transaction of the Institution of Mining and Metallurgy (Section B: Earth Sciences), 103, pp B57-B67.

Evans, D.M., and Spratt, J., 2000, *Platinum and palladium oxides/hydroxides from the Great Dyke, Zimbabwe and thoughts on their stability and possible extraction*, In: Rammlair et al. (eds), Applied Mineralogy, AA Balkema, Rotterdam, pp 289-292.

Feng, D., and Aldrich, C., 1999, *Effect of particle size on flotation performance of complex sulphide ores,* Minerals Engineering, vol 12, no. 7, pp 721-731.

Jones, R.T., 1999, *Platinum smelting in South Africa*, South African Journal of Science, vol 95, pp 525-534.

Hoffman, E., and Maclean, W.H., 1976, *Phase relations of michenerite and merenskyite in the Pd-Bi-Te system*. Economic Geology, Issue 71, pp 1461-1468.

Kinloch, E.D., 1982, *Regional trends in the platinum-group mineralogy of the Critical Zone of the Bushveld Complex*, South Africa, Economical Geology, vol 77, pp 1328-1347.

Klimpel, R.R., 1984, *Froth flotation: The kinetic approach*, Proceedings of Mintek 50, Johannesburg, South Africa.

Lidsay, N.M., and Sellschop, J.P.F., 1988, *Routine SIMS microanalysis: trace Au and Pt sulphides*, Nucl. Instr. Meth. Phys. Res. B35, pp 358-363.

Makovicky M., Makovicky, E., and Rose-Hansen, J., 1986, *Experimental studies on the solubility and distribution of platinum-group elements in base metal sulphides in platinum deposits, In Metallogeny of Basic and Ultrabasic Rocks*, Edited by M.J. Gallagher, R.A., Ixer, C.R., Neary and H.M. Prichard. The Institution of Mining and Metallurgy, London, pp 415-425.

Merkle, R.K.W., 2004, *Personal communication.*

Merkle, R.K.W. and Harney, D.M.W., 1990, *Pt-Pd Minerals from the Upper Zone of the Eastern Bushveld Complex*, Canadian Mineralogist, vol.28, pp 619-628.

Merkle, R.K.W and McKenzie, A.D., 2002*, The Mining and Beneficiation of South African PGE ores – An Overview*, The Geology, Geochemistry, Mineralogy and Mineral Beneficiation of Platinum-Group Elements, Edited by L.J. Cabri. Canadian Institute of Mining, Metallurgy and Petroleum, Special volume 54, pp 793-810.

Michell, R.H., and Keays, R.R., 1987, *Abundance and distribution of gold , palladium and iridium in some spinel and garnet lherzolites: Implications for the nature and origin of precious metal-rich intergranular components in the upper mantle*, Geochimica et Cosmochimica Acta, 45, pp 2425-2442.

Nguyen, A.V., Ralston, J., and Schulze, H.J., 1998, *On modelling of bubble-particle attachment probability in flotation*, International Journal of mineral processing, vol 53, pp 225-249.

Oberthür, T., 2002b, *Platinum-Group Element Mineralization of the Great Dyke, Zimbabwe*, The Geology, Geochemistry, Mineralogy and Mineral Beneficiation of Platinum-Group Elements, Edited by L.J. Cabri. Canadian Institute of Mining, Metallurgy and Petroleum, Special volume 54, pp 793-810.

Oberthür, T., 2002c, *Personal communication*.

Oberthür, T., Kojonen, K., and Weiser, T.W., 2002a, *Local variations and regional trends in PGE geochemistry and mineralogy in the Main Sulphide Zone of the Great Dyke, Zimbabwe*, Proceedings: 9th International Platinum Symposium, Billings, Montana, USA, 21-25 July, 2002.

Oberthür, T., Melcher, F., Weiser, T.W., and Gast, L., 2002d, *Distribution of PGE and PGM in oxidised ores from the Main Sulphide Zone of the Great Dyke*, Zimbabwe, Proceedings: 9th International Platinum Symposium, Billings, Montana, USA, 21-25 July.

Oberthür, T., Weiser, T.W., Cabri, L.J., and McMahon, G., 1997, *Pt, Pd and trace elements in sulphides of the Main Sulphide Zone, Great Dyke Zimbabwe – A reconnaissance study*, Canadian Mineralogists, 35, pp 597-609.

Oberthür, T., Weiser, T.W., Müller, P., and Lodziak, Je., 1998, *New observations on the distribution of platinum group elements (PGE) and minerals (PGM) in the MSZ at Hartley Mine, Great Dyke, Zimbabwe*, Proceedings: 8th International Platinum

Symposium of the South African Institute of Mining and Metallurgy, Johannesburg, South Africa, pp 293.

Osseo-Asare, K., 2004, *Complex Liquids in solvent extraction: extractants and microemulsions, polymers and aqueous two-phase systems*, Metal Separation Technologies III: Proceedings of the Symposium in Honour of Professor Lauri E. Holappa of the Helsinki University of Technology, Helsinki University of Technology, Laboratory of Metallurgy, Espoo, Finland.

Parry, S., 1980, *Simultaneous determination of the noble metals in geological materials by radiochemical neutron-activation analysis*, Analyst, vol 105, pp 1157-1162.

Pourbaix, M., 1974, *Atlas of electrochemical equilibria in aqueous solutions*, Houston : National Association of Corrosion Engineers.

Penberthy, C.J., Oosthuyzen, E.J., and Merkle, R.K.W., 2000, *The recovery of platinum-group elements from the UG-2 chromitite, Busheveld Complex – a mineralogical perspective*, Mineralogy and Petrology, vol. 68, pp 213-222.

Peyerl, W., 1983, *The metallurgical implications of the mode of occurrence of the platinum-group metals in the Merensky reef and UG-2 chromitite of the Bushveld Complex*, Special Publication of the Geological Society of South Africa, 7, pp 295-300.

Prendergast. M.D., 1988a, *An investigation of the Stratigraphy and Petrology of the Peroxinite No. 1 layer of the Great Dyke of Zimbabwe, with special reference to the characteristic features and origin of the platinum-Group Element-bearing Main Sulphide Zone*. PhD thesis, University of Zimbabwe.

Prendergast. M.D., 1988b, *The geology and economic potential of the PGE-rich Main Sulphide Zone of the Great Dyke, Zimbabwe*, Geo-platinum 87, pp 281-302.

Prendergast. M.D., 1990, *Platinum-group minerals and hydrosilcate 'alteration' in the Wedza-Mimosa platinum deposit, Greta Dyke, Zimbabwe – genetic and metallurgical implications,* Transaction of the Institution of Mining and Metallurgy (Section B: Earth Sciences), 99, pp B91-B105.

Pyke, B., Fornasiero, D., and. Ralston, J., 2003, *Bubble particle heterocoagulation under turbulent conditions*, Journal of colloid and interface science, vol. 265, pp. 141-151.

Ralston, J., 1991, *E_h and its consequences in sulphide mineral flotation,* Minerals Engineering, vol.4, pp. 859-878.

Schubert, H., 1999*, On the turbulence-controlled microprocesses in flotation machines*, International journal of mineral processing, vol. 56, pp 257-276.

Senior, G D; Shannon, L K; and Trahar, W J, 1994, *The flotation of pentlandite from pyrrhotite with particular reference to the effects of particle size*, International journal of mineral processing, vol. 42, pp 169-190.

Sizgoric, M.B., 1984*, Tracking platinum-group minerals in the milling of Cu-Ni ores from at Sadbury*, Reference 10, pp 923-932.

Steyen, J., Knopjes, B., and Goodall, C.M., 2001, *Milling and flotation test work at Lonmin Platinum's pilot plant,* South Africa Institute of Mining and Metallurgy Colloqium – Developments in the Metallurgical Processing in the Platinum Industry.

Stribrny,B., Wellmer, F.W., Burgath, K.P., Oberthur, T., Tarkain, M., Pheiffer, T., 2000, *Unconventional PGE occurances and PGE mineralization in the Great Dyke: metallogenic and economic aspects*, Mineralium Deposita, Vol 35, pp 260-281.

Tortorelli, J.P., Craven, J.W., Toguri, J.M., Dobby, G.S., and Agar, G.E., 1997, *The effect of gas/slurry contact on the flotation of fine particles*, Minerals Engineering, vol 10, pp 1127 – 1138.

Van der Maas, J., and Visser, T., 1987, *Group frequency correlation table*, Laboratory Methods in Vibrational Spectroscopy, John Wiley & Sons LTD.

Van Wouw, K., 2000, *Internal report: Mineralogical investigation of the platinum-group minerals from Mimosa Platinum Mine.*

Van Wouw, K., 2003, *Internal report: Mineralogical investigation of the platinum-group minerals in flotation products from Mimosa Platinum Mine*.

Van Wouw, K., 2004, *Personal communication.*

Volyanskii, B. M., Ostorozhnaya, E.E., Geonya, N.I., Gorstein, A.E., and Illyuvieva, G.V., 1985, *Sulphydryl Collector reaction with the surface of sperrylite*, Soviet Journal of Non-ferrous metals, vol 26, no 1, pp 96-98.

Weast,R.C., 1982, *CRC Handbook of Chemistry and Physics*, 62nd edition, CRC Press, Florida, pp B78 – B79.

Weiser, T.W., Oberthür, T., and Kojonen, K.K., 1998, *Distribution of trace PGE in pentlandite and of PGM in the Main Sulphide Zone (MSZ) at Mimosa Mine, Great Dyke, Zimbabwe*, Proceedings: 8th International Platinum Symposium of the South African Institute of Mining and Metallurgy, Johannesburg, South Africa, pp 443-445.

Wilson, M.G.C., 1998, *The mineral resources of South Africa,* Council of Geoscience, Sixth edition.

Wilson, A.H., Coghill, B.M., *Platinum-group minerals in the Selukwe Subchamber, Great Dyke, Zimbabwe: implications for PGE collection mechanisms and post-formational redistribution*, Mineralogical Magazine, December, 1993, Vol. 57, pp 613-633.

Woods, R., 1971, *The oxidation of ethyl xanthate on platinum, gold, copper and galena electrodes. Relation to the mechanism of mineral flotation*, The Journal of Physical Chemistry, Vol. 75, pp 354-362.

Woods, R., 1972, *The anodic oxidation of ethyl xanthate on metal and galena electrodes*, The Australian Journal of Chemistry, Vol. 25, pp 2329-2335.

Woods, R., Basilio, C.I., Kim, D.S., and Yoon, R.-H., 1994, *Chemisorption of ethyl xanthate on silver-gold alloys*, Colloids and surfaces A: Physicochemical and Engineering Aspects, vol 83, pp 1-7.

Woods, R., and Gardner, J.R., 1974, *An Electrochemical investigation of Contact Angle and of Flotation in the presence of Alkylxanthates. I Platinum and Gold Surfaces*, Australian Journal of Chemistry, vol 27, pp 2139-2148.

Woods, R., and Gardner, J.R., 1977, *An Electrochemical investigation of Contact Angle and of Flotation in the presence of Alkylxanthates. II Galena and Pyrite Surfaces*, Australian Journal of Chemistry, vol 30, pp 981-991.

Woods, R., and Gardner, J.R., 1997, *The hydrophobic nature of gold and platinum*, Journal of electroanalytical chemistry, vol 81, pp 285-290.

Woods, R., Hope, G.A., and Brown, G.H., 1998a, *Spectroelectrochemical investigations of the interaction of ethyl xanthate with copper, silver and gold: II. SERS of xanthate absorbed on silver and copper surfaces*, Colloids and surfaces A: Physicochemical and Engineering Aspects, vol 137, pp 329-337.

Woods, R., Hope, G.A., and Brown, G.H., 1998b, *Spectroelectrochemical investigations of the interaction of ethyl xanthate with copper, silver and gold: III. SERS of xanthate absorbed on gold surfaces*, Colloids and surfaces A: Physicochemical and Engineering Aspects, 1998, vol 137, pp 339-344.

Woods, R., Hope, G.A., and Watling, K., 2000, *Surface enhancement Raman Scattering Spectroscopic studies of the adsorption of flotation collectors*, Minerals Engineering, vol 13, pp. 345-356.

Woods, R., Young, C.A., and Yoon, R. –H., 1990, Ethyl xanthate chemisorption isotherms and Eh-pH diagrams for copper/ water/ xanthate and chalcocite / water xanthate systems, International journal of mineral processing, vol 30. pp. 17-33.

Zhong-Qun, T., Bin, R., and De-Yin, W., 2002, *Surface-enhancement Raman Scattering: From Noble to Transitional Metals and from Rough Surfaces to Ordered Nanostructures*, The Journal of Physical Chemistry B, vol 106, no. 37, pp 9463-9483.

Zeng, X., and Osseo-Asare, K., 2001, *Partition of pyrite and hematite in aqueous biphase systems: effects of pH and surfactants*, Colloids and surfaces A: physiochemical and engineering aspects, vol 177, pp 247 – 254.

Zolfaghari, A., Conway, B.E., and Jerkiewicz, G., 2002, *Elucidation of the effects of competitive adsorption of Cl^- and Br^- ions on the initial stages of Pt surface oxidation by means of electrochemical nonogravimetry,* Electrochimica Acta, vol. 47, pp 1173-1187.

12. Appendices

Appendix 1

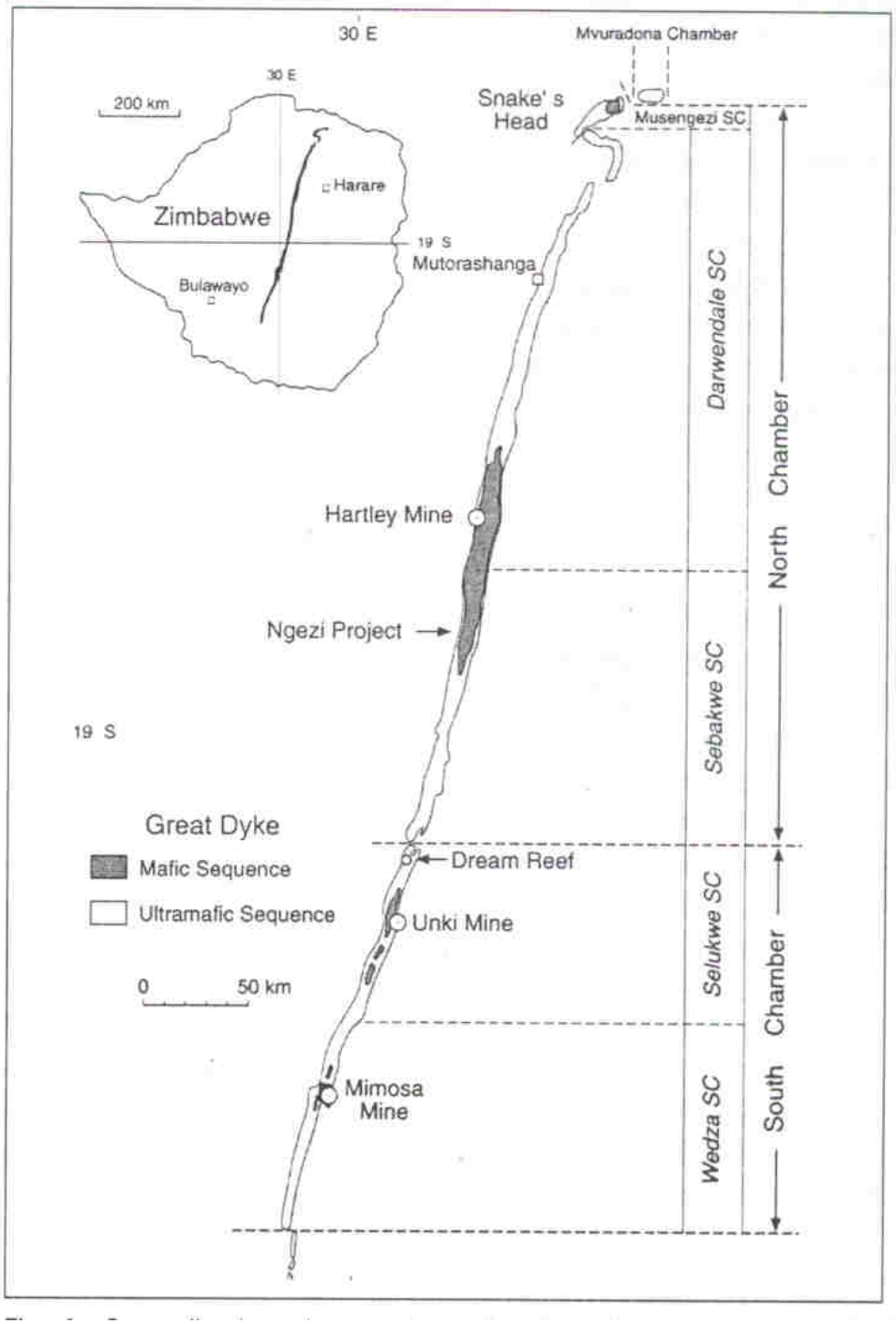

Figure: Great Dyke of Zimbabwe (Oberthür, 2002b)

Appendix 2

Microprobe analysis of natural PGMs from Mimosa Mine, Zimbabwe

$PtAs_2$ (proportions are by weight)																		
Sample	Ru	Rh	Pd	Os	Ir	Pt	Fe	Cu	Ni	Co	S	Se	Te	As	Sb	Bi	Ag	Hg	Total
As5219a	0.03	0.10	0.09	0.06	0.00	54.78	0.75	0.02	0.04	0.02	0.46	0.00	0.05	43.76	0.00	0.02	0.03	0.03	100.24
As5220a	0.15	0.32	0.05	0.07	3.64	50.80	2.01	0.14	0.02	0.00	1.32	0.02	0.06	42.45	0.00	0.01	0.00	0.05	101.11
As5291	0.09	0.05	0.05	0.01	0.00	56.13	0.59	0.03	0.02	0.00	0.35	0.06	0.03	44.07	0.03	0.00	0.00	0.00	101.51
As5296	0.01	0.03	0.03	0.00	0.00	53.43	2.07	0.61	0.09	0.00	0.38	0.01	0.00	44.92	0.00	0.07	0.00	0.00	101.65
As5299	0.81	3.62	0.00	0.03	1.17	48.95	1.56	0.03	0.21	0.01	3.17	0.16	0.00	40.13	0.02	0.12	0.15	0.09	100.23
As5301	0.03	0.55	0.00	0.00	0.00	52.69	1.80	0.18	1.36	0.08	0.92	0.17	0.00	43.33	0.03	0.00	0.12	0.00	101.26
	0.02	1.10	0.05	0.00	0.00	53.12	1.14	0.65	0.23	0.00	0.86	0.17	0.00	43.49	0.00	0.25	0.00	0.01	101.09
As5305	0.00	0.00	0.00	0.00	0.26	53.16	1.35	0.22	0.06	0.00	0.51	0.02	0.01	44.92	0.00	0.11	0.00	0.00	100.64
As5309	0.05	0.04	0.00	0.05	1.24	54.45	0.73	0.04	0.07	0.00	0.70	0.07	0.03	43.35	0.00	0.00	0.00	0.00	100.82
	0.04	0.14	0.00	0.00	0.46	53.72	1.36	0.04	0.03	0.01	0.51	0.04	0.00	44.12	0.03	0.02	0.06	0.00	100.58
As5310	0.03	0.08	0.00	0.05	0.39	53.48	2.97	0.10	0.09	0.06	0.92	0.03	0.03	43.00	0.10	0.04	0.00	0.00	101.37
As5311	0.03	0.21	0.00	0.21	0.00	53.84	1.21	0.00	0.30	0.01	0.74	0.01	0.05	43.83	0.04	0.14	0.00	0.00	100.76
As5314	0.15	0.00	0.00	0.00	0.00	54.21	1.23	0.00	0.00	0.00	0.48	0.03	0.00	44.30	0.01	0.00	0.00	0.00	100.68
	0.06	0.00	0.00	0.00	0.00	53.95	1.12	0.00	0.00	0.00	0.49	0.00	0.12	43.64	0.07	0.12	0.00	0.00	99.89
As5434	0.03	0.14	0.27	0.00	0.14	52.77	1.48	1.49	0.14	0.14	0.57	0.04	0.18	43.39	0.07	0.10	0.00	0.00	100.63
As5435	0.01	0.13	0.04	0.00	0.00	54.56	1.09	0.05	0.01	0.01	0.55	0.06	0.00	43.88	0.01	0.17	0.00	0.00	100.56
	0.00	0.06	0.00	0.00	0.02	54.88	0.55	0.02	0.03	0.00	0.29	0.00	0.04	43.87	0.00	0.07	0.00	0.00	99.97
As5436	0.04	0.03	0.00	0.01	0.22	53.67	1.10	0.00	0.09	0.01	0.49	0.05	0.03	43.54	0.06	0.00	0.14	0.06	99.54
	0.09	0.07	0.00	0.00	0.64	53.59	0.96	0.78	0.19	0.01	0.42	0.07	0.00	44.07	0.00	0.00	0.00	0.17	101.06
	0.09	0.08	0.01	0.03	0.06	54.46	0.61	0.45	0.01	0.01	0.26	0.00	0.00	44.25	0.00	0.00	0.00	0.00	100.32
As5441	0.00	0.16	0.00	0.02	0.00	54.25	0.98	0.17	0.45	0.02	0.26	0.07	0.00	44.60	0.11	0.12	0.05	0.00	101.26
As5444	0.05	0.00	0.03	0.10	0.37	55.81	0.50	0.01	0.08	0.01	0.33	0.11	0.05	42.76	0.00	0.05	0.00	0.00	100.26
As5446	0.45	1.05	0.00	0.12	0.14	52.68	0.97	0.29	0.27	0.04	1.47	0.00	0.02	42.60	0.09	0.09	0.00	0.00	100.28
As5538	0.11	0.09	0.07	0.06	0.91	55.87	0.76	0.00	0.02	0.00	0.65	0.13	0.02	41.94	0.03	0.00	0.10	0.00	100.76
As5937	0.06	0.07	0.00	0.09	0.01	55.74	1.35	0.08	0.02	0.00	0.37	0.09	0.01	43.54	0.04	0.00	0.00	0.00	101.51
As5939	0.08	0.03	0.03	0.08	0.02	54.93	0.55	0.74	0.02	0.00	0.17	0.02	0.01	43.78	0.06	0.00	0.06	0.00	100.58
	0.06	0.14	0.00	0.09	1.46	54.93	0.33	0.00	0.04	0.00	0.55	0.04	0.06	42.71	0.10	0.00	0.00	0.00	100.59
	0.07	0.05	0.00	0.09	2.17	53.62	0.48	0.07	0.12	0.00	0.65	0.00	0.07	42.86	0.21	0.08	0.17	0.02	100.73
Average	**0.09**	**0.30**	**0.03**	**0.04**	**0.48**	**53.87**	**1.13**	**0.22**	**0.14**	**0.02**	**0.67**	**0.05**	**0.03**	**43.47**	**0.04**	**0.06**	**0.03**	**0.02**	**100.71**
Stdev	**0.16**	**0.71**	**0.05**	**0.05**	**0.83**	**1.51**	**0.58**	**0.35**	**0.26**	**0.03**	**0.57**	**0.05**	**0.04**	**0.97**	**0.05**	**0.07**	**0.05**	**0.04**	**0.52**
High	**0.81**	**3.62**	**0.27**	**0.21**	**3.64**	**56.13**	**2.97**	**1.49**	**1.36**	**0.14**	**3.17**	**0.17**	**0.18**	**44.92**	**0.21**	**0.25**	**0.17**	**0.17**	**101.65**
Low	**0.00**	**0.00**	**0.00**	**0.00**	**0.00**	**48.95**	**0.33**	**0.00**	**0.00**	**0.00**	**0.17**	**0.00**	**0.00**	**40.13**	**0.00**	**0.00**	**0.00**	**0.00**	**99.54**
95% Confidence	**0.06**	**0.26**	**0.02**	**0.02**	**0.31**	**0.56**	**0.22**	**0.13**	**0.10**	**0.01**	**0.21**	**0.02**	**0.02**	**0.36**	**0.02**	**0.02**	**0.02**	**0.01**	**0.19**

Table: Composition of natural $PtAs_2$ (proportions by mass) (Oberthür, 2002c).

Pt-Pd-Bi-Te (proportions are by mass)																	
Sample	Pd	Os	Ir	Pt	Fe	Cu	Ni	Co	S	Se	Te	Sb	Bi	Pb	Ag	Hg	Total
As5287	6.74	0.00	0.00	24.76	1.21	0.00	2.13	0.03	0.05	0.00	43.40	0.00	21.50	0.00	0.19	0.06	100.09
As5292	0.70	0.00	0.00	37.94	1.01	0.00	0.02	0.00	0.05	0.00	39.65	0.01	21.26	0.18	0.15	0.00	100.97
	0.00	0.00	0.15	36.50	1.73	0.84	0.34	0.02	0.22	0.02	32.37	0.00	26.56	0.00	0.06	0.00	98.81
As5537	0.00	0.00	0.00	35.71	0.40	0.09	0.00	0.00	0.05	0.04	21.74	0.00	41.60	0.00	0.32	0.00	99.95
	0.00	0.00	0.00	37.35	0.55	0.06	0.03	0.00	0.04	0.03	33.89	0.02	27.56	0.00	0.00	0.00	99.53
	2.18	0.00	0.00	33.96	1.21	0.49	0.06	0.00	0.07	0.00	34.43	0.00	27.30	0.00	0.00	0.00	99.70
As5941	0.02	0.02	0.00	36.48	1.90	0.58	1.49	0.00	0.22	0.00	32.74	0.07	26.43	0.43	0.00	0.00	100.38
	1.26	0.00	0.00	35.34	0.72	0.24	0.06	0.00	0.05	0.00	35.94	0.00	26.48	0.00	0.19	0.00	100.28
As5492	0.00	0.00	0.00	35.69	2.24	1.76	0.79	0.00	0.18	0.00	31.01	0.08	28.57	0.31	0.12	0.00	100.75
Average	**1.21**	**0.00**	**0.02**	**34.86**	**1.22**	**0.45**	**0.55**	**0.01**	**0.10**	**0.01**	**33.91**	**0.02**	**27.47**	**0.10**	**0.11**	**0.01**	**100.05**
Stdev	**2.21**	**0.01**	**0.05**	**3.96**	**0.63**	**0.57**	**0.78**	**0.01**	**0.08**	**0.02**	**6.00**	**0.03**	**5.89**	**0.17**	**0.11**	**0.02**	**0.66**
High	**6.74**	**0.02**	**0.15**	**37.94**	**2.24**	**1.76**	**2.13**	**0.03**	**0.22**	**0.04**	**43.40**	**0.08**	**41.60**	**0.43**	**0.32**	**0.06**	**100.97**
Low	**0.00**	**0.00**	**0.00**	**24.76**	**0.40**	**0.00**	**0.00**	**0.00**	**0.04**	**0.00**	**21.74**	**0.00**	**21.26**	**0.00**	**0.00**	**0.00**	**98.81**
95% Confidence	**1.37**	**0.00**	**0.03**	**2.45**	**0.39**	**0.35**	**0.48**	**0.01**	**0.05**	**0.01**	**3.72**	**0.02**	**3.65**	**0.10**	**0.07**	**0.01**	**0.41**

Table: Composition of natural Pt-Pd-Bi-Te (proportions by mass) (Oberthür, 2002c)

	Pd-Pt-Bi-Te (Proportions in mass%)																			
Sample no.	Rh	Pd	Os	Ir	Pt	Fe	Cu	Ni	Co	S	Se	Te	As	Sb	Bi	Pb	Ag	Au	Hg	Total
	0.00	24.17	0.00	0.00	0.00	2.02	0.00	0.03	0.00	0.06	0.04	31.38	0.00	0.23	42.46	0.05	0.10	0.03	0.00	100.57
As5313	0.00	24.15	0.00	0.00	0.00	1.05	0.25	0.04	0.00	0.01	0.00	29.30	0.00	1.17	43.72	0.15	0.06	0.01	0.06	99.97
	0.00	38.50	0.00	0.00	0.00	0.95	0.20	0.07	0.03	0.04	0.00	21.17	0.00	1.56	38.70	0.02	0.24	0.00	0.00	101.48
As5449	0.00	34.50	0.00	0.02	0.00	3.80	0.08	0.02	0.00	0.53	0.00	10.14	0.00	2.95	48.65	0.00	0.29	0.00	0.00	100.98
As5451	0.00	23.66	0.05	0.21	0.00	1.04	0.00	0.56	0.02	0.05	0.00	26.72	0.00	0.03	47.02	0.06	0.00	0.06	0.00	99.48
As5443	0.00	38.51	0.04	0.00	0.00	0.39	0.20	0.40	0.00	0.03	0.00	22.43	0.00	0.20	38.11	0.05	0.31	0.00	0.00	100.67
As5940	0.00	23.54	0.00	0.00	0.00	3.25	1.06	0.07	0.13	0.44	0.02	31.79	0.10	0.40	41.70	0.00	0.00	0.00	0.00	102.50
	0.00	24.02	0.00	0.00	0.00	1.18	0.11	1.02	0.29	0.01	0.00	28.42	0.00	0.10	46.61	0.05	0.00	0.06	0.00	101.87
	0.00	23.48	0.00	0.29	0.10	0.78	0.00	0.12	0.17	0.19	0.00	28.84	0.26	0.09	45.48	0.02	0.20	0.00	0.00	100.20
	0.00	23.68	0.00	0.00	0.00	0.83	0.35	0.02	0.03	0.04	0.00	28.96	0.00	0.00	46.97	0.02	0.01	0.06	0.00	100.97
	0.00	23.84	0.00	0.12	0.00	0.56	0.23	0.03	0.02	0.02	0.00	29.34	0.00	0.00	46.63	0.00	0.00	0.00	0.00	100.79
As5943	0.00	23.69	0.00	0.01	0.00	2.38	0.34	0.03	0.01	0.08	0.00	29.99	0.00	0.02	44.25	0.14	0.00	0.02	0.00	100.97
Average	**0.00**	**27.15**	**0.01**	**0.05**	**0.01**	**1.52**	**0.24**	**0.20**	**0.06**	**0.13**	**0.01**	**26.54**	**0.03**	**0.56**	**44.19**	**0.05**	**0.10**	**0.02**	**0.01**	**100.87**
Stdev	**0.00**	**6.13**	**0.02**	**0.10**	**0.03**	**1.10**	**0.29**	**0.31**	**0.09**	**0.18**	**0.01**	**6.09**	**0.08**	**0.90**	**3.38**	**0.05**	**0.12**	**0.03**	**0.02**	**0.82**
High	**0.00**	**38.51**	**0.05**	**0.29**	**0.10**	**3.80**	**1.06**	**1.02**	**0.29**	**0.53**	**0.04**	**31.79**	**0.26**	**2.95**	**48.65**	**0.15**	**0.31**	**0.06**	**0.06**	**102.50**
Low	**0.00**	**23.48**	**0.00**	**0.00**	**0.00**	**0.39**	**0.00**	**0.02**	**0.00**	**0.01**	**0.00**	**10.14**	**0.00**	**0.00**	**38.11**	**0.00**	**0.00**	**0.00**	**0.00**	**99.48**
95% Confidence		**3.21**	**0.01**	**0.05**	**0.02**	**0.58**	**0.15**	**0.16**	**0.05**	**0.09**	**0.01**	**3.19**	**0.04**	**0.47**	**1.77**	**0.03**	**0.07**	**0.01**	**0.01**	**0.43**

Table: Composition of natural Pd-Bi-Te (proportions by mass) (Oberthür, 2002c)

Appendix 3

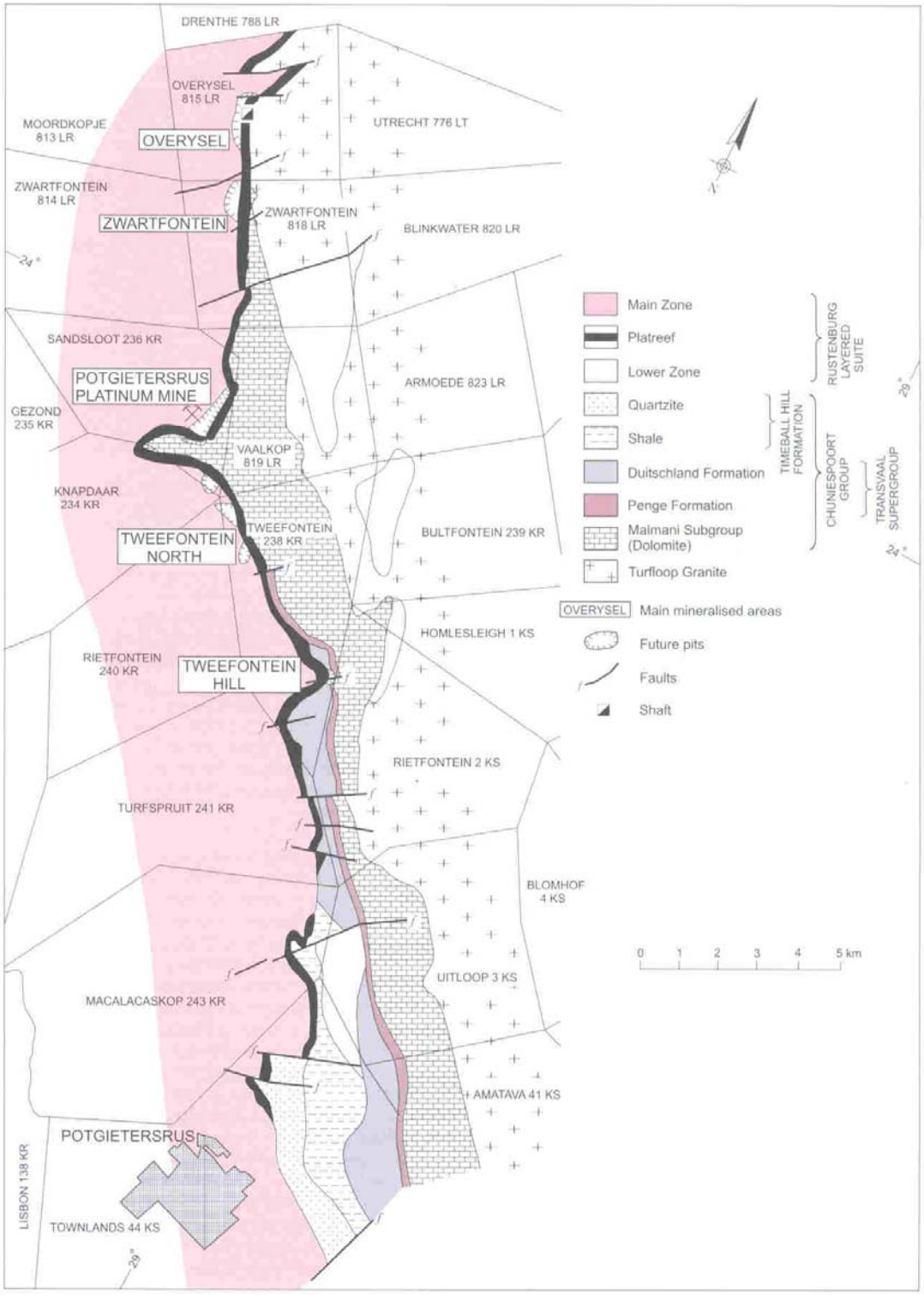

Figure: Platreef showing the location of possible open pits (Wilson,1998).

Appendix 4

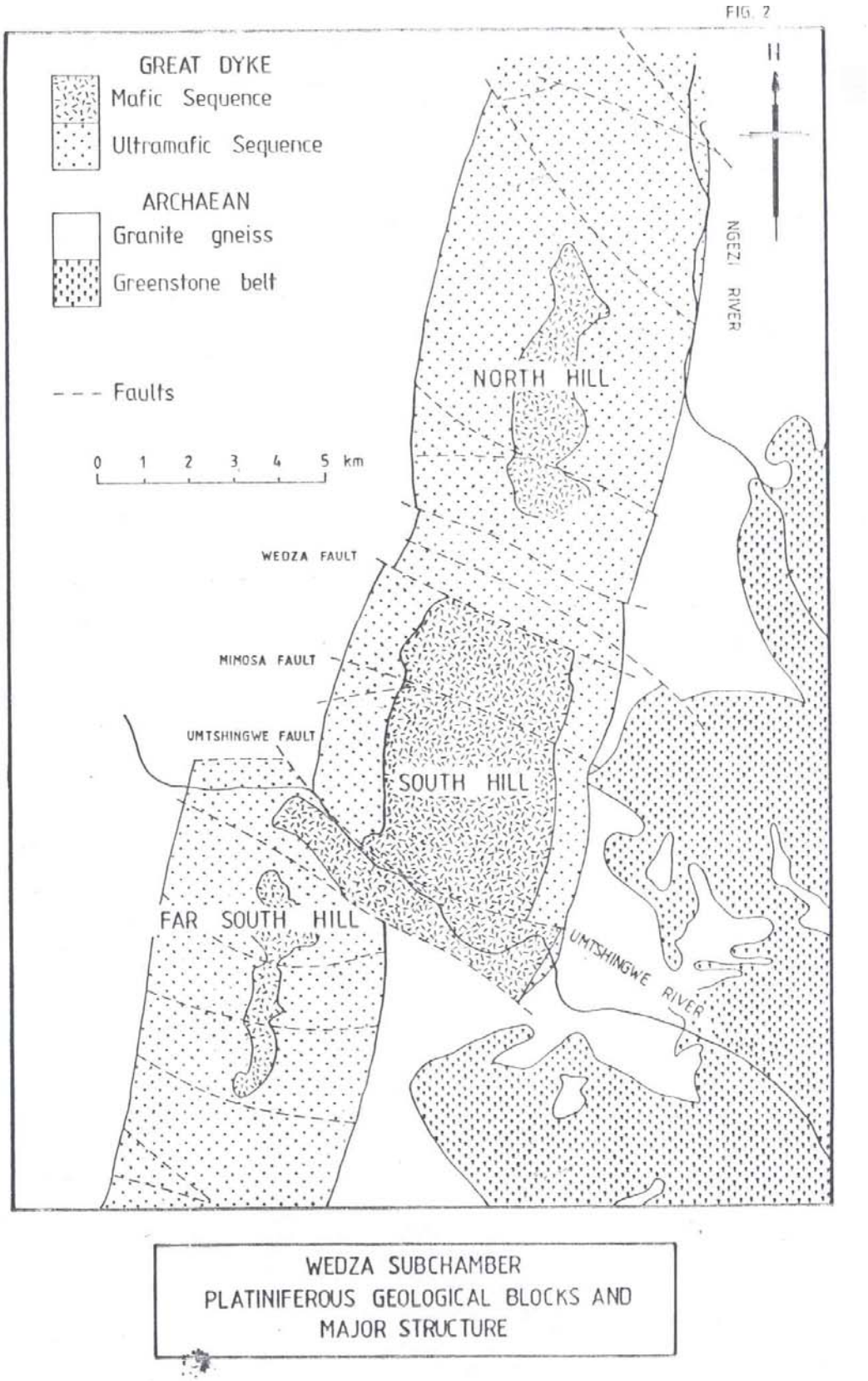

Figure: The geological complex of Mimosa Mine, Zimbabwe (Van Wouw, 2004).

Appendix 5

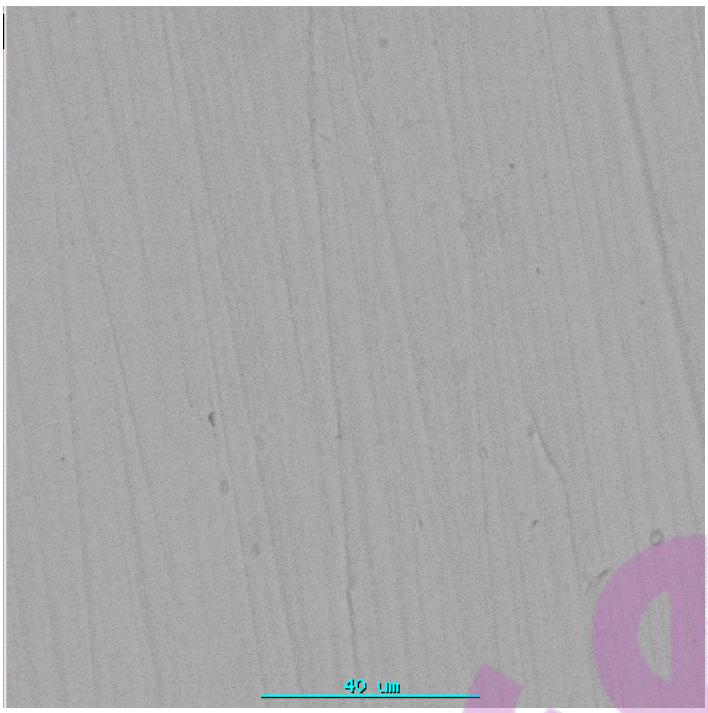

Figure: Back-scattered electron micrograph of the synthetically prepared michenerite (PdBiTe) heat-treated at 480^{o}C for 60 days. Accelerating voltage 25kV.

Appendix 6

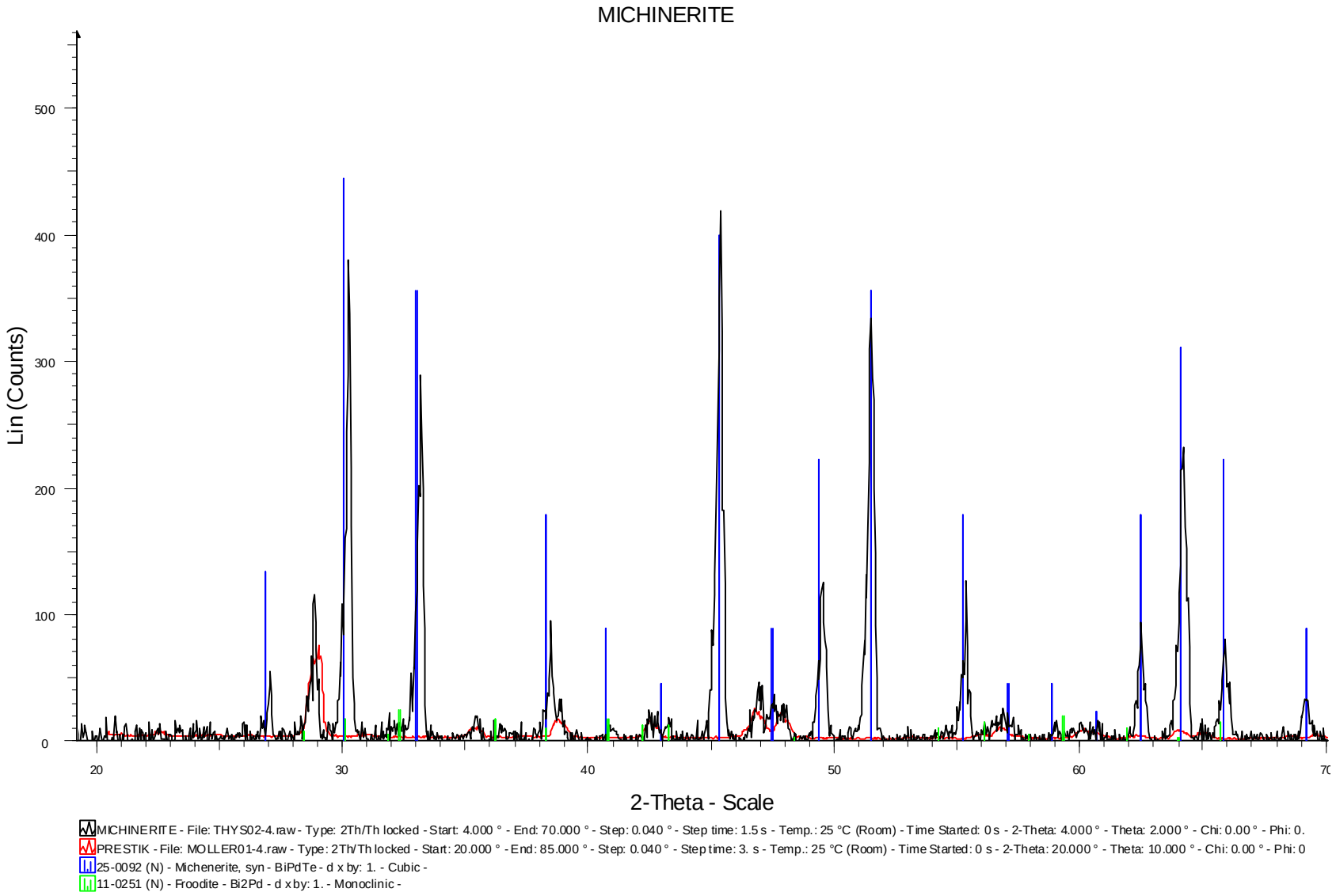

Figure: XRD Spectrum of synthetic Pd-Bi-Te (Michenerite)

Appendix 7

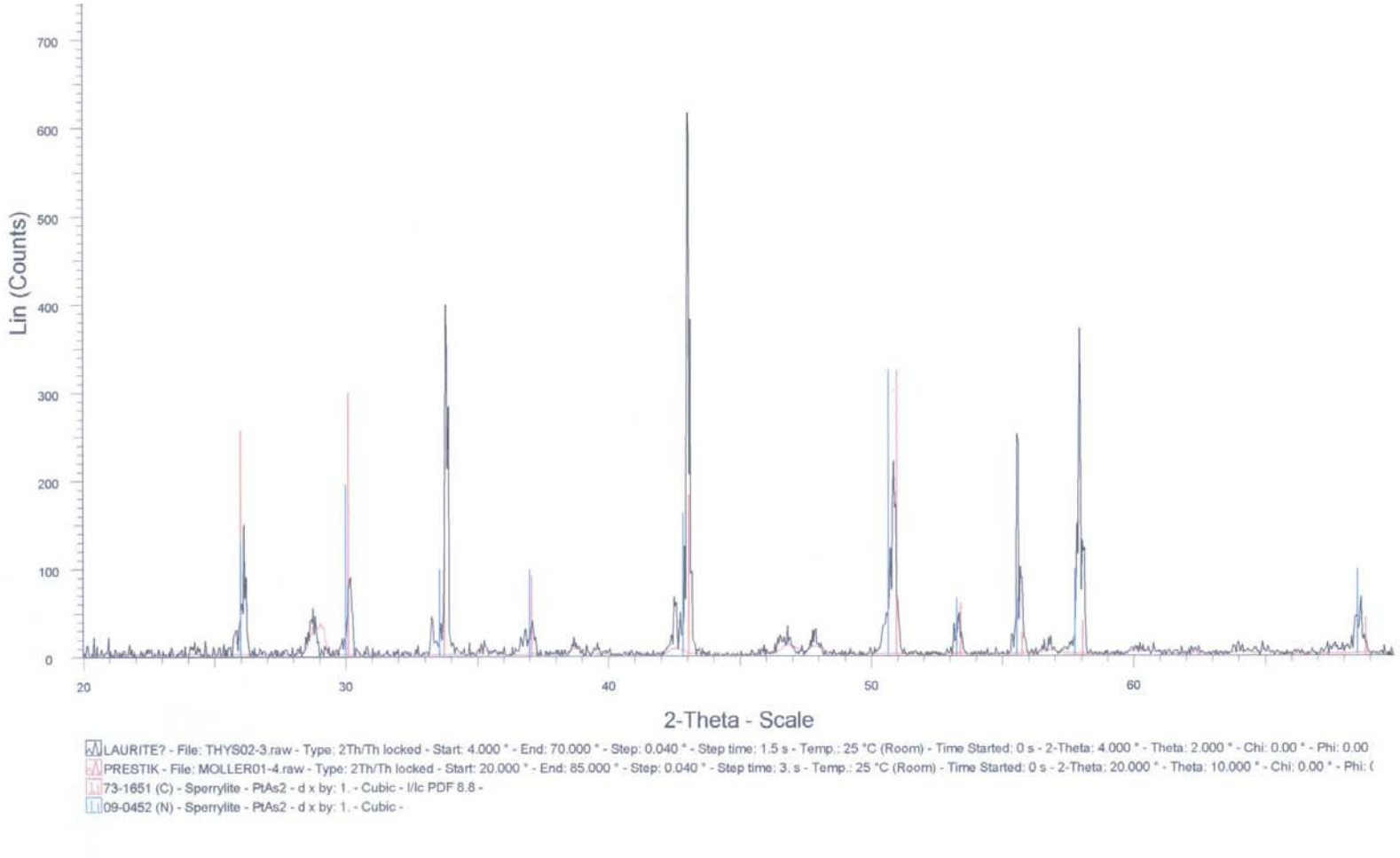

Figure: XRD Spectrum of $PtAs_2$ (Sperrylite)

Appendix 8

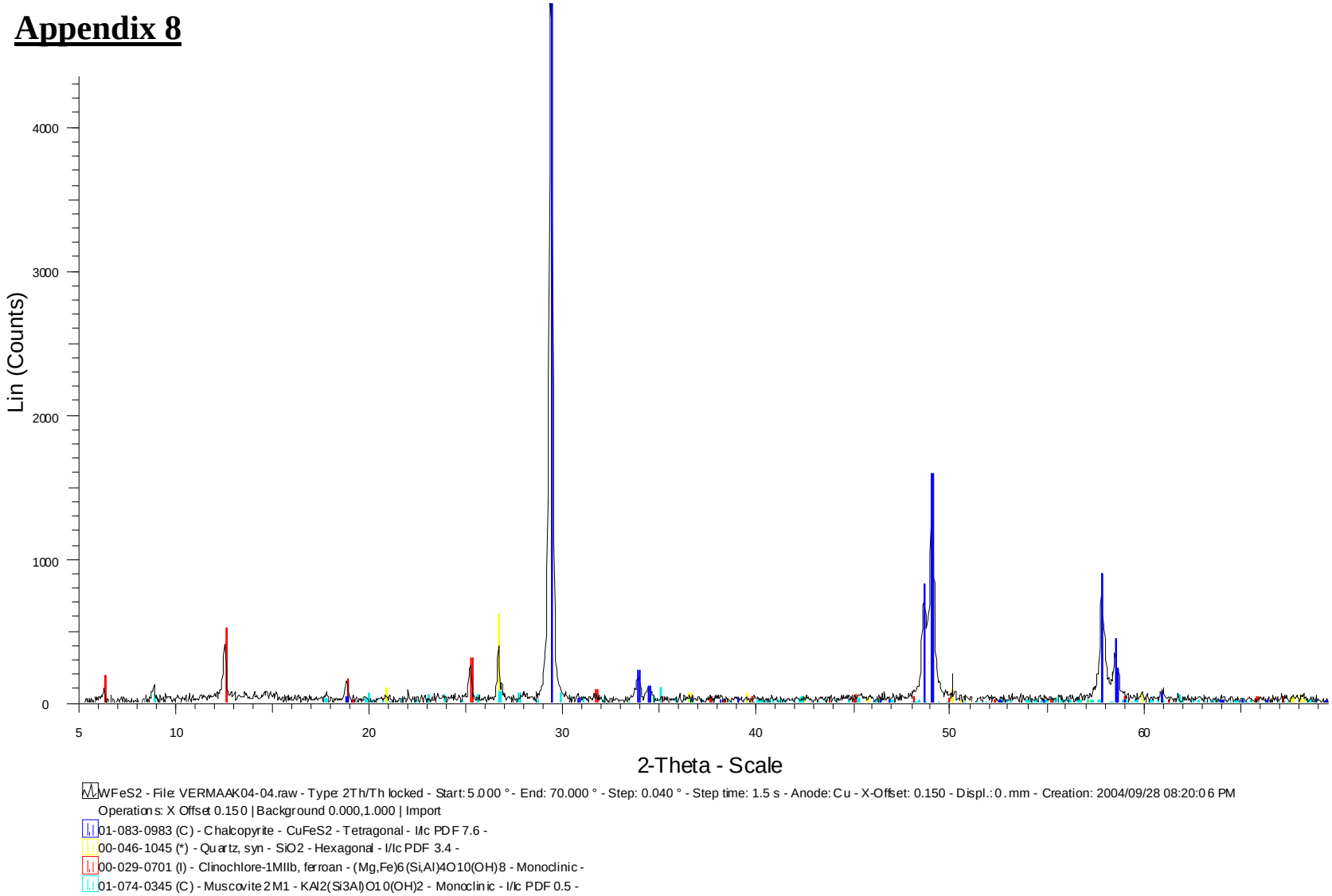

Figure: XRD Spectrum of natural $CuFeS_2$ (Chalcopyrite)

Appendix 9

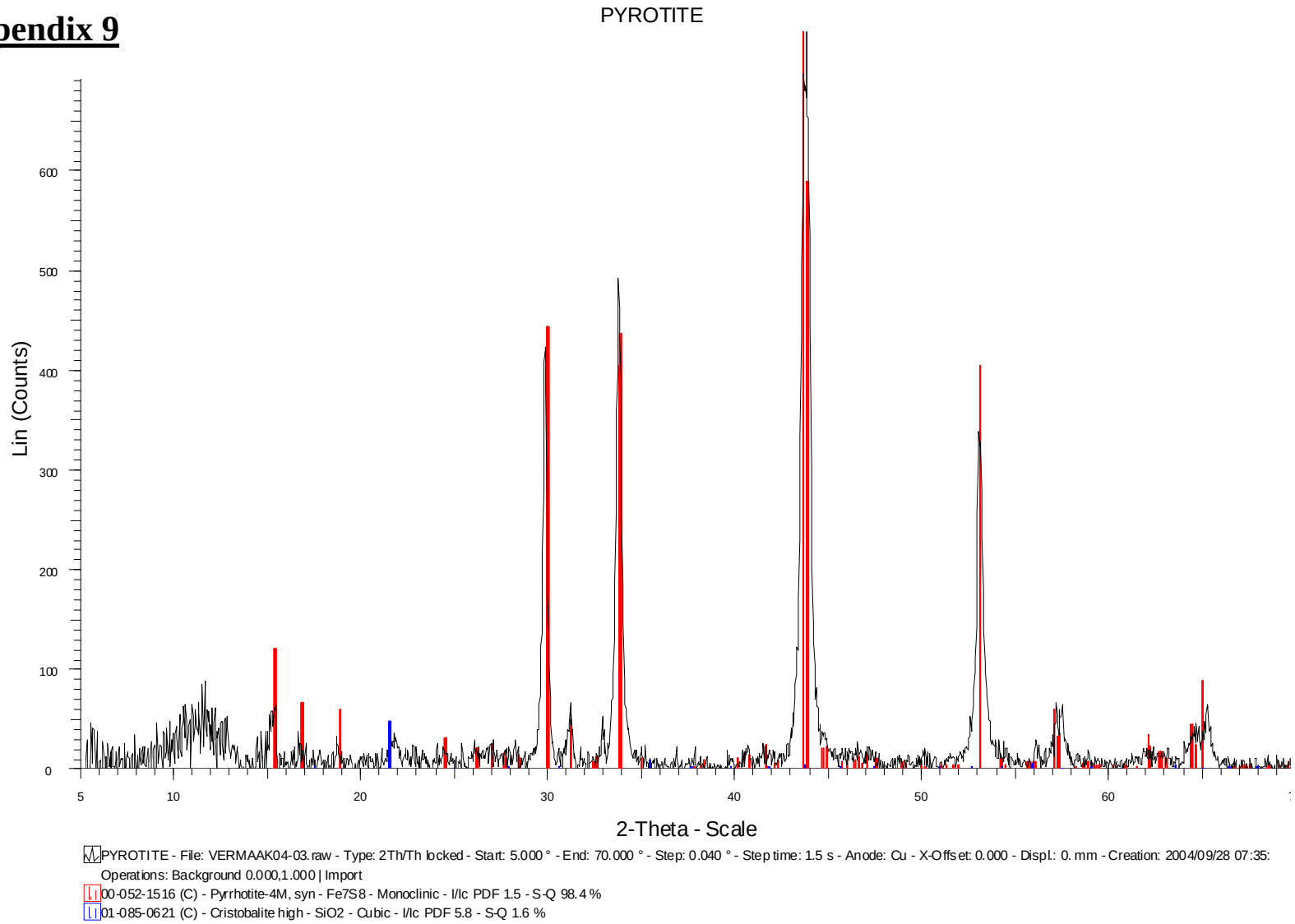

Figure: XRD Spectrum of natural pyrrhotite

Appendix 10

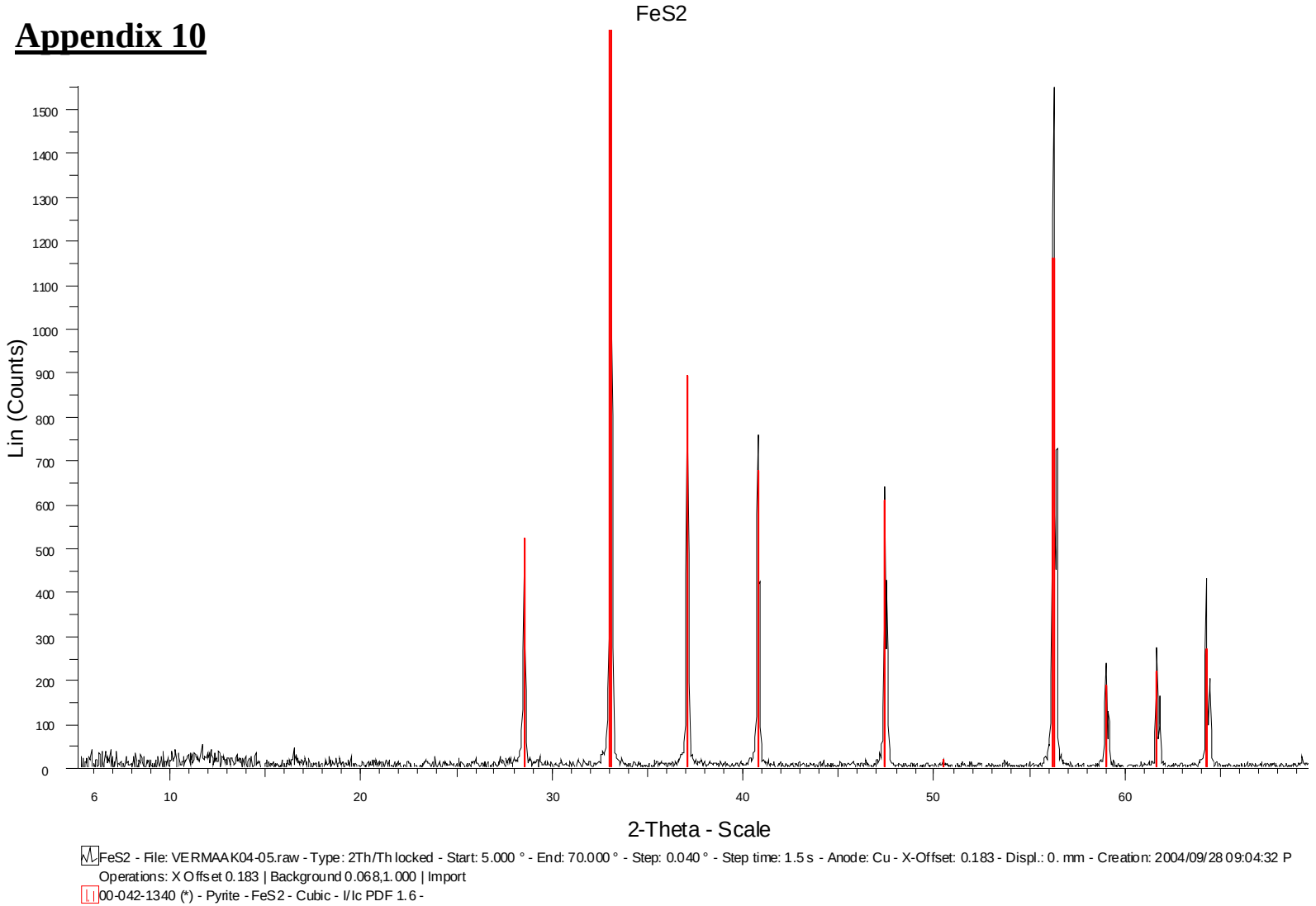

Figure: XRD Spectrum of natural pyrite

Appendix 11

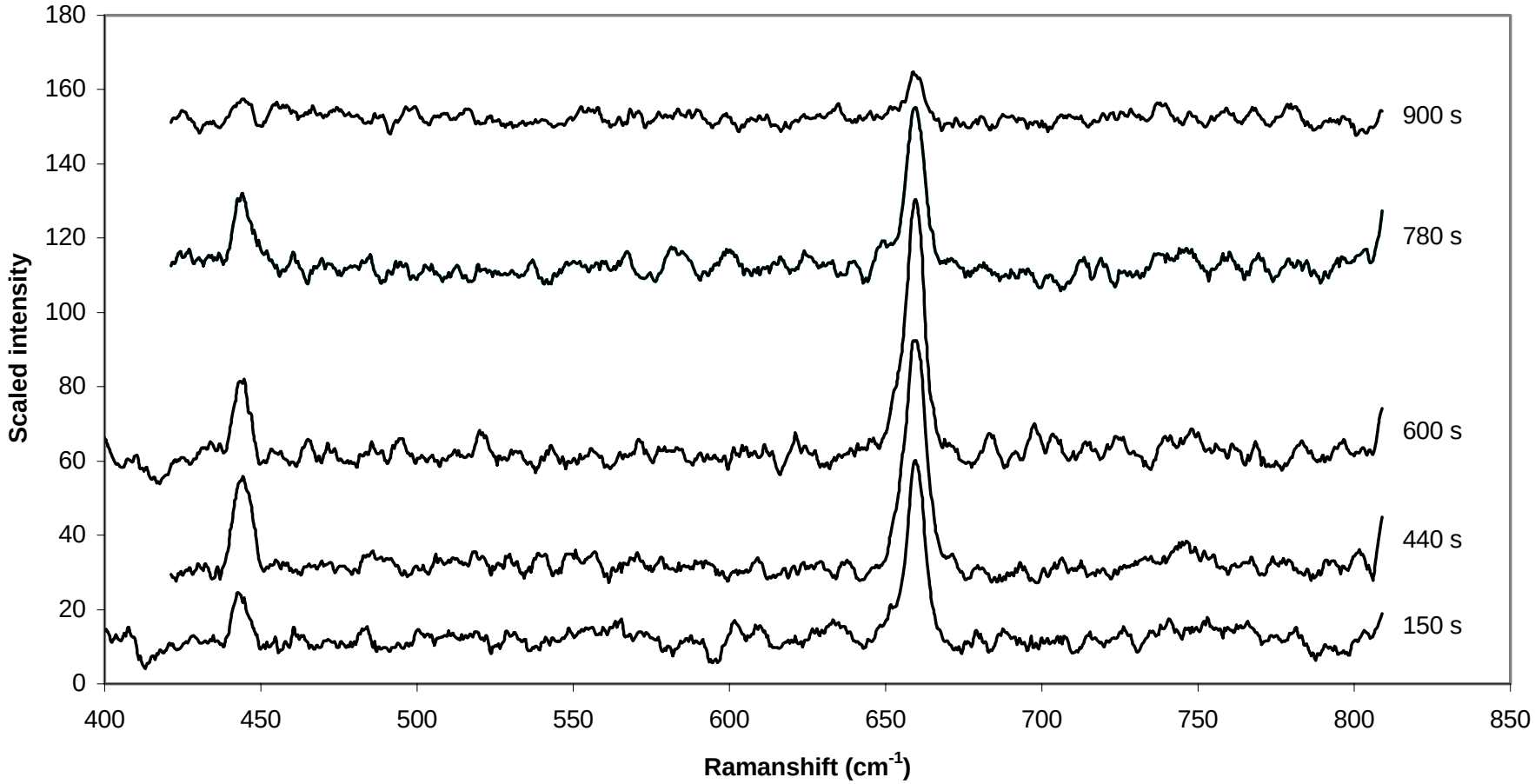

Figure: Raman spectra of Pd-Bi-Te electrode polarized for different lengths of time at 0.3V (SHE) in 0.05M $Na_2B_4O_7$ solution containing $1x10^{-3}$ M potassium ethyl xanthate

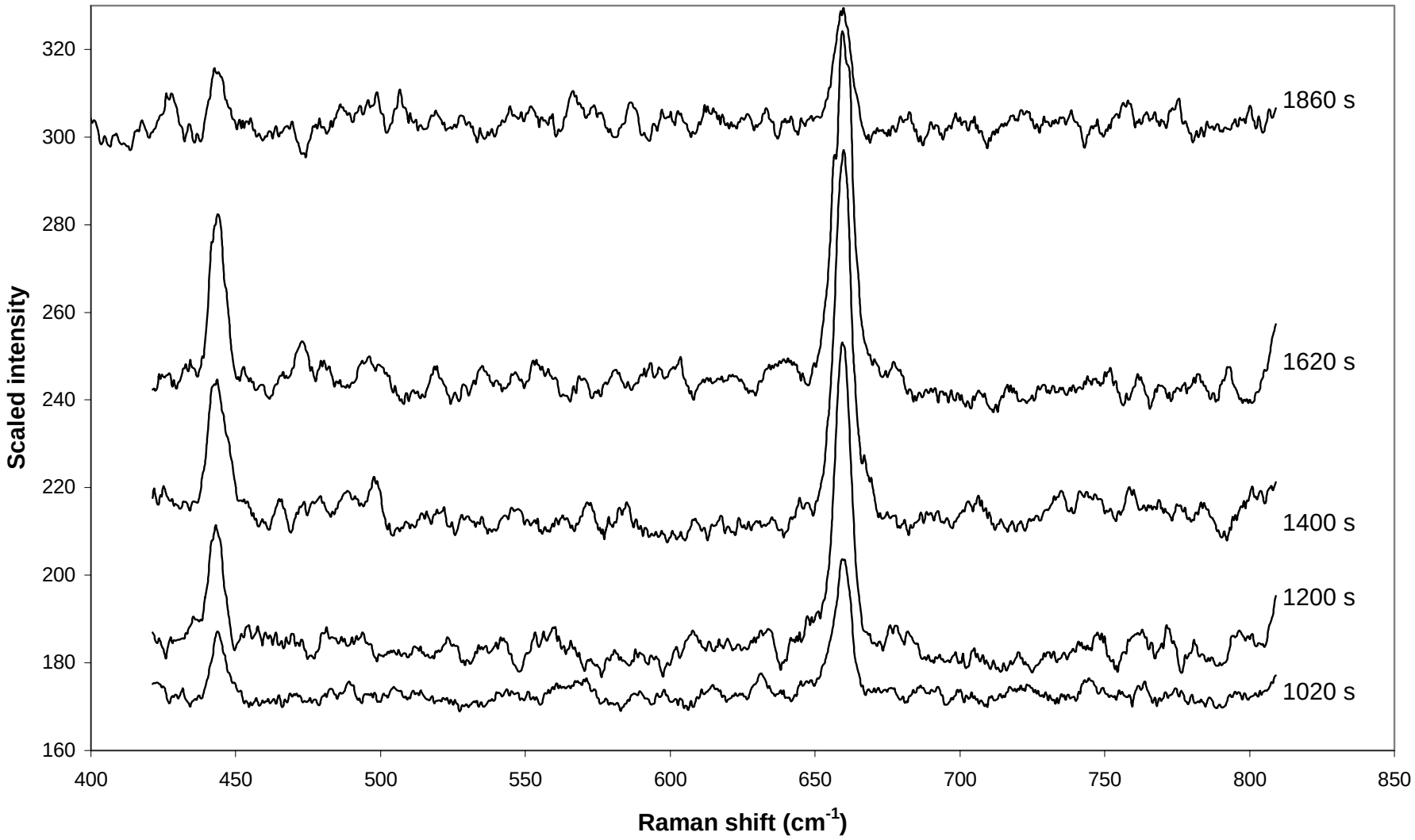

Figure: Raman spectra of Pd-Bi-Te electrode polarized for different lengths of time at 0.3V (SHE) in 0.05M $Na_2B_4O_7$ solution containing $1x10^{-3}$ M potassium ethyl xanthate

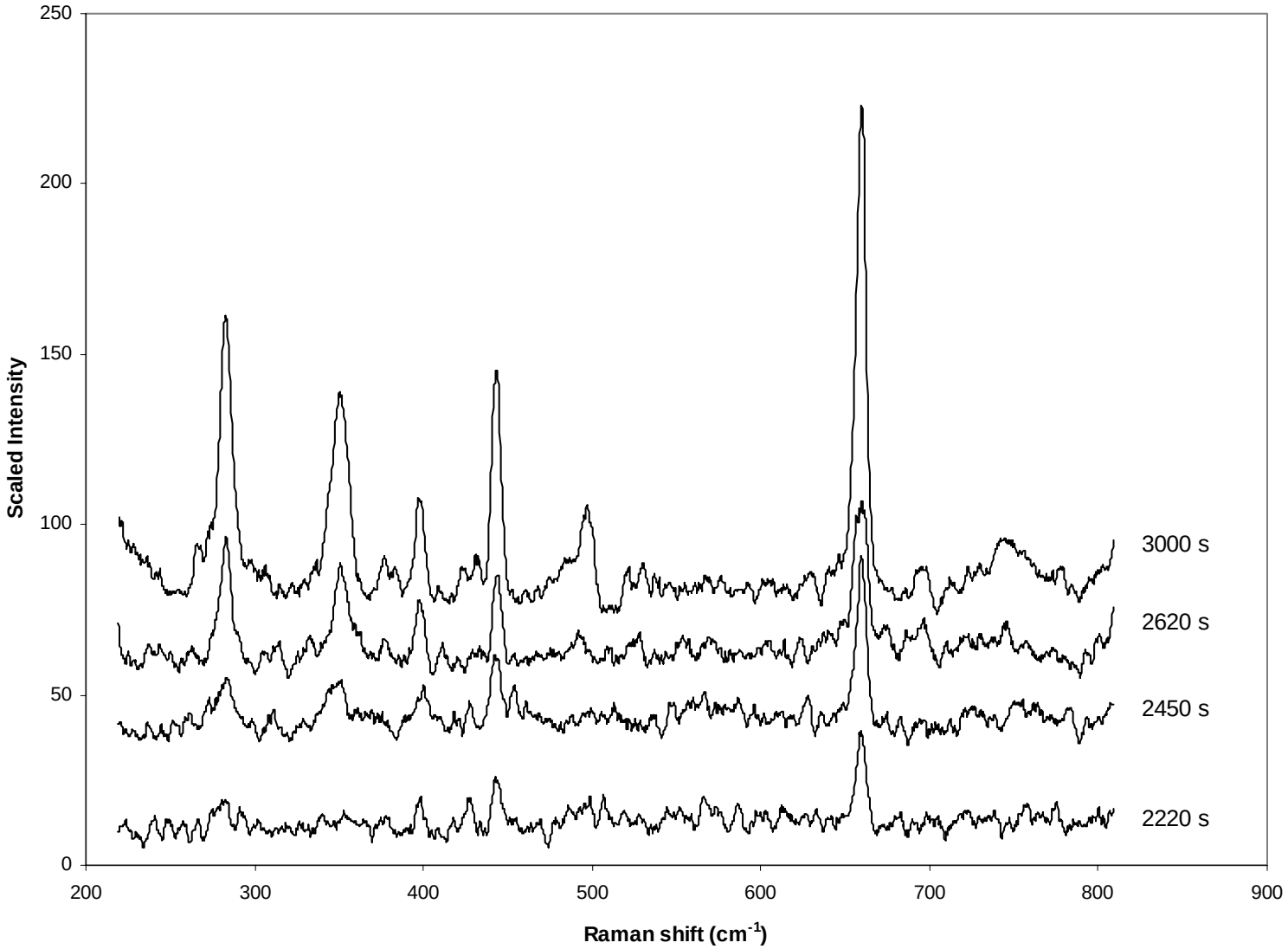

Figure: Raman spectra of Pd-Bi-Te electrode polarized for different lengths of time at 0.3V (SHE) in 0.05M $Na_2B_4O_7$ solution containing $1x10^{-3}$ M potassium ethyl xanthate

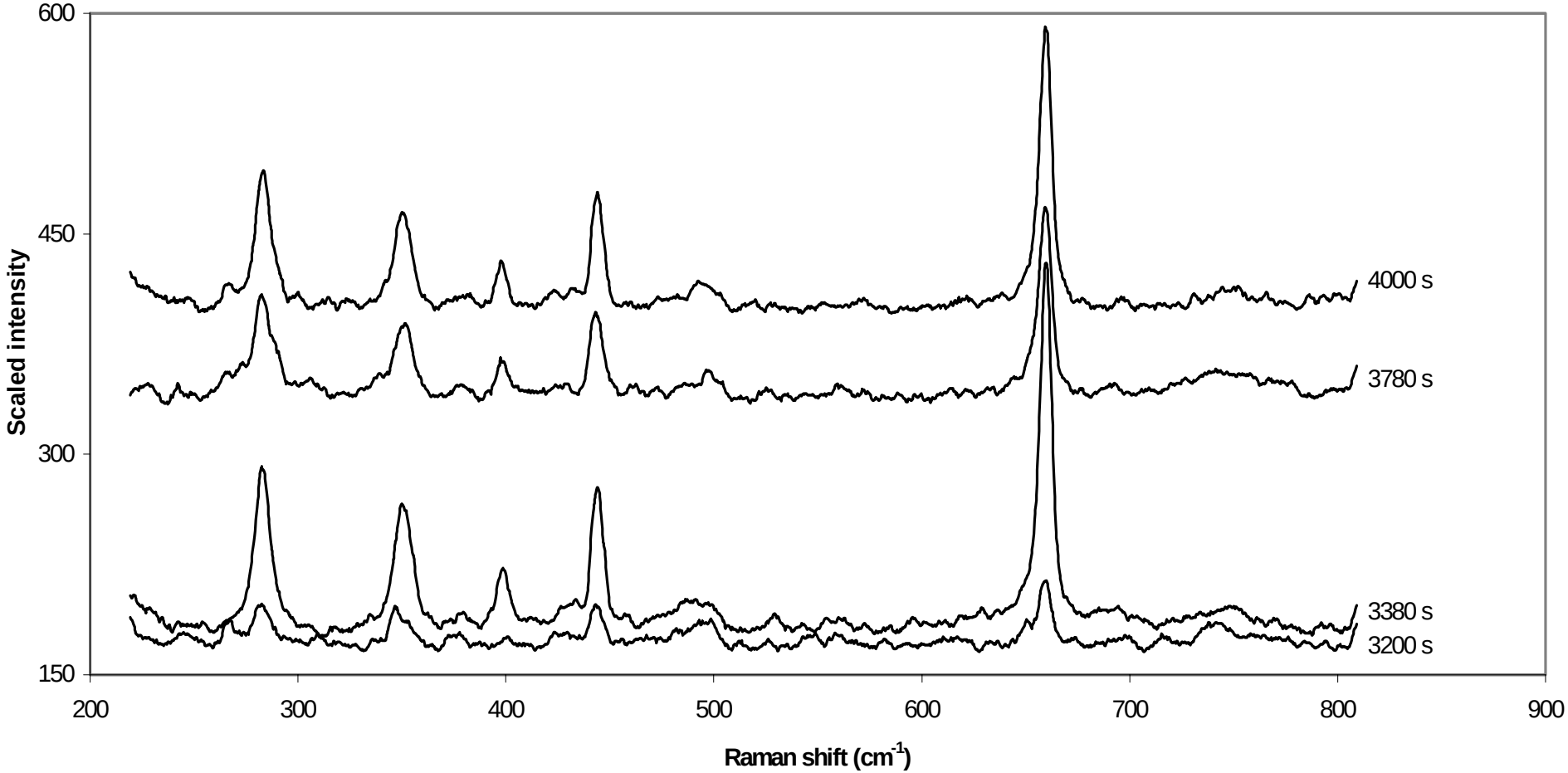

Figure: Figure: Raman spectra of Pd-Bi-Te electrode polarized for different lengths of time at 0.3V (SHE) in 0.05M $Na_2B_4O_7$ solution containing $1x10^{-3}$ M potassium ethyl xanthate

Table : Summary of intensity ratios as functions of anodic polarization time

Time (s)	743 cm^{-1} peak intensity	660 cm^{-1} peak intensity	498 cm^{-1} peak intensity	660 cm^{-1}: 743 cm^{-1} ratio	498 cm^{-1}: 743 cm^{-1} ratio	498 cm^{-1}: 743 cm^{-1} ratio		660 cm^{-1}: 743 cm^{-1} ratio	
						Average	Stedev	Average	Stdev
150	7.90	62.34	3.64	7.89	0.46				
440	8.37	69.28	6.00	8.28	0.72				
600	6.80	44.79	2.85	6.59	0.42				
780	6.01	14.10	5.12	2.35	0.85	0.61	0.21	6.27	2.72
1000	6.02	33.57	4.24	5.57	0.70				
1200	6.45	72.51	6.48	11.25	1.01				
1400	8.64	85.78	11.69	9.93	1.35				
1620	6.68	82.77	9.64	12.39	1.44				
1860	7.85	55.79	8.08	7.11	1.03	1.11	0.30	8.37	4.48
2220	133.11	155.41	136.59	1.17	1.03				
2450	7.49	50.00	5.54	6.68	0.74				
2620	11.06	45.99	7.89	4.16	0.71				
3000	15.93	140.73	24.59	8.84	1.54	1.01	0.39	5.63	3.30
3200	15.05	43.08	17.11	2.86	1.14				
3380	17.16	125.59	16.73	7.32	0.97				
3780	16.55	247.37	18.62	14.94	1.12				
4000	13.42	188.45	17.28	14.04	1.29	1.21	0.22	9.79	4.99